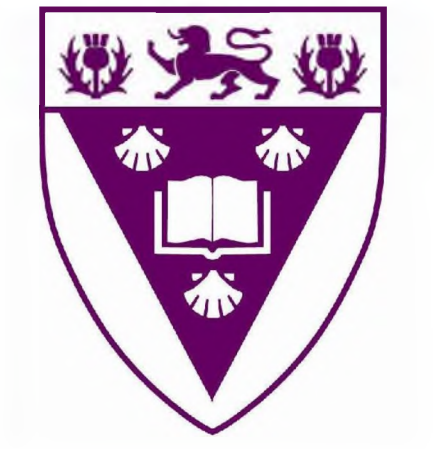

Development and Optimisation of a Novel *Plasmodium falciparum* Hsp90-Hop Interaction Assay

Thesis submitted in fulfilment of the requirements for the degree of

MASTER OF SCIENCE IN BIOCHEMISTRY

Department of Biochemistry and Microbiology
Rhodes University
Grahamstown
South Africa

By

Lynn Wambua

December 2017

Supervisor: H.C. Hoppe

Abstract

Protein-protein interactions are involved in a range of disease processes and thus have become the focus of many drug discovery programs. Widespread drug resistance to all currently used antimalarial drugs drives the search for alternative drug targets with novel mechanisms of action that offer new therapeutic options. Molecular chaperones such as heat shock proteins facilitate protein folding, play a role in protein trafficking and prevent protein misfolding in cells under stress. Heat shock protein 90 (Hsp90) is a well-studied chaperone that has been the focus of cancer drug development with moderate success. In *Plasmodium falciparum* (*P. falciparum*), heat shock proteins are thought to play a vital role in parasite survival of the physiologically diverse habitats of the parasite lifecycle and because Hsp90 is prominently expressed in *P. falciparum*, the chaperone is considered a potentially ideal drug target. Hsp90 function in cells is regulated by interactions with co-chaperones, which includes Heat shock protein 70-Heat shock protein 90 organising protein (Hop). As opposed to directly inhibiting Hsp90 activity, targeting Hsp90 interaction with Hop has recently been suggested as an alternative method of Hsp90 inhibition that has not been explored in *P. falciparum*. The aim of this research project was to demonstrate *Pf*Hsp90 and *Pf*Hop robustly interact *in vitro* and to facilitate high-throughput screening of *Pf*Hsp90-*Pf*Hop inhibitors by developing and optimising a novel plate capture Hsp90-Hop interaction assay. To establish the assay, the respective domains of the proteins that mediate Hsp90-Hop interaction were used (Hsp90 C-terminal domain and Hop TPR2A domain). The human Hsp90 C-terminal domain and glutathione-S-transferase (GST) coding sequences were cloned into pET-28a(+) and murine and *P. falciparum* TPR2A sequences into pGEX-4T-1 plasmids to enable expression of histidine-tagged and GST fusion proteins, respectively, in *Escherichia coli*. The *P. falciparum* Hsp90 C-terminal domain sequence cloned into pET-28a(+) was supplied by GenScript. The constructs were transformed into T7 Express *lysY* competent *E. coli* cells and subsequent small-scale expression studies showed the recombinant proteins were expressed in a soluble form allowing for subsequent protein purification. Purification of the recombinant proteins was achieved using nickel-NTA and glutathione affinity chromatography for the His-tagged (Hsp90 C-terminal domains and GST) and GST fusion proteins (TPR2A domains), respectively. The purified proteins were used to establish and optimise mammalian and *P. falciparum* Hsp90-Hop interaction assays on nickel-coated plates by immobilising the His-tagged C-terminal domains on the plates and detecting the binding of the GST-TPR2A domains using a colorimetric GST enzyme assay. Z'-factor values above 0.5 were observed for both assays

indicating good separation between the protein interaction signals and negative control background signals, although relatively high background signals were observed for the mammalian interaction due to non-specific binding of murine TPR2A to the plate. Designed human and *P. falciparum* TPR peptides were observed to be effective inhibitors of the mammalian and *P. falciparum* interactions, demonstrating the assay's ability to respond to inhibitor compounds. Comparison of assay performance using GST assay kit reagents and lab-prepared reagents showed the assay was more efficient using lab-prepared reagents, however, lower GST signals were observed when comparing assay performance using a custom prepared Ni-NTA plate to a purchased Ni-NTA plate. The Hsp90-Hop interaction assays were also performed using an alternative assay format in which the GST-TPR2A fusion proteins were immobilised on glutathione-coated plates and binding of the His-tagged C-terminal domains detected with a nickel-horseradish peroxidase (HRP) conjugate and a colorimetric HRP substrate. The assay showed higher interaction signals for the *P. falciparum* proteins but comparatively low signals for the mammalian proteins. Z'-factor values for the assay were above 0.8 for both protein sets, suggesting this assay format is superior to the GST assay. However, further optimisation of this assay format is required. This study demonstrated direct binding of *Pf*Hsp90-*Pf*Hop *in vitro* and established a novel and robust *Pf*Hsp90-*Pf*Hop interaction assay format that can be used in future screening campaigns.

Table of Contents

Abstract i
Table of Contents iii
List of Figures vi
List of Tables viii
List of Abbreviations ix
Acknowledgements xiii

Chapter 1: Introduction 1
1.1 Protein-Protein Interactions 1
1.1.1 Types of PPIs 1
1.1.2 PPIs in Drug Discovery 2
1.2 PPI Assays 3
1.2.1 PPI Detection 3
1.2.1.1 *In vivo* detection methods 3
1.2.1.2 *In vitro* detection methods 5
1.2.2 PPIs and Drug Screening 7
1.3 Malaria 10
1.4 Chaperones as Drug Targets 14
1.4.1 Hsp90 15
1.4.2 Hop 19
1.5 Problem Statement 22
1.6 Aims and Objectives 23

Chapter 2: Methods and Materials 24
2.1 Molecular cloning 24
2.1.1 Primer Design 24
2.1.2 PCR Amplification 24
2.1.3 Agarose Gel Electrophoresis 25
2.1.4 PCR Product Purification 25
2.1.5 Vector Preparation 25
2.1.5.1 Transformation 25
2.1.5.2 Alkaline Lysis Miniprep 26
2.1.5.3 Restriction Digestion 26

2.1.5.4 Long Term Vector Storage 26
2.1.5.5 Vector Purification 27
2.1.6 Cloning 27
2.1.7 Cloning Verification 27
2.2 Protein Expression 28
2.2.1 Transformation of T7 Express *lysY* cells 28
2.2.2 Long Term Storage of Expression Constructs 28
2.2.3 Small-scale Protein Expression 28
2.2.4 SDS-PAGE Analysis 29
2.2.5 Large-scale Protein Expression 29
2.2.6 Protein Purification of His-tagged Proteins 30
2.2.7 Protein Concentration Determination 30
2.2.8 Desalting 31
2.2.9 Protein Concentration 31
2.2.10 Recharging the Ni-NTA Column 31
2.2.11 Preparation of Glutathione Agarose Column 32
2.2.12 Protein Purification of GST-tagged Proteins 32
2.2.13 Glutathione-Agarose Column Cleaning 32
2.3 C-domain – TPR2A Interaction Assays 33
2.3.1 Nickel plate GST Assay 33
2.3.2 Preparation of Ni-NTA plates 34
2.3.3 Glutathione plate HRP assay 34

Chapter 3: Cloning, Expression and Purification of pET-hCdom, pET-*Pf*Cdom, pET-GST, pGEX-mTPR2A and pGEX-*Pf*TPR2A 35
3.1 Introduction 35
3.2 Results 38
3.2.1 PCR amplification 38
3.2.2 Cloning 39
3.2.3 Small-scale expression analysis 42
3.2.4 Protein purification 46
3.2.5 Final protein work-up and storage 50
3.3 Discussion 51

Chapter 4: Establishment and Optimisation of the C-domain-TPR2A interaction assay 55

4.1 Introduction 55

4.2 Results 58

4.2.1 Initial GST assay 58

4.2.2 *P. falciparum* C-domain-TPR2A interaction assay 60

4.2.3 Mammalian C-domain-TPR2A interaction assay 66

4.2.4 Comparison of P. falciparum and mammalian C-domain-TPR2A interaction 71

4.2.5 Determining C-domain-TPR2A affinity 71

4.2.6 Comparing kit and lab-prepared GST assay components 72

4.2.7 C-domain-TPR2A inhibition 75

4.2.8 C-domain-TPR2A Glutathione plate assay 77

4.3 Discussion 80

Chapter 5: General Conclusions 84

References 87

Appendices 99

Appendix A: Designed Primers 99

Appendix B: Gene sequences amplified by PCR and cloned into pET-28a(+) and pGEX-4T-1 99

Appendix C: pET-28a(+) and pGEX-4T-1 plasmid maps 102

Appendix D: Summary of sequencing (performed by Inqaba Biotec™ South Africa 103

Appendix E: Bradford assay standard curve 105

List of Figures

Figure 1: Countries endemic for malaria in 2016 (WHO Malaria Report, 2016) 11
Figure 2: The lifecycle of malaria-causing *Plasmodium* (White, 2004) 12
Figure 3: Agarose gel of GST, hCdom, *Pf*Cdom, mTPR2A and *Pf*TPR2A PCR products 39
Figure 4: Agarose gel showing diagnostic restriction digests of pET-GST, pGEX-*Pf*TPR2A and pGEX-mTPR2A using BamHI and XhoI 40
Figure 5: Agarose gel showing PCR confirmation of hCdom cloned into pET-28a 41
Figure 6: Agarose gel showing restriction of pET-*Pf*Cdom using NheI and XhoI 41
Figure 7: SDS-PAGE analysis of hCdom small-scale expression samples 43
Figure 8: SDS-PAGE analysis of hGST small-scale expression samples 43
Figure 9: SDS-PAGE analysis of mTPR2A small-scale expression samples 44
Figure 10: SDS-PAGE analysis of *Pf*TPR2A small-scale expression samples 44
Figure 11: SDS-PAGE analysis of *Pf*Cdom small-scale expression samples 45
Figure 12: SDS-PAGE analysis of hCdom protein purification samples 46
Figure 13: SDS-PAGE analysis of *Pf*Cdom protein purification samples 47
Figure 14: SDS-PAGE analysis of mTPR2A protein purification samples 48
Figure 15: SDS-PAGE analysis of *Pf*TPR2A protein purification samples 48
Figure 16: SDS-PAGE analysis of uGST protein purification samples from *E. coli* transformed with pGEX-4T-1 49
Figure 17: SDS-PAGE analysis of hGST protein purification samples from *E. coli* transformed with pET-GST 50
Figure 18: Schematic diagram of the C-domain-TPR2A interaction GST assay 56
Figure 19: Schematic diagram of the GST positive and negative controls 57
Figure 20: His-tagged GST Ni-NTA binding capacity 58
Figure 21: Untagged GST Ni-NTA binding capacity 59
Figure 22: GST assay Z'-factor experiment 60
Figure 23: *Pf*C-domain-*Pf*TPR2A interaction GST assay at equimolar concentrations 61
Figure 24: Non-specific binding of *Pf*TPR2A at different concentrations 62
Figure 25: *Pf*C-domain-*Pf*TPR2A interaction GST assay at varying *Pf*TPR2A concentrations 63
Figure 26: *Pf*C-domain-*Pf*TPR2A interaction GST assay - control for *Pf*TPR2A background signal 64

Figure 27: *Pf*C-domain-*Pf*TPR2A interaction GST assay - control for *Pf*C-domain-uGST interaction 65
Figure 28: Mammalian C-domain-TPR2A interaction GST assay at equimolar concentrations 66
Figure 29: Non-specific binding of mTPR2A at different concentrations 67
Figure 30: Mammalian C-domain-TPR2A interaction GST assay at different mTPR2A concentrations 68
Figure 31: hC-domain-mTPR2A interaction GST assay - control for mTPR2A background signal 69
Figure 32: Mammalian C-domain-TPR2A interaction GST assay – control for hC-domain-uGST interaction 70
Figure 33: Comparison of the *P. falciparum* and mammalian C-domain-TPR2A interaction signals 71
Figure 34: hC-domain-*Pf*TPR2A and *Pf*C-domain-mTPR2A interaction 72
Figure 35: *P. falciparum* C-domain-TPR2A interaction GST assay using kit reagents and lab-prepared reagents 73
Figure 36: Mammalian C-domain-TPR2A interaction GST assay using kit reagents and lab-prepared reagents 73
Figure 37: Mammalian C-domain-TPR2A interaction GST assay in purchased and prepared Ni-NTA plates 74
Figure 38: Mammalian C-domain-TPR2A inhibition with hTPR peptide and *Pf*TPR peptide 75
Figure 39: *P. falciparum* C-domain-TPR2A inhibition with *Pf*TPR peptide and hTPR peptide 76
Figure 40: *P. falciparum* and mammalian C-domain-TPR2A interaction HRP assay 77
Figure 41: *P. falciparum* C-domain-TPR2A interaction HRP assay: Z'-factor experiment 78
Figure 42: Mammalian C-domain-TPR2A interaction HRP assay: Z'-factor experiment 79
Figure 43: pET-28a(+) plasmid map (obtained from Novagen) 102
Figure 44: pGEX-4T-1 plasmid map generated by SnapGene 102
Figure 45: Bradford assay standard curve 105

List of Tables

Table 1: Protein-protein interactions for which small molecule inhibitors have been discovered by fluorescence polarization, FRET and ELISA-based screening methods (adapted from Heeres and Hergentother, 2011) 10

Table 2: Hsp90 client proteins and their role in tumorigenesis (adapted from Sidera and Patsavoudi, 2014) 16

Table 3: Concentration of the purified proteins determined using a Bradford assay 51

Table 4: Z'-factor values at various time points of the GST assay 60

Table 5: Z'-factor values at various time points of the *P. falciparum* C-domain-TPR2A interaction GST assay 64

Table 6: Z'-factor values at various time points of the *P. falciparum* C-domain-TPR2A and C-domain-uGST interaction GST assay 65

Table 7: Z'-factor values at various time points of the mammalian C-domain-TPR2A interaction GST assay 69

Table 8: Z'-factor values at various time points of the mammalian C-domain-TPR2A and C-domain-uGST interaction GST assay 70

Table 9: Percentage inhibition of the mammalian and *P. falciparum* C-domain-TPR2A interaction by *Pf*TPR and hTPR peptides 76

Table 10: Z'-factor values at various time points of the *P. falciparum* C-domain-TPR2A interaction HRP assay 78

Table 11: Z'-factor values at various time points of the mammalian C-domain-TPR2A interaction HRP assay 79

Table 12: Primers used for PCR amplification 99

List of Abbreviations

$(His)_6$	Polyhistidine tag
µl	Microliters
µm	Micrometre
µM	Micromolar
17-AAG	17-allyamino-17-demethoxygeldanamycin
ACT	Artemisinin-based combination therapy
ADP	Adenosine diphosphate
AGE	Agarose gel electrophoresis
Alpha	Amplified luminescent proximity homogenous assay
Antp	Cell-penetrating peptide
Arg (R)	Arginine
ARMD	Accelerated resistance to multiple drugs
Asn	Asparagine
AT	Adenine thymine
ATP	Adenosine triphosphate
bp	Base pairs
BRET	Bioluminescence resonance energy transfer
BSA	Bovine serum albumin
CBP	Calmodulin-binding peptide
CCR5	C-C chemokine receptor type 5
Cdc37	Cell division cycle 37
CDNB	2,4-Dinitrochlorobenzene
CFP	Cyan fluorescent protein
crt	Chloroquine resistance transporter
DHFR	Dihydrofolate reductase
DHPS	Dihydropteroate synthase
DMSO	Dimethyl sulfoxide
DNA	Deoxyribonucleic acid
DPBS	Dulbecco's phosphate-buffered saline
E.coli	*Escherichia coli*

EDTA	Ethylenediaminetetraacetic acid
ELISA	Enzyme-linked immunosorbent assay
FDA	Food and drug administration
FRET	Fluorescence resonance energy transfer
GA	Geldanamycin
GC	Guanine cytosine
GFP	Green fluorescent protein
Glu	Glutamic acid
Gly	Glycine
Grp94	Endoplasmic reticulum heat shock protein 90 kilodaltons
GST	Glutathione S-transferase
GTE	Glucose-Tris-EDTA
hC-domain (hCdom)	Human Hsp90 C-domain
HCl	Hydrogen chloride
hGST	His-tagged GST
HIV	Human immunodeficiency virus
Hop	Heat shock protein 70-Heat shock protein 90 organising protein
HPPK	Hydroxymethylpterin pyrophosphokinase
HRP	Horse radish peroxidase
Hsp	Heat shock protein
Hsp110	Heat shock protein 110 kilodaltons
Hsp40	Heat shock protein 40 kilodaltons
Hsp70	Heat shock protein 70 kilodaltons
Hsp90	Heat shock protein 90 kilodaltons
hTPR	Human tetratricopeptide repeat
HTS	High-throughput screening
IgG	Immunoglobulin G
Ile	Isoleucine
IMAC	Immobilised metal-affinity chromatography
IPTG	Isopropyl β-D-1- thiogalactopyranoside
kDa	Kilodaltons
lacI	Lac repressor

LB	Luria-Bertani
Lys (K)	Lysine
M	Molar
mg/ml	Milligrams per millilitre
ml	Millilitres
mM	Millimolar
MS	Mass spectrometry
mTPR2A	Murine Hop TPR2A domain
Ni^{2+}	Nickel
nm	Nanometre
NTA	Nitriloacetic acid
OD_{600}	Absorbance at 600 nm
P. falciparum (*Pf*)	*Plasmodium falciparum*
PBS	Phosphate-buffered saline
PCA	Protein fragment complementation assay
PCR	Polymerase chain reaction
pET-GST	pET-28a(+) containing GST gene
pET-hCdom	pET-28a(+) containing hC-domain gene
pET-*Pf*Cdom	pET-28a(+) containing *Plasmodium falciparum* C-domain gene
*Pf*C-domain (*Pf*Cdom)	*Plasmodium falciparum* Hsp90 C-domain
*Pf*Hop	*Plasmodium falciparum* Hsp70-Hsp90 organising protein
*Pf*Hsp90	*Plasmodium falciparum* heat shock protein 90 kilodatons
*Pf*TPR	*Plasmodium falciparum* tetratricopeptide repeat
*Pf*TPR2A	*Plasmodium falciparum* Hop TPR2A domain
pGEX-mTPR2A	pGEX-4T-1 containing murine TPR2A gene
pGEX-*Pf*TPR2A	pGEX-4T-1 containing *Plasmodium falciparum* TPR2A gene
PMSF	Phenylmethylsulfonylfluoride
PPI	Protein-protein interactions
SDS	Sodium dodecyl sulfate
SDS-PAGE	Sodium dodecyl sulfate - polyacrylamide gel electrophoresis
Ser	Serine
sHsp	Small heat shock protein

T. evansi	*Trypanasoma evansi*
TAP	Tandem affinity protein
TBE	Tris-Borate-EDTA
TBS	Tris-buffered saline
TE	Tris-EDTA
TEMED	N,N,N',N'-Tetramethyl-ethylenediamine
TEV	Tobacco etch virus
TNF	Tumour necrosis factor
TPR	Tetratricopeptide repeat
uGST	GST from pGEX-4T-1
V	Volts
v/v	Volume per volume
w/v	Weight per volume
WHO	World health organisation
X	Times
xg	Times gravity
Y2H	Yeast two-hybrid
YFP	Yellow fluorescent protein

Acknowledgements

I would like to thank my supervisor Professor Heinrich Hoppe for his patience, advice and support throughout this project. I am extremely grateful for the guidance you have provided over the last two years. I would also like to thank my parents, Gregory and Jacinta and my brother Lloyd for their unwavering encouragement and faith in me.

Thank you to the members of Lab 302 for all the help and motivation particularly Dumisani Mnkandhla for teaching me protein expression and purification. Leigh-anne Derry, you are the T75 flask to my HeLa cells, the APS to my TEMED, the snap to my pea, the Cyan to my Venus, the fluorescence to my spectrophotometer and the person who just speaks too much during movies and 'my 600 lb life'.

To my dearest friend Farrah Khan, I would like to take this moment to thank you for your friendship, and to say that you are better than anything and everything that life has to offer. Better than everything on the planet, everything in the solar system, everything that exists – past, present and future, in all discovered and undiscovered dimensions. You are truly the red blood cell to my *Plasmodium falciparum*.

My sincere gratitude goes out to Glynis Oree, Shantal Maharaj and Sarah Kituyi for all the lunches and their friendship and support over the years. I would also like to thank Helpmekkar-Studiefonds for their financial support.

This work was funded by a Deutsche Forschungsgemeinschaft (DFG) German-African co-operation in Infectiology grant: "Molecular Interactions of *Pf*Hop as a target for anti-malarial drug development". Additional support was provided by a Medical Research Council SA University Flagship Project award: "Integration of bioassay capacity, target identification and multidisciplinary research for the discovery of drug lead compounds (CCBR-RU)".

Chapter 1

Introduction

1.1 Protein-Protein Interactions

Most of the functions mediated by proteins in cells occur as a result of interactions between proteins (Szilagyi and Zhang, 2014). Intentional and specific physical contact between individual proteins by molecular docking is known as protein-protein interaction (De Las Rivas and Fontanillo, 2010). Protein-protein interactions (PPIs) play a key role in fundamental biological processes in cells (Peng *et al.*, 2016). They often have a structural function, e.g. the formation of cytoskeletal structures through protein oligomerization into filaments or tubules, cell-cell or cell-matrix adhesion and tethering proteins that stabilise organelles (Phizicky and Fields, 1995). Relatively stable PPIs are used to form large, functional protein complexes, for example ribosome large and small subunits are composed of 49 and 33 proteins respectively, and nuclear pores that mediate protein entry into the nucleus consist of complexes of up to 30 different nucleoporins (Fox, 2010). Metabolic enzymes are often multimeric (e.g. pyruvate dehydrogenase consists of up to 60 protein subunits) and their substrate specificity, kinetic properties and activity can be modulated by interacting proteins (Phizicky and Fields, 1995). Protein trafficking relies on numerous temporary PPIs during vesicle formation, migration and fusion, while transient PPIs that activate or deactivate interaction partners through conformational changes are particularly prevalent in signal transduction pathways (Calakos *et al.*, 1994; Vidal, 2002). PPIs can be classified based on their interaction surface, their stability or their lifetime (Rao *et al.*, 2014).

1.1.1 Types of PPIs

Based on protein interaction surfaces, PPIs can be homo-oligomeric or hetero-oligomeric (Rao *et al.*, 2014). If PPIs occur between identical polypeptide chains, homo-oligomeric complexes are formed whereas PPIs between non-identical chains forms hetero-oligomeric complexes (Keskin *et al.*, 2016). Homo-oligomeric complexes provide a good scaffold for stable macromolecules as they are symmetric and tend to be permanent and optimized (Jones and Thornton, 1996; Ozbabacan *et al.*, 2011). Hetero-oligomeric complexes can vary in stability and may be permanent or temporary, depending on external factors (Jones and Thornton, 1996; Ozbabacan *et al.*, 2011). Based on stability, PPIs can be obligate or non-obligate (Rao *et al.*, 2014). Obligate PPIs occur when the proteins involved are unstable on their own whereas the

protein involved in non-obligate interactions are stable independently (Ozbabacan *et al.*, 2011). Based on interaction lifetime, PPIs can be permanent or transient (Peng *et al.*, 2016). Permanent PPIs are typically very stable and irreversible, usually resulting in the formation of a stable complex (Ozbabacan *et al.*, 2011; Peng *et al.*, 2016). Transient interactions occur under certain biological conditions and associate and dissociate temporarily (Peng *et al.*, 2016). Most non-obligate PPIs are transient while obligate PPIs are usually permanent (Ozbabacan *et al.*, 2011).

1.1.2 PPIs in Drug Discovery

Existing pharmaceutical drugs typically act by inhibiting (or occasionally stimulating) enzyme activity or signalling receptor-ligand interactions (Makley and Gestwicki, 2012). Enzymes and receptors contain substrate/co-factor/ligand binding pockets that can be occupied or allosterically altered by drug-like molecules (i.e. compounds that adhere to Lipinsky's rule of five) (Yin and Hamilton, 2005). However, despite increased investment and improvements in drug discovery methodologies, there has been an alarming decrease in new drug chemical entities entering the marketplace (Vasaikar *et al.*, 2016). This has led some analysts to conclude that alterative drug target types need to be explored more vigorously (Vasaikar *et al.*, 2016). Cellular processes involved in disease-related pathways are often regulated by transient PPIs, thus understanding these interactions allows for potential discovery and development of inhibitors that can serve as therapeutics (Ozbabacan *et al.*, 2011). There are an estimated 130,000-1 million human PPIs and thus a large source of novel drug targets are potentially available (Keskin *et al.*, 2016; Sheng *et al.*, 2015). Recently there has been great interest in targeting the interfaces between interacting proteins, however the characteristics of these interfaces makes it challenging (Wells and McClendon, 2007). PPI contact surfaces are typically large and generally flat therefore they lack the significant grooves and pockets which would allow for binding of small molecules (Fry, 2015; Wells and McClendon, 2007). Contact surfaces are often hydrophobic thus any potential effective PPI inhibitors must cover a large surface and have the capacity for hydrophobic interactions (Sheng *et al.*, 2015). Such an inhibitor would face pharmacokinetic issues due to its size and poor solubility (Sheng *et al.*, 2015). Recent studies have shown a limited number of amino acids at the contact surface mediate most of the key interactions between proteins and contribute most of the free energy of binding (Fry, 2015; Sheng *et al.*, 2015). These areas are known as 'hot-spots' and are usually found at the centre of the contact surface (Wells and McClendon, 2007). Proteins involved in PPIs often bind to several other protein targets using the same hot-spot region, thus the design

and development of PPI inhibitors that are small 'drug-like' molecules has made considerable progress by targeting the hot-spots (Sheng *et al.*, 2015).

1.2 PPI Assays

1.2.1 PPI Detection

1.2.1.1 *In vivo* detection methods

Protein interactions can be detected and analysed by *in vivo*, *in silico* and *in vitro* methods (Rao *et al.*, 2014). Studying protein interactions *in vivo* allows for understanding of the cellular environment in which the protein interactions take place, which can be used to re-create the protein-protein interactions in a controlled environment *in vitro* (Piehler, 2005). The most commonly used *in vivo* PPI detection methods are yeast two-hybrid (Y2H) techniques, protein fragment complementation and resonance energy transfer (Rao *et al.*, 2014). The Y2H method is widely used for the detection and screening of PPIs (Berggård *et al.*, 2007). In the Y2H assay, two expression plasmids are constructed, one with the coding sequence of a transcription factor DNA binding domain fused to one interacting protein partner, another with a transcription factor activation domain fused to the second interaction protein partner (Phizicky and Fields, 1995). The two hybrid constructs are co-expressed in the same cell containing a reporter gene regulated by a promoter which is recognised by the transcription factor DNA binding domain (Phizicky and Fields, 1995). If the proteins interact, they form a functional transcriptional activator (as a result of the close proximity between the DNA binding domain and the activation domain) which is detected by the expression of the reporter gene (Berggård *et al.*, 2007). The Y2H method has several advantages: it is relatively inexpensive, simple to set up and requires little optimization (Berggård *et al.*, 2007). However, the method works best with proteins localized to the nucleus as extranuclear proteins are unable to activate reporter genes (Rao *et al.*, 2014). The biggest disadvantage of the method is the large number of false positives it generates - estimated to be as high as 50% of identified interactions - therefore any interacting partners identified by Y2H must be verified by other methods (Berggård *et al.*, 2007).

To study extranuclear protein interactions, protein fragment complementation assays (PCAs) were developed (Piehler, 2005). The principle of PCAs is based on splitting a reporter protein into two fragments, genetically fusing these to the two potentially interacting proteins respectively and expressing the two fusion constructs in cells (Morell *et al.*, 2009). Should the proteins interact, the two halves of the reporter protein are re-joined and its function is restored

(Piehler, 2005). The reporter proteins used are typically enzymes which have chromogenic or fluorogenic substrates such as dihydrofolate reductase (DHFR), galactosidase or lactamase, or *Renilla* luciferase which metabolizes coelenterazine to produce luminescence (Morell *et al.*, 2009). An additional useful reporter is the green fluorescent protein (GFP) (Cabantous *et al.*, 2013). The N- and C-terminal domains of GFP are fused to the two respective interaction protein partners and GFP fluorescence is restored when the two proteins bind to each other (also known as the 'split-GFP assay') (Cabantous *et al.*, 2013). Although PCAs are widely used and have high specificity, the method often requires a lot of optimization and high background signals are a commonly reported issue (Piehler, 2005).

For resonance energy transfer experiments, two formats are employed: fluorescence resonance energy transfer (FRET) or bioluminescence resonance energy transfer (BRET) (Couturier and Deprez, 2012). For FRET assays, the two protein interaction partners are fused to two different fluorescent proteins that have overlapping emission and excitation spectra (donor and acceptor fluorophores) and co-expressed in cells (Degorce *et al.*, 2009). Commonly used donor/acceptor fluorophore pairs are variants of cyan fluorescent protein (CFP) and yellow fluorescent protein (YFP) (Broussard *et al.*, 2013). If the two proteins under investigation interact, the CFP and YFP fusion partners are brought into close proximity (Couturier and Deprez, 2012). Excitation of CFP at 430 nm produces fluorescence emission at 470 nm, which in turn excites YFP to emit fluorescence at 535 nm (Hou *et al.*, 2011). Interaction of the proteins can thus be measured as an increase in YFP fluorescence emission (or decrease in CFP emission, due to its absorption by YFP) (Couturier and Deprez, 2012). An additional advantage of FRET is that the interaction can be detected using confocal microscopy, allowing the sub-cellular location of the interaction to be studied (Sekar and Periasamy, 2003). BRET operates on the same principle as FRET, except that the CFP donor fluorophore is replaced with *Renilla* luciferase (Couturier and Deprez, 2012). Addition of a coelenterazine substrate causes the luciferase to produce bioluminescence which excites YFP and results in fluorescence emission at 535 nm (Dacres *et al.*, 2012).

1.2.1.2 *In vitro* detection methods

Due to the high number of false positive results generated by *in vivo* PPI assays, validation of these interactions is required *in vitro* (Piehler, 2005). A number of *in vitro* techniques can be used to detect PPIs such as: Tandem Affinity Purification-Mass Spectrometry (TAP-MS), co-immunoprecipitation and protein microarrays (Rao *et al.*, 2014) (note that the discussion below is not exhaustive and does not include, for example, electrophoresis gel shift or chromatography co-elution assays). Co-immunoprecipitation is perhaps the most commonly used method for PPI verification (Gurung *et al.*, 2017). In a typical co-immunoprecipitation experiment, a bait protein is captured from a whole cell extract using an antibody which is immobilised on sepharose beads (Markham *et al.*, 2007). After washing the beads to remove unbound cell lysate proteins, the antibody, bait protein and any proteins bound to the bait protein are eluted (Gurung *et al.*, 2017). The immunoprecipitated proteins and their interaction partners can be identified by mass spectrometry or, more commonly, western blotting (Free *et al.*, 2009). This method allows for the study of native endogenous proteins, thus avoiding any artefactual effects due to affinity tags or overexpression which is inherent in the *in vivo* techniques described above (Berggård *et al.*, 2007). Alternatively, co-immunoprecipitation experiments can be conducted using an epitope-tagged bait protein for which commercially available antibodies immobilised on beads are used (Phizicky and Fields, 1995). Bait proteins may also be fused to a protein tag such as Glutathione S-Transferase (GST) for which glutathione beads are commercially available for rapid purification of the GST-tagged protein and any interaction partners which eliminates the need for highly specific antibodies (Phizicky and Fields, 1995).

Techniques such as co-immunoprecipitation were refined for protein study by TAP (Piehler, 2005). The principle of TAP is based on the use of a TAP tag fused to the bait protein of interest (Berggård *et al.*, 2007). TAP tag consists of two IgG-binding units of protein A of *Staphylococcus aureus* and a calmodulin-binding peptide (CBP) domain separated by a tobacco etch virus (TEV) protease cleavage site (Xu *et al.*, 2010). There are two forms of the TAP tag- a C-terminal TAP tag and an N- terminal TAP tag- determined by which terminus the protein A domain is located (Puig *et al.*, 2001). The tagged protein is expressed in a target cell and the bait protein as well as any interaction partners are subsequently purified (Berggård *et al.*, 2007). During purification, the TAP-tagged bait protein binds tightly to an IgG matrix (via the protein A domain) after which TEV-proteinase is added and the TAP tag is cleaved, leaving the CBP-tagged bait protein unbound (Xu *et al.*, 2010). The CBP-tagged bait protein is then mixed with

calmodulin-coated beads in the presence of calcium and the bait protein complex is obtained by elution using buffer containing egtazic acid (Puig *et* al., 2001). The protein complex is subsequently analysed by SDS-PAGE and mass spectrometry (Rao *et al.*, 2014). The TAP method is highly selective and sensitive and has resulted in the identification of numerous protein complexes in yeast, however transient interactions are often not detected (Xu *et al.*, 2010). TAP has limited success in mammalian cells thus an alternative TAP tag (GS-TAP) was developed for the study of protein complexes in mammalian cells (Berggård *et al.*, 2007). The GS-TAP tag is based on protein G and the streptavidin-binding peptide (Xu *et al.*, 2010). Protein complex purification using the GS-TAP tag is 10 times more efficient than other TAP tags (Berggård *et al.*, 2007).

Protein microarrays are quickly becoming a powerful way to detect proteins and determine protein interactions as well as protein functions (Rao *et al.*, 2014). A protein microarray is a solid support (typically glass) on which different proteins are immobilised at different locations in an organised manner (Piehler, 2005). Metal chelators or affinity capture by streptavidin, glutathione or Ni^{2+}-NTA is often used for direct protein immobilisation although capture antibodies, adsorption onto a nitrocellulose membrane and covalent immobilization can also be used to capture proteins (Sutandy *et al.*, 2013). Protein microarrays require a probe protein which is typically labelled with a fluorophore (Zhu and Snyder, 2003). Any interaction between the probe protein and the immobilised protein results in fluorescence which can be detected by a laser scanner-based system (Zhu and Snyder, 2003). Fluorescence observed at a particular location on the protein micro array indicates protein-protein interaction thus the probe protein interaction partners can be determined (Piehler, 2005). Fluorescent dyes such as Cy3 and Cy5 are commonly used as they have a wide linear detection range compared to other labelling systems (Sutandy *et al.*, 2013). Chemiluminescent probes such as horseradish peroxidase are also popular detection methods (Sutandy *et al.*, 2013). Protein microarrays aim for efficient, high-throughput, sensitive protein analysis with great progress, however protein microarrays require large amounts of highly purified proteins, expensive equipment for sample handling and detection which limits its use in protein studies (Piehler, 2005; Rao *et al.*, 2014).

In vivo and *in vitro* methods have results in the advancement of PPI detection methods, however experimental methods have limitations (Rao *et al.*, 2014). Not all PPIs can be detected using existing experimental methods thus various computational approaches have been developed to support PPIs detected by experimental methods as well as to predict PPIs (Shen *et al.*, 2007). Most of the computational methods can be grouped into simulation based and

statistical/machine-learning based approaches (Keskin *et al.*, 2016). Simulation based methods are often used to determine the strength of PPIs or the dynamics of interactions as they model the forces involved in protein interaction but due to high computational cost, they are mostly used to model existing (known) interactions and rarely used to predict which proteins interact (Keskin *et al.*, 2016). Statistical/ machine-learning based methods use information known from interacting proteins to predict other possible protein-protein interactions (Zahiri *et al.*, 2013). Features representing PPIs and using an appropriate learning algorithm results in a reliable PPI prediction method (Rao *et al.*, 2014).

1.2.2 PPIs and Drug Screening

As previously stated, PPIs are involved in a range of disease processes and thus are the focus of many drug discovery programs (Arkin *et al.*, 2012). It has been difficult to find peptide or small molecule inhibitors of PPIs for 3 reasons:

i. PPI interfaces are flat and often lack grooves or pockets in which small molecules can bind;
ii. PPI interfaces often have large contact areas which generally exceeds the surface area of a potential drug molecule;
iii. Screening libraries often follow the 'Rule of 5' which might not suit PPI inhibitors

Lipinski's 'Rule of 5' states that orally active drugs must have a molecular weight less than 500, 5 or less hydrogen bond donors, no more than 10 hydrogen bond acceptors and a lipophilicity of 5 or less (Lipinski, 2004). Despite the lack of drug-like characteristics exhibited by PPI inhibitors, a number of PPI modulators have proceeded to clinical trials, indicating PPIs can be inhibited by small molecules (Gul and Hadian, 2014). To screen for PPI inhibitors methods similar to those used to detect protein-protein interactions described in the previous sections can also be used, but there are limitations (Couturier and Deprez, 2012). Identifying PPI inhibitors in screening projects may involve interrogating thousands (or more) compounds in compound libraries (Janzen, 2014). To enable the simultaneous testing of multiple compounds, this necessitates an assay format that can be performed in multi-well plates and produces robust read-outs that can be detected in a plate reader (Hughes *et al.*, 2011). As a result, co-precipitation assays (for example) are not amenable to screening campaigns (Janzen, 2014). The *in vivo* cell-based assays described above may in principle be used but also have logistical and experimental limitations, for example the continuous maintenance of transgenic cell lines, inter-experimental variation due to the use of live cells and often relatively low

signal/background ratios (Moore and Rees, 2001). Consequently, biochemical assays involving purified recombinant proteins heterologously expressed in *E. coli* (or other convenient expression hosts) are more practical (Moore and Rees, 2001).

There are 4 types of biochemical assay formats that are generally used for screening: Fluorescence Resonance Energy Transfer (FRET)/Bioluminescence Resonance Energy Transfer (BRET), fluorescence polarization, Enzyme Linked Immunosorbent Assay (ELISA)-like assays and bead based assays such as AlphaScreen (PerkinElmer) (Arkin *et al.*, 2012). As described above, FRET/BRET assays involve the use of compatible energy donor and acceptor couples each linked to one of the interacting proteins (Couturier and Deprez, 2012). For resonance energy transfer to occur, the energy donor emission wavelength must overlap the excitation wavelength of the energy acceptor (Degorce *et al.*, 2009). Resonance energy transfer can only occur if the two partners interact, bringing the energy donor and energy acceptor together by a distance of 10 nm or less (Couturier and Deprez, 2012). In FRET, the donor and acceptor are both fluorophores whereas in BRET the donor is a bioluminescent enzyme that converts its substrate into light that is compatible with a fluorescent acceptor (Dacres *et al.*, 2012).

Fluorescence polarization is an in-solution type assay that requires a fluorescently labelled probe and linearly polarized light (Gul and Hadian, 2014). Binding of the small fluorescently labelled probe (a PPI interaction partner 1500 Da to 5000 Da in size) to its protein partner is monitored by change in light polarization (Arkin *et al.*, 2012). The degree of polarization is inversely proportional to the molecular rotation (Lea and Simeonov, 2012). When the molecule is free in solution, it has fast molecular rotation and will emit depolarized light (Heeres and Hergenrother, 2011). On the other hand, when the fluorescent molecule is bound to a larger molecule e.g. a protein interaction partner, it forms a larger, more ridged complex with a slower molecular rotation thus the light emitted remains polarized (Gul and Hadian, 2014). In the assay, the fluorescently labelled molecule is excited by polarized light and emits polarized light when bound to its protein partner (Lea and Simeonov, 2012). In the presence of an inhibitor, the PPI complex dissociates leaving the fluorescently labelled probe free in solution thus when excited by polarised light, depolarised light is emitted i.e. no change in light polarization indicates no PPI inhibition (Lea and Simeonov, 2012).

Enzyme-linked immunosorbent assay (ELISA)-like assays use the traditional method of binding one of the protein partners to a microtitre plate (Arkin *et al.*, 2012). The protein is

attached to the plate surface - either by affinity recognition or non-specific adhesion – and the second protein then binds to its protein partner (Arkin *et al.*, 2012). Detection of the second protein can occur by binding of an enzyme-labelled antibody, direct labelling of the protein with a signal generating enzyme or by binding of an unlabelled primary antibody followed by addition of a labelled secondary antibody (Arkin *et al.*, 2012). Detection methods can be colorimetric, luminescent or fluorometric (Arkin *et al.*, 2012). ELISAs are very flexible, typically inexpensive and sensitive (Arkin *et al.*, 2012).

The AlphaScreen (Amplified Luminescent Proximity Homogenous Assay) method is a bead-based assay developed by PerkinElmer that uses donor and acceptor beads to detect binding partners (Janzen, 2014). AlphaScreen donor beads contain a phthalocyanine photosensitizer that excites oxygen to a singlet state while AlphaScreen acceptor beads contain thioxene, anthracene and rubrene (chemical dyes) (Yasgar *et al.*, 2017). The binding partners are captured on donor and acceptor beads respectively and, upon their interaction, the resulting energy transfer leads to the emission of a fluorescent signal (Gul and Hadian, 2014). Excitation of the donor beads by high energy irradiation at 680 nm excites ambient oxygen to a singlet oxygen state which diffuses to the acceptor beads (if they are within 200 nm), resulting in emission of light in the 520- 620 nm range due to a chemical reaction cascade that occurs inside the acceptor beads – thioxene reacts with the singlet oxygen and generates light that is transferred to anthracene and subsequently to rubrene (Janzen, 2014; Yasgar *et al.*, 2017). This technique is highly sensitive as singlet oxygen has a relatively short lifetime in aqueous solution, background signals are low and the beads are usually added at low concentrations thus non-specific interactions are rare (Yasgar *et al.*, 2017). However, the complex chemistry involved in producing the signal often gives false positives in small molecule screening (Gul and Hadian, 2014).

The above-mentioned assay formats are often used for primary high-throughput screening (HTS) to select for compounds that are active against the PPIs as well as for dose-response assays (Arkin *et al.*, 2012). Table 1 shows the small molecule inhibitors of protein-protein interactions discovered through fluorescence polarization, FRET-based HTS and ELISA-based HTS (Heeres and Hergenrother, 2011).

Table 1: Protein-protein interactions for which small molecule inhibitors have been discovered by fluorescence polarization, FRET and ELISA-based screening methods (adapted from Heeres and Hergentother, 2011).

Method	Protein-Protein Interaction*	Biological function
Fluorescence polarization	Bcl-XL-Bak	Cell death induction
	ZipA-FtsZ	Bacterial cell division
	JNK-JIP	Signal transduction in cancer cells
FRET	Myc-Max	Cancer cell proliferation and apoptosis
	PKCi-Par6	Growth of cancer cells
	LRH-1-TIF2	Regulates gene expression for steroid synthesis and cell cycle progression
ELISA-based assays	TCF_4-β-catenin	Control of c-Myc expression in colorectal cancer
	RNAP-σ	Bacterial RNA polymerase assembly
	LFA-1-ICAM-1	Leukocyte cell adhesion

*Bcl-XL: B-cell lymphoma-extra large; Bak: Bcl-2 antagonist killer; JNK: c-Jun N-terminal Kinase; JIP: JNK Interacting Protein; Max: myc-associated factor X; PKCi: Protein Kinase C iota; Par6: Partitioning defective 6; LRH-1: Liver Receptor Homolog-1; TIF2: Transcriptional Intermediary Factor 2; TCF4: T-cell Factor 4; RNAP: RNA Polymerase; σ: sigma factor; LFA-1: Lymphocyte Function Associated Antigen-1; ICAM-1: Intercellular adhesion molecule 1.

The table above shows numerous PPIs have already been subjected to screening and yielded promising compounds - An oral alternate of the Bcl-XL-Bak inhibitor (ABT-737) is currently in clinical trials (Harazono *et* al., 2014; Ianov *et al.*, 2013). The availability of Maraviroc (a CCR5/gp120 interaction inhibitor) and Titrobifan (a glycoprotein IIb/IIa interaction inhibitor) on the market as anti-HIV and cardiovascular drugs respectively as well as the clinical trial success of several anti-cancer compounds has highlighted the potential of targeting PPIs in disease treatment (Ianov *et al.*, 2013).

1.3 Malaria

Malaria is one of the most prevalent parasitic diseases found in Africa, the Americas and Asia (Biamonte *et al.*, 2013). According to the World Health Organisation Malaria Report, there was an estimated 212 million cases of malaria in 2015 and 429,000 deaths worldwide (WHO, 2016). Of the estimated deaths, 92 % occurred in the African region, with children under five years most affected (WHO, 2015).

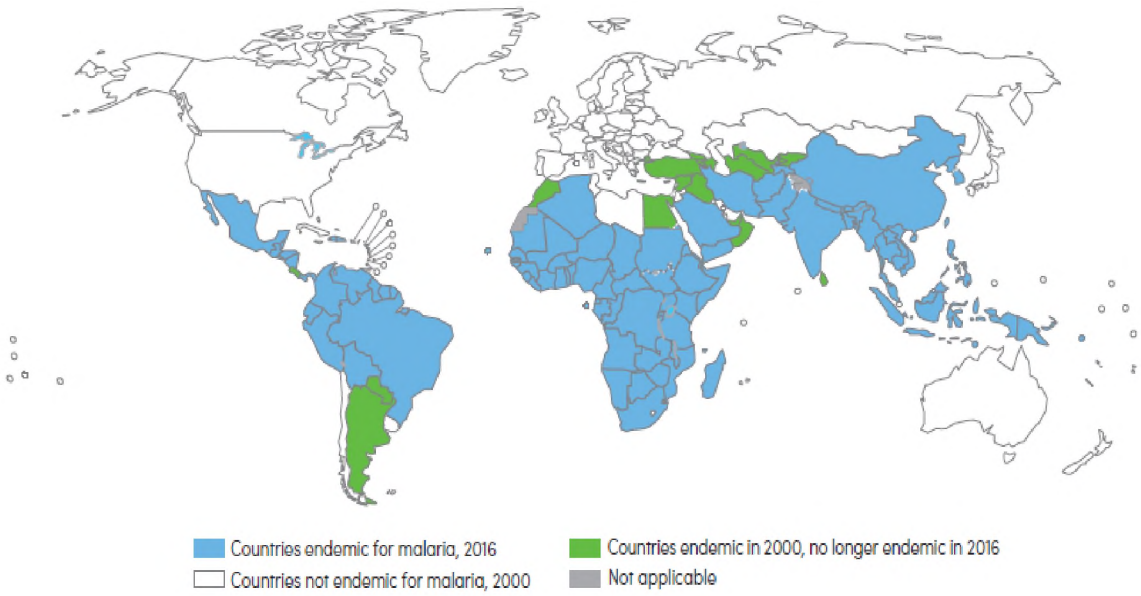

Figure 1: Countries endemic for malaria in 2016 (WHO Malaria Report, 2016).

In regions where malaria is endemic (shown in Figure 1), delayed economic development has been observed (Flannery *et al*., 2013). The economic burden in Africa is estimated at $12 billion per year (Biamonte *et al*., 2013). Malaria is caused by protozoan parasites of the genus *Plasmodium* (Flannery *et al*., 2013). There are five *Plasmodium* species that cause malaria in humans: *Plasmodium ovale*, *Plasmodium falciparum*, *Plasmodium vivax*, *Plasmodium malariae* and *Plasmodium knowlesi* (Tangpukdee *et al*., 2009).

Plasmodium falciparum (*P. falciparum*) is the most lethal of the five species and is predominantly found in Africa (Biamonte *et al*., 2013). There are four stages in the parasite lifecycle: liver stage, erythrocyte stage, transmission stage and mosquito stage (Biamonte *et al*., 2013). The parasite lifecycle is shown in Figure 2. Human infection begins once an infected *Anopheles* mosquito bites and inoculates parasites (sporozoites) into the blood stream (Biamonte *et al*., 2013). The parasites migrate to the liver and invade liver cells where replication occurs, producing schizonts - known as the liver stage (Flannery *et al*., 2013). The parasite enters the erythrocyte stage after approximately two weeks (Flannery *et al*., 2013). In the erythrocyte stage, the liver cells burst releasing merozoites which invade red blood cells and proliferate asexually by schizogony (Aguiar *et al*., 2012). The red blood cells burst and release more merozoites which invade new red blood cells, thus re-initiating the erythrocyte stage cycle (Aguiar *et al*., 2012).

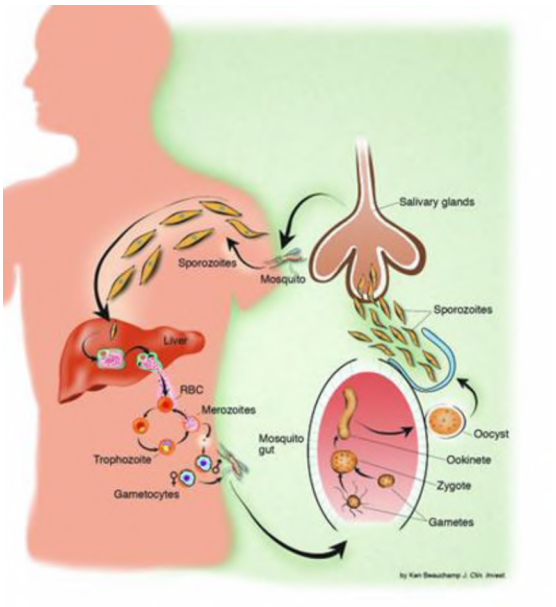

Figure 2: The lifecycle of malaria-causing *Plasmodium* (White, 2004).

Infected red blood cells are responsible for the clinical manifestations of malaria such as headaches, chills, fever, anaemia and prostration (Kalra *et al*., 2006). In severe cases, delirium, multi-organ system failure, cerebral malaria, coma and death can occur (Kalra *et al*., 2006). In the transmission stage, gametocyte generation occurs – some parasites undergo sexual differentiation, developing into male and female gametocytes (Biamonte *et al*., 2013). Parasites enter the mosquito stage when the gametocytes are ingested by mosquitos, where they fuse in the midgut and form a zygote, which further develops into new sporozoites that invade the salivary glands (Kalra *et al*., 2006). There is no clinically approved malaria vaccine and treatment relies heavily on the use of a few anti-malarial drugs as a result of increasing drug resistance (Wagner *et al*., 2013). Transmission control by insecticide sprays and use of insecticide-treated nets is also hampered by increased mosquito resistance to insecticides thus malaria control is becoming increasingly dependent on pharmacological methods (Santos and Torres, 2013).

Currently there are three types of drugs used to treat malaria – quinolines, artemisins and antifolates (Santos and Torres, 2013). These drugs vary in mechanism, but all seem to target the erythrocyte stage of the parasite lifecycle (Santos and Torres, 2013). Quinolines interfere with the detoxification of haem produced by haemoglobin digestion in the parasite digestive vacuole, resulting in cell death, while antifolates inhibit the synthesis of tetrahydrofolate, an essential cofactor in amino acid and nucleic acid metabolism, by inhibiting two key enzymes in the pathway: dihydrofolate reductase (DHFR) and dihydropteroate synthase (DHPS) (Kar

and Kar, 2010; Santos and Torres, 2013). The mechanism of action of artemisinin is yet to be established although it is thought that heme and free intracellular iron molecules lead to the bioactivation of artemisinin which then leads to the drug binding to macromolecules throughout the parasite (Muller and Hyde, 2010). The targeted macromolecules are still under debate - artemisinin has been shown to interact with heme, parasite proteins and parasite membranes - and a single molecular target which plays a direct role in cell death is yet to be identified (O'Neill *et al.*, 2010). Resistance has emerged to all existing drugs (Shahinas *et al.*, 2013). Development of resistance in *Plasmodium* depends on multiple factors: the mutation rate of the parasite, the fitness costs associated with resistance mutations, the overall parasite load, the strength of drug selection and treatment compliance (Petersen, Eastman and Lanzer, 2011). Drug resistant *P. falciparum* strains develop due to chromosomal mutations (Le Bras and Durand, 2003). Resistance mechanisms for quinoline amino-alcohols such as quinine and mefloquine are unclear (Petersen, Eastman and Lanzer, 2011). However, genetic and biochemical approaches have shown mutations in the *P. falciparum* chloroquine resistance transporter (*Pf*crt) gene result in efflux of chloroquine out of the parasite digestive vacuole, lowering chloroquine concentrations within the digestive vacuole and thus conferring chloroquine resistance (Petersen, Eastman and Lanzer, 2011).

Point mutations (typically one to four mutations) in the DHFR gene result in moderate to high levels of resistance to type-2 antifolate drugs (DHFR inhibitors) such as pyrimethamine while mutations in the DHPS gene result in resistance to type-1 antifolates (DHPS inhibitors) such as sulphadoxine (Saifi et al., 2013). Parasite treatment with the sulphadoxine-pyrimethamine drug combination selects for the following DHFR variants; Ile(51), Arg(59) and Asn(108) and the following DHPS variants; Ser(436), Gly(437) and Glu(540) (Le Bras and Durand, 2003). Multiple-drug chemoresistance – resistance to several antimalarial drugs – has been observed in *P. falciparum* (Le Bras and Durand, 2003). Multiple-drug resistance can emerge as a result of large-scale, simultaneous use of several antimalarial drugs creating strong selective pressure or due to cross-resistance which is linked to the common modes of action between several antimalarial drugs and possibly their resistance mechanisms (Le Bras and Durand, 2003). Studies have shown clones resistant to traditional antimalarials acquire resistance to new ones at a high frequency, known as accelerated resistance to multiple drugs (ARMD) (Le Bras and Durand, 2003). Due to increased resistance, antimalarial drugs are used in combination to treat uncomplicated malaria – typically artemisinin-based combination therapies (ACTs) - as it

reduces the risk of resistance developing (Biamonte *et al.*, 2013). Combinations of drugs with different mechanisms of action are commonly used (Kar and Kar, 2010).

Artemisinin resistance was first reported in Western Cambodia in 2009 and since then, resistance has emerged in other areas of Southeast Asia (Dhorda *et al.*, 2014). Resistance has been observed in *P. falciparum* and is characterised by a reduction in parasite clearance rate which is demonstrated by an increased parasite clearance half-life or the presence of detectable parasites on the third day of ACT (Fairhurst and Dondorp, 2016). Studies have shown that mutations in the 'propeller' region of a *P. falciparum* kelch protein (K13) confer artemisinin resistance in a number of clinical parasite isolates, however the mechanism is yet to be determined (Ariey *et al.*, 2016). At present, only 20 of 124 K13-propeller mutations have been associated with artemisinin resistance and only 4 of the 20 have been validated (by *in vitro and in vivo* methods) thus a number of studies are required before the exact mutations in the K13-protein associated with resistance are known (Fairhurst and Dondorp, 2016). As ACTs are the first line of treatment, increasing reports of ACT failures in Southeast Asia and surrounding regions poses a threat to malaria treatment worldwide (Dondorp, 2013). The World Health Organisation launched the Global Plan for Artemisinin Resistance Containment in 2013 with the aim of eliminating all *P. falciparum* parasites in areas where artemisinin resistance had emerged to prevent it from spreading (Dondorp, 2013). Despite this, there is concern that *P. falciparum* malaria in some regions of Southeast Asia are becoming resistant to all antimalarial drugs making it untreatable and likely to re-emerge which signifies the importance of finding alternative drug targets (Fairhurst and Dondorp, 2016).

Widespread drug resistance drives drug development research into alternative drug targets with different mechanisms of action (Shahinas *et al.*, 2013). New drugs should also be safe for pregnant women and children, fast-acting, affordable and ideally allow for single-dose administration as compliance is often an issue (Biamonte *et al.*, 2013). Antimalarials with alternative mechanisms of action minimise the risk of cross-resistance and allows for possible use in combination with existing antimalarials as a therapeutic option (Shahinas *et al.*, 2013).

1.4 Chaperones as Drug Targets

Chaperones are a set of proteins that have been targeted for drug development over the last 20 years (Ahmad and Muzaffar, 2016). Molecular chaperones facilitate protein folding and also prevent and reverse protein misfolding when cells are in stressful conditions (Shonhai, 2010). In addition, chaperones are required for protein trafficking, particularly the translocation of

cytoplasmic proteins into the endoplasmic reticulum and mitochondria (Odunuga *et al.*, 2004). Heat shock proteins (Hsps) make up a major fraction of the molecular chaperone family (Shonhai, 2010). Heat shock proteins are named according to their molecular size in kilodaltons and most are stress-inducible (Odunuga *et al.*, 2004). The principle heat shock proteins are: small heat shock proteins (sHsps), Hsp40, Hsp70, Hsp90 and Hsp110 (Kim *et al.*, 2013).

In *P. falciparum*, heat shock proteins are thought to regulate parasite infectivity and pathogenesis, thermo-protection of the parasite, parasite protein trafficking as well as export of parasite proteins to the red blood cell (Shonhai, 2010). The two physiologically diverse habitats of the parasite lifecycle (humans and mosquitoes) indicates parasites must have the ability to adapt to and survive in the two environments (Kumar *et al.*, 2007). The vital role heat shock proteins play in parasite survival make them potentially ideal drug targets (Acharya *et al.*, 2007). Two heat shock proteins are prominently expressed in *P. falciparum*: Hsp70 and Hsp90 (Gitau *et al.*, 2012). It is thought that Hsp70 and Hsp90 regulate the activities of transcription factors and protein kinases and help folding of newly synthesised proteins (Kim *et al.*, 2013).

1.4.1 Hsp90

Hsp90 is a well-studied dimeric heat shock protein made up three domains: an N-terminal ATP-binding domain (25 kDa), a middle domain (35 kDa) and a C-terminal domain (12 kDa) (Shonhai, 2010). The C-terminal domain is crucial for dimerization of Hsp90 while the N-terminal domain and middle domain are responsible for ATP binding and client protein binding respectively (Banerji, 2009). Hsp90 provides regulatory mechanisms that maintain the functional conformation of regulatory proteins when proteins misfold and aggregate in response to stress (Kim *et al.*, 2013). The mechanism by which Hsp90 functions is not well understood (Saibil, 2013). Hsp90 exists as a dimer through the mutual binding of the C-terminal domains of two individual proteins (Saibil, 2013). When the N-terminal domains of the Hsp90 proteins are bound to ADP, the dimer adopts a V-shaped 'open' conformation (Li and Buchner, 2013). When the chaperone receives a client protein, the Hsp90 N-terminal domains bind to each other forming a 'molecular clamp' thus the chaperone assumes a 'closed' conformation (Brandt and Blagg, 2009). This conformational change is mediated by the exchange of ADP for ATP (Banerji, 2009). Subsequent hydrolysis of ATP to ADP results in the return of Hsp90 to its 'open' conformation and release of the folded client protein (Li and Buchner, 2013). Aspects of this cycle – loading of the client protein, stimulation of ADP-ATP exchange and stimulation of ATPase activity – are mediated by co-chaperones e.g. Cell-

Division Cycle 37 (Cdc37) and Hop (client protein loading) and Aha1 (stimulation of ATPase activity) (Butler *et al.*, 2015).

'Normal' mammalian cells have molecular machinery to regulate cell growth, differentiation, proliferation and death (Miyata *et al.*, 2013). On the other hand, cancer cells proliferate rapidly and evade the cell's apoptotic and growth-inhibitory machinery and thus have limitless replication ability and a propensity towards metastasis (Miyata *et al.*, 2013). As a result of this, cancer cells experience nutrient deprivation, hypoxia and acidosis amongst other types of stress (Moser *et al.*, 2009). Increased expression of chaperone proteins, Hsp90 in particular, in tumour cells seems to help cancer cells successfully adapt to these stress conditions. Presumably Hsp90 does so by preventing/correcting protein misfolding or denaturation due to cell stress, thus maintaining a functional proteome in cancer cells and promoting tumour survival and growth (Bagatell and Whitesell, 2004). Importantly, Hsp90 client proteins include a number of proteins known to be important in oncogenesis/tumorigenesis and metastasis (Table 2)

Table 2: Hsp90 client proteins and their role in tumorigenesis (adapted from Sidera and Patsavoudi, 2014).

Client Protein*	Role in Tumorigenesis
Telomerase; n-TERT	Unlimited replicative potential
Cdk4; cyclin D; PIK-1	Insensitivity to anti-growth signals
Bcl2; P53; Akt; Rip	Evasion of apoptosis
Raf; Akt; EGFR; MEK	Self-sufficiency in growth signals
c-MET; MMP-2	Metastasis/Tissue invasion
HIF1; Akt; Src; FAK	Sustained Angiogenesis

*n-TERT: N-terminal telomerase reverse transcriptase; Cdk4: Cyclin dependent kinase 4; PIK-1: Pelle/IL-1 receptor associated transcriptase; Bcl2: B-cell lymphoma 2; P53: tumour protein 53; Akt: protein kinase B; Rip: Receptor-interacting kinase; Raf: Rapidly accelerated fibrosarcoma kinase: EGFR: Epidermal Growth Factor; MEK: Mitogen-activated protein kinase; c-MET: tyrosine protein kinase Met; MMP-2: Matrix Metalloproteinase-2; HIF1: Hypoxia-inducible factor 1; Src: tyrosine protein kinase Src; FAK: Focal Adhesion Kinase.

The table above shows various Hsp90 client proteins and the roles they play in tumorigenesis. Thus inhibition of Hsp90 may result in the disruption of numerous signalling pathways and lead to degradation of proteins involved in various aspects of tumorigenesis such as limitless replicative potential, metastasis and evasion of apoptosis (Miyata *et al.*, 2013; Trepel *et al.*, 2010; Holzbeierlein *et al.*, 2010). Studies have also shown that Hsp90 in cancer cells has a higher ATP-binding affinity and higher activity than Hsp90 found in normal cells (Holzbeierlein *et al.*, 2010). This suggests that, upon treatment with an Hsp90 inhibitor, cancer cells will have a higher sensitivity for the inhibitor than normal cells, resulting in decreased toxicity to normal cells (Bagatell and Whitesell, 2004). Most of the Hsp90 inhibitors in clinical trials and under development target the N-terminal domain of the chaperone (Necker, 2007).

The first reported Hsp90 inhibitors were natural products geldanamycin (GA) and radicicol, which inhibit Hsp90 ATPase activity by binding to the N-terminal ATP-binding domain, keeping the chaperone in its ADP-bound form thus inhibiting chaperone function and resulting in client protein destabilisation and proteosomal degradation (Sidera and Patsavoudi, 2014). Geldanamycin has poor solubility, limited stability *in vivo* and hepatoxicity (Kumalo *et al.*, 2015). Radicicol is metabolically and chemically unstable *in vivo* thus derivatives for radicicol and GA were developed to combat these issues (Wang *et al.*, 2016). The first GA derivative to proceed to clinical trials was 17-allyamino-17-demethoxy geldanamycin (17-AAG) which has shown promising results in breast cancer patients (Sidera and Patsavoudi, 2014). Since then, a few radicicol derivatives (such as triazole derivative STA-9090 [Synta] and isoxazole derivative NVP-AUY922/VER2296 [Cancer Research UK]) and numerous GA derivatives have entered clinical trials (Kumalo *et al.*, 2015). Other N-terminus binding Hsp90 inhibitors are purine-scaffold inhibitors- synthetic Hsp90 inhibitors developed based on a purine scaffold which mimic the features observed in ATP-binding to Hsp90- and peptidomimetrics- small protein-like molecules that mimic peptides and bind to the N-terminus, inhibiting ATP binding and hydrolysis (Kumalo *et al.*, 2015).

Novobiocin is a coumarin antibiotic and is the first known Hsp90 C-terminal domain inhibitor (Holzbeierlein *et al.*, 2010). The compound binds to the ATP-binding domain site at the C-terminus, resulting in destabilisation of the Hsp90 complex and the release and subsequent degradation of client proteins, but it has weak affinity for the binding site hence the compound is not clinically useful (Wang *et al.*, 2016). Analogues of novobiocin have been developed to improve its poor Hsp90 inhibition activity with some success, however, further validation (*in vivo*) of these analogues is needed before they can be considered for clinical use (Holzbeierlein *et al.*, 2010).

Over 20 Hsp90 inhibitors have entered clinical trials to date (all N-terminus inhibitors) but none has successfully entered the market although many clinical trials produce promising results (Wang *et al.*, 2016). This may be due to toxicity and dosage limitations and although combination of these compounds with traditional chemotherapy appears to improve efficacy and improve the toxicity problem, FDA approval for a Hsp90 inhibitor in cancer treatment is yet to be obtained (Kumalo *et al.*, 2015).

Many of the factors that make Hsp90 a good drug target in cancer are also why the chaperone is currently explored as a potential drug target in malaria treatment i.e. its support of cell

growth, cell signalling and cell development (Corbett and Berger, 2010). The *Pf*Hsp90 (*Plasmodium falciparum* Hsp90) gene is located on a fragment of chromosome 7of the parasite genome (Banumathy *et al.*, 2003). *Pf*Hsp90 has 64 % sequence identity with human Hsp90 including conserved ATP-binding motifs (Acharya *et al.*, 2007). The biggest difference between *Pf*Hsp90 and human Hsp90 is found in a region adjacent to the N-terminal ATP binding domain known as the 'linker' region which studies suggest affects Hsp90 ATPase activity and overall Hsp90 regulation (Pallavi *et al.*, 2010). Two additional paralogs of Hsp90 are found in both humans and *P. falciparum*: Hsp90-TNF receptor-associated protein which is found in mitochondria while Hsp90-Grp94 is localised in the endoplasmic reticulum (Shahinas *et al.*, 2013). Both the human and malaria genome encode two cytosolic Hsp90 proteins (Shonhai, 2010). Both human cytosolic Hsp90 proteins have a C-terminal EEVD motif which is required for binding to the co-chaperone Hop (described in section 1.4.2 below) whereas only one *Pf*Hsp90 contains the EEVD motif (Shahinas *et al.*, 2013). A study by Pallavi *et al.* (2010) found *Pf*Hsp90 binds and hydrolyses ATP more efficiently than human Hsp90 and that GA binds to *Pf*Hsp90 with high affinity, resulting in substantial inhibition of *Pf*Hsp90 ATPase activity.

Studies show treatment of *P. falciparum* in culture with GA inhibits parasite development from the ring stage to the trophozoite stage and leads to parasitemia clearing in mouse models which indicates *Pf*Hsp90 is essential for parasite growth and development in erythrocytes (Banumathy *et al.*, 2003; Wang *et al.*, 2016). Functional studies suggest *Pf*Hsp90 regulates parasite growth and development during the frequent febrile episodes characteristic of malaria i.e. the *Pf*Hsp90's stress response is activated after an increase in temperature, allowing for parasite survival (Kumar *et al.*, 2007). Geldanamycin inhibition of *Pf*Hsp90 ATPase activity and parasite development as well as *Pf*Hsp90's essential role in parasite survival presents *Pf*Hsp90 as a promising malaria drug target (Kumar *et al.*, 2007). The location of *Pf*Hsp90 on chromosome 7 – a region associated with chloroquine resistance- suggests *Pf*Hsp90 may play a role in the development of drug resistance in parasites, perhaps by maintaining a functional parasite proteome in the face of drug-induced cell stress (Wang *et al.*, 2016). This indicates that targeting *Pf*Hsp90 may not only have a therapeutic effect but may also help circumvent drug resistance to traditional antimalarials (Shahinas *et al.*, 2013).

A study conducted by Pallavi *et al.* (2010) found that 17-AAG not only inhibited parasite growth *in vitro* and in pre-clinical mouse models, it also inhibited *Trypanasoma evansi* (*T.evansi*) parasite growth and cured mice infected with *T.evansi*, thereby supporting *Pf*Hsp90

as a potential drug target for malaria treatment and also suggesting Hsp90 in other protozoan parasites may be potential drug targets for treatment of parasitic human and animal diseases.

1.4.2 Hop

Although Hsp90 functions as an independent chaperone, it is also known to exist in a functional partnership with Hsp70, allowing for some peptide substrates to be passed between the two chaperones (Kim *et al.*, 2013). Essentially Hsp70 is thought to initiate the folding of client proteins and the partially folded protein is then transferred to Hsp90 to complete the folding process (Li *et al.*, 2012). Hsp70 and Hsp90 are functionally linked by an 'adaptor' protein known as the Hsp70-Hsp90 organising protein (Hop) (Gitau *et al.*, 2012). Hop is an 'adaptor' protein that coordinates Hsp70 and Hsp90 interaction by simultaneously binding to both proteins without acting as a chaperone itself (Hernandez *et al.*, 2002). Hop is made up of nine tetratricopeptide repeat (TPR) motifs grouped into three domains: TPR1 domain, TPR2A domain and TPR2B domain (Blatch and Edkins, 2015). The TPR domains interact specifically with Hsp70 and Hsp90 C-terminal domains: TPR1 and TPR2B bind preferentially to the Hsp70 C-terminal domain whereas TPR2A binds preferentially to the Hsp90 C-terminal domain. Particularly important in these interactions is the recognition of the C-terminal EEVD motifs of the Hsp proteins (GPTIEEVD in the case of Hsp70 and MEEVD in the case of Hsp90) by the respective Hop TPR domains (Alvira *et al.*, 2014). In addition to acting as an adaptor protein, Hop is a co-chaperone known to modulate the ATPase activities of Hsp70 and Hsp90 and is also involved in a number of Hsp70 and Hsp90-independent complexes, suggesting additional cellular functions that are still being delineated (Blatch and Edkins, 2015).

As with Hsp90, Hsp70 has ATPase activity which causes conformational changes allowing client protein binding and folding (Mayer and Bukau, 2005). Hsp70 generally functions in collaboration with J-proteins or Hsp40s that transfer client proteins to Hsp70. Hsp70s generally consist of a 45 kDa N-terminal ATPase domain and a 25 kDa C-terminal domain which is made up of a β-sandwich subdomain and an α-helical subdomain (Vabulas *et al.*, 2010). The β-sandwich subdomain recognises extended segments enriched with hydrophobic amino acids (approximately 7 residues) typically found in nascent unfolded protein chains (Hartl *et al.*, 2011). The ability for a peptide to bind to Hsp70 is regulated by the α-helical subdomain and a conformational change in the β-sandwich subdomain which is ATP dependent (Vabulas *et al.*, 2010). In the ATP-bound form, the α-helical subdomain adopts an open conformation, allowing for Hsp40-mediated peptide binding (Mayer and Bukau, 2005). Hydrolysis of ATP to ADP is

accelerated by Hsp110 and leads to a conformational change of the α-helical subdomain (adopts a closed conformation) and subsequently stable binding of Hsp70 to the peptide (Hartl *et al.*, 2011). After hydrolysis, various nucleotide exchange factors e.g. Hsp110 bind to the Hsp70 ATPase domain and catalyse ADP-ATP exchange which causes the α-helical subdomain to adopt an open conformation, releasing the peptide (Vabulas *et al.*, 2010). The released client protein buries its hydrophobic residues (in fast-folding molecules) while proteins that require more time to fully fold re-bind to Hsp70 to avoid aggregation (Hartl *et al.*, 2011).

As mentioned previously, Hsp90 often acts on the partially folded proteins released by Hsp70 to complete the folding process (Whitesell and Lindquist, 2005). Hsp90 receives its client proteins from Hsp70 in a reaction that is dependent on Hop which acts as a scaffold protein and reversibly links Hsp70 and Hsp90 to allow for the transfer of client proteins (Scheufler *et al.*, 2000; Butler *et al.*, 2015). The ADP-bound form of Hsp70 and Hsp90 is favoured for Hop binding (Hernandez *et al.*, 2002; Odunuga *et al.*, 2004). Hop binds to Hsp90 and the Hsp90-Hop complex binds to peptide-bound Hsp70, aligning the client protein to one of two substrate binding sites on Hsp90, opposite the Hop binding site (Alvira *et al.*, 2014). ATP binding to Hsp90 weakens the Hsp90-Hop complex, resulting in dissociation of Hop and the client protein proceeds through the Hsp90 cycle described in section 1.4.1 (Onuoha *et al.*, 2008). Apart from facilitating client protein transfer between Hsp70 and Hsp90, Hop regulates the ATPase activity of Hsp90 – it inhibits ATP hydrolysis by Hsp90 which keeps the Hsp90 dimer in an open conformation and facilitates client protein binding. (Butler *et* al., 2014; Sidera and Patsavoudi, 2014).

Similar to human Hop, the malaria counterpart *Pf*Hop also appears to act as an adaptor protein and forms a functional complex with *Pf*Hsp70 and *Pf*Hsp90 to facilitate protein folding (Zininga *et al.*, 2015). *Pf*Hop co-localises with *Pf*Hsp70 and *Pf*Hsp90 in the parasite cytosol and co-elutes and co-precipitates with the two proteins in gel filtration and immunoprecipitation experiments conducted on parasite lysates. Like its human counterpart, an *E. coli*-based GFP complementation experiment suggests that it interacts with the C-terminal domain of *Pf*Hsp70 via the TPR1 and TPR2B domains and with the *Pf*Hsp90 C-terminal domain via the TPR2A domain (Gitau *et al.*, 2012; Zininga *et al.*, 2015). Bioinformatics analysis shows sequence variation between human Hop and *Pf*Hop which may allow for inhibition of *Pf*Hop without affecting human Hop (Gitau *et al.*, 2012).

As described previously, Hsp90 is being extensively pursued as a cancer drug target and current evidence suggests that it may likewise be a target for treatment of parasitic diseases, including malaria. Current Hsp90 drug candidates in clinical trials or in development target the N-terminal ATP binding site (e.g. geldanamycin and related compounds), with a minority also aimed at the C-terminal domain which appears to contain a second ATP binding site (e.g. novobiocin). However, it has been suggested that targeting the interactions of Hsp90 with its co-chaperones, including Hop, may be a fruitful alternative avenue for suppressing Hsp90 function as a therapeutic strategy (Brandt and Blagg, 2009; Edkins, 2016).

Interference of the Hsp90-Hop interaction is thought to possibly inhibit Hsp90 by preventing Hsp90 client proteins from being transferred from Hsp70 and by preventing Hop-mediated inhibition of Hsp90 ATPase activity which facilitates the stabilization of the Hsp90 open conformation and client protein binding, however no natural inhibitors have been described that target this interaction (Sidera and Patsavoudi, 2014). In 2011, Horibe *et al.* used a designed cell permeable peptidomimetric hybrid Antp-TPR peptide to inhibit Hsp90 interaction with the TPR2A domain of Hop. The peptide contained a cell-penetrating peptide sequence (Antp) and a sequence of the Hop TPR2A domain thought be important for Hsp90 binding (TPR). This study showed inhibition of the Hsp90-Hop interaction induced cell death in multiple cancer cell lines, resulted in significant anti-tumour activity in a xenograft model of human pancreatic cancer in mice and had no effect on the viability of normal cells, indicating that the Hsp90-Hop complex is a viable drug target for cancer treatment (Horibe *et al.*, 2011). Yi and Regan (2008) designed TPR-domain fragments as Hsp90 inhibitors and used AlphaScreen based screening to identify several small molecules capable of disrupting Hsp90-Hop interaction, by binding to the TPR2A domain interaction surface however optimization of these compounds has not been reported. The first HTS assay to screen for Hsp90-Hop inhibitors was established by Yi *et al.* (2009) based on AlphaScreen technology using a peptide corresponding the C-terminal 20 amino acids of Hsp90 and the TPR2A domain of Hop. As previously mentioned, AlphaScreen technology is highly sensitive but prone to false positives in small molecule screening (Gul and Hadian, 2014). With these promising results observed for Hsp90-Hop inhibition in cancer cells, it is reasonable to hypothesize that inhibition of the *Pf* Hsp90-*Pf*Hop interaction may lead to similar results and provide a viable alternative drug target for malaria treatment.

1.5 Problem Statement

Widespread drug resistance in *P. falciparum* has limited treatment options for malaria worldwide. Understanding the genome and biochemistry of the malaria parasite has advanced the search for alternative drug targets with novel mechanisms of action that may offer new therapeutic options, combat cross resistance and possibly reverse resistance to traditional antimalarials through synergy (Shahinas *et al.*, 2013).

As previously mentioned, ATP binding at the N-terminal domain of Hsp90 has been the focus of cancer drug development, with moderate success. However, the compounds are plagued with toxicity and pharmacokinetic problems and the clinical trials of some of these compounds showed an increase in heat shock response (Gomez-Monterrey *et al.*, 2012). This means that heat shock proteins are upregulated in treated cells and could compensate for the inhibition of Hsp90. Recently inhibition of Hsp90-co-chaperone interactions have been considered as possible drug targets, including Hsp90-Hop interaction (Banerji, 2009). Besides the AlphaScreen assay published by Yi *et al.* (2009), a suitable medium to high-throughput assay for screening inhibitors of Hsp90-Hop interaction has not been described. The ability of Hsp90 inhibitors to inhibit malaria parasite growth *in vitro* and *in vivo* suggests *Pf*Hsp90 is a valid drug target for malaria treatment, and *Pf*Hsp90-*Pf*Hop interaction is suggested by co-elution and co-precipitation assays. According to Shahinas *et al.* (2013), the functional domains of *Pf*Hop show sequence variation when compared to the human counterpart thus inhibition of the *P. falciparum* Hsp90-Hop interaction may be a viable drug target that to date, has not been explored. Direct *in vitro* binding of *Pf*Hsp90 to *Pf*Hop using purified proteins has not been demonstrated, neither has a screening assay format for this interaction been described.

1.6 Aims and Objectives

The objective of this research project was to develop and optimize a novel *P. falciparum* Hsp90-Hop interaction assay in order to demonstrate, firstly, that the proteins robustly interact *in vitro* and, secondly, to facilitate high-throughput screening of protein-protein interaction inhibitors. Our hypothesis was that this may be achieved by a novel plate capture assay using the heterologously expressed C-terminal domain of *Pf*Hsp90 and TPR2A domain of *Pf*Hop. The proposed assay format was to immobilise a His-tagged version of one of the interaction partners (*Pf*Hsp90 C-domain was chosen for this purpose) on nickel-coated 96-well plates and detect the binding of the *Pf*Hop TPR2A domain, fused to glutathione-S-transferase (GST), by a colorimetric GST enzyme assay. The corresponding mammalian Hsp90 and Hop domains were used as comparative controls.

In order to achieve this, the following objectives were pursued:

1. Clone *P. falciparum* and human Hsp90 C-terminal domains and GST into the pET-28a(+) *E. coli* expression plasmid and *P. falciparum* and mouse TPR2A domains into the pGEX-4T-1 *E. coli* expression plasmid.
2. Express and purify the His-tagged *Pf*Hsp-90 C-terminal domain, human Hsp90 C-terminal domain and GST, and the GST-tagged *Pf*TPR2A domain and Mouse TPR2A domain.
3. Establish the GST-assay using His-tagged GST immobilised on Nickel plates (positive control) and untagged GST (negative control).
4. Detect and optimise the interaction of human Hsp90 C-domain (hCdom) and murine Hop TPR2A domain (mTPR2A) using the assay.
5. Detect and optimise the interaction of the *Pf*Hsp90 C-domain (*Pf*Cdom) and *Pf*Hop TPR2A domain (*Pf*TPR2A) using the assay.
6. Explore alternative assay formats using the purified tagged proteins.

Chapter 2

Methods and Materials

2.1 Molecular Cloning

2.1.1 Primer Design

Primers were designed for polymerase chain reaction (PCR) amplification of the coding sequences of the human C-domain, *Pf* C-domain, mouse TPR2A domain, *Pf* TPR2A domain and glutathione-S-transferase (GST). The primers were designed according to the following InFusion® HD EcoDry™ Cloning Kit (Clontech, (CA) USA) user manual guidelines:

- The 5' end must contain 15 bases homologous to 15 bases at one end of the linearized vector
- The 3' end must contain the sequence specific to the insert, contain 40% to 60% GC content and be 18-25 bases in length
- The last 5 nucleotides at the 3' end must have no more than two cytosines and guanines

The primers were synthesised by Integrated DNA Technologies (Appendix A). Lyophilised primers were re-constituted in Tris-EDTA (TE) buffer (10 mM Tris, 0.1 mM EDTA, pH 8.0).

2.1.2 PCR Amplification

Human C-domain, *Pf* C-domain, *Pf* TPR2A, mouse TPR2A and GST coding sequences were amplified by hot start PCR using pYFP-hCdom, pYFP-*Pf*Cdom, pCFP-*Pf*TPR2A, pCFP-mTPR2A (Leigh-anne Derry, Rhodes University) and pGEX-4T-1 (GE Healthcare, (IL) USA) plasmids as templates, respectively. The template plasmids provided by L. Derry contain the human hsp90 C-domain, murine TPR2A domain, malaria (*P. falciparum*) hsp90 and TPR2A domain coding sequences cloned into mammalian expression plasmids derived from pEGFP-N1 (Clontech, (CA) USA). The malaria sequences had been codon-optimised for expression in human cells by Genscript (Hong Kong). PCR reactions were set up in a total reaction volume of 50 µl using KAPA HiFi PCR Kit (KK2101) components: 37.5 µl sabax water (water for irrigation), 1X KAPA HiFi buffer, 0.2 mM KAPA dNTP mix, 0.5 µl plasmid DNA and 3 µM of each primer. In a SimpliAmp Thermal Cycler (*life* technologies), the reactions were heated at 94 ºC for 2 minutes and 0.5 units of KAPA HiFi DNA polymerase was added. The PCR cycle was resumed for 30 cycles with the following parameters: 94 ºC for 40 seconds, 66 ºC

for 45 seconds and 70 °C for 2 minutes followed by a final step at 70 °C for 5 minutes. The PCR reactions were cooled, stored at 4°C and analysed by agarose gel electrophoresis.

2.1.3 Agarose Gel Electrophoresis

DNA products were analysed by agarose gel electrophoresis (AGE) on 0.8 % (w/v) agarose gels. Agarose gels were prepared by dissolving agarose (SeaKem® LE Agarose; Lonza, Switzerland) in 1X TBE buffer (0.02 M Tris, 1.3 mM EDTA, 0.02 M Boric acid) followed by addition of ethidium bromide to a final concentration of 0.6 µM. Sample loading buffer (1X TBE, 30 % glycerol and 0.25 % bromophenol blue) was added to the DNA samples in a 1:1 ratio. Electrophoresis was performed in 1X TBE buffer at 90 V for 1 hour. A 1 Kb DNA ladder (Promega, (WI) USA) was used to estimate the size of the samples. The gels were visualised and photographed under UV using a ChemiDoc™ XRS+ (Bio-Rad) gel documentation system. Agarose gels used for DNA purification were visualised using a UVITEC transilluminator (Cambridge).

2.1.4 PCR Product Purification

The PCR products were analysed by AGE as describe in section 2.1.3 at 80 V for 1 hour in a sample to sample loading buffer ratio of 6:1. The gel was visualised using a UVITEC transilluminator. The PCR bands were excised and purified using the Isolate II PCR and Gel Purification Kit (Bioline, UK) as per the kits instructions. The concentration and purity of the purified PCR products was quantified using a NanoDrop 2000 spectrophotometer (Thermo Scientific).

2.1.5 Vector Preparation

2.1.5.1 Transformation

pET-HPPK (contains the coding sequence of *E. coli* hydroxymethylpterin pyrophosphokinase cloned into the BamHI/XhoI sites of pET-28a(+) and provided by Genscript) and pGEX-4T-1 (GE Healthcare, (IL) USA) cloning vectors (Appendix C) were transformed into competent XL-10 gold *Escherichia coli* (*E. coli*) cells (Stratagene, (CA) USA). Competent XL-10 gold cells were thawed on ice and 1 µl plasmid DNA was added to a 50 µl aliquot of the cells. The cells were mixed briefly and incubated on ice for 30 minutes. The cells were heat shocked at 42.5 °C for 1 minute and incubated on ice for a further 5 minutes. LB broth (Millers) (10 g/L tryptone, 10 g/L NaCl and 5 g/L yeast extract) without antibiotic was added to the cells and the culture was incubated stationary at 37 °C for 1 hour. The transformation culture was plated

onto LB-Agar plates (15 g/L agar, 10 g/L tryptone, 5 g/L yeast extract and 5 g/L NaCl) containing 50 µg/ml ampicillin (Sigma-Aldrich, Germany) for the pGEX plasmid or 50 µg/ml kanamycin (Sigma-Aldrich, Germany) for the pET plasmid. The plates were incubated overnight in an inverted position at 37 ºC.

2.1.5.2 Alkaline Lysis Miniprep

Plasmids were isolated from transformed XL-10 gold *E. coli* cells by alkaline lysis miniprep. A single colony was inoculated into 5 ml LB broth containing 50 µg/ml ampicillin or kanamycin and incubated overnight at 37 ºC with shaking at 150-180 rpm. In sterile microfuge tubes, a 3ml aliquot of the overnight cultures was centrifuged at 3099 *xg* for 3 minutes in a Centrifuge 5148 (Eppendorf). The bacterial pellets were resuspended in GTE buffer (30 mM glucose, 25 mM Tris, 10 mM EDTA and 10 µg/ml RNase, pH 8.0). NaOH/SDS lysis solution (0.2 N NaOH, 1 % (w/v) SDS) was added to the suspensions with brief but vigorous shaking. Potassium acetate (5M) was added to the suspensions with immediate shaking. The suspensions were centrifuged at 16,873 *xg* for 5 minutes. The supernatants were added to sterile microfuge tubes and absolute ethanol was added with brief mixing. The microfuge tubes were centrifuged at 16,873 *xg* for 6 minutes. The supernatant was discarded and 70 % (v/v) ethanol was added to the pellets. The microfuge tubes were re-centrifuged at 16,873 *xg* for 3 minutes and the supernatants were discarded. The DNA pellet was dried at 37 ºC for 15 minutes. The pellet was dissolved in 50 µl sabax water and incubated at 37 ºC for 10 minutes.

2.1.5.3 Restriction Digestion

The plasmids isolated from transformed XL-10 gold cells were used to set up restriction enzyme digestions. The restriction digest reactions consisted of: 8.5 µl water, 12 µl plasmid miniprep, 2.5 µl Cut Smart® buffer (New England Biolabs, (MA) USA), 1 µl XhoI (New England Biolabs, (MA) USA) and 1µl BamHI (New England Biolabs, (MA) USA). The reactions were incubated overnight at 37 ºC and analysed by AGE as described in section 2.1.3.

2.1.5.4 Long Term Vector Storage

Following verification of the plasmids by restriction digestion, sterile glycerol was added to 850 µl of the overnight culture from section 2.1.5.2 to a final concentration of 17 % (v/v) and stored in sterile cryotubes at -80 ºC.

2.1.5.5 Vector Purification

The AGE analysed restriction digests (section 2.1.5.3) were visualised on a UVITEC transilluminator and the pET-28a(+) and pGEX-4T-1 bands were excised and purified using the Wizard® SV Gel and PCR Clean-Up Kit (Promega, (WI) USA) according to the kit's instructions. The concentration and purity of the purified vector samples was determined by a NanoDrop 2000 spectrophotometer (Thermo Scientific).

2.1.6 Cloning

The purified GST, human C-domain, mouse TPR2A and *Pf* TPR2A PCR products were ligated into restriction digested and purified pET-28a(+) and pGEX-4T-1 plasmid vectors using the InFusion® HD EcoDry™ Cloning Kit (Clontech, (CA) USA) according to the kit's instructions. GST and human C-domain PCR products were cloned into pET-28a(+) and *Pf*TPR2A and murine TPR2A PCR products were cloned into pGEX-4T-1.Attempts to clone the *Pf*C-domain into the pET-28a(+) plasmid by this procedure were unsuccessful. The *Pf*C-domain sequence, codon optimised for *E. coli* expression and cloned into the NheI and XhoI sites of pET-28a(+) was custom prepared and supplied by GenScript. The cloning reactions and *Pf*C-domain-pET-28a(+) construct were transformed into competent XL-10 gold cells as described in section 2.1.5.1. The transformed cells were plated onto LB-Agar plates containing 50 µg/ml ampicillin for pGEX-4T-1 constructs and 50 µg/ml kanamycin for pET-28a(+) constructs.

2.1.7 Cloning Verification

The cloned constructs were extracted from transformed XL-10 gold cells by alkaline lysis miniprep as described in section 2.1.5.2. The presence of the PCR insert was confirmed by restriction digestion as described in section 2.1.5.3. BamHI and XhoI restriction enzymes (New England Biolabs, (MA) USA) were used for pET-GST, pGEX-mTPR2A and pGEX-*Pf*TPR2A constructs. NheI and XhoI restriction enzymes (New England Biolabs, (MA) USA) were used for the pET-*Pf*Cdom construct. Cloning of pET-hCdom was confirmed by PCR as described in section 2.1.2 using cloned hCdom-pET-28a(+) plasmid as the DNA template. The PCR reaction and restriction digests were subsequently analysed by AGE as described in section 2.1.3 on 0.8 % (w/v) agarose gels containing 1.2 µM ethidium bromide. Electrophoresis was conducted at 80 V for 1 hour. The gels were visualised and photographed under UV using a ChemiDoc™ XRS+. For further verification, the plasmids were sequenced by Inqaba Biotec

(South Africa). *E. coli* cultures containing confirmed constructs were stored in glycerol as described in section 2.1.5.4.

2.2 Protein Expression

2.2.1 Transformation of T7 Express *lys*Y cells

pET-GST, pET-hCdom, pET-*Pf*Com, pGEX-4T-1, pGEX-mTPR2A and pGEX-*Pf*TPR2A plasmids were transformed into T7 Express *lys*Y competent *E. coli* cells (New England Biolabs, (MA) USA). The competent cells were thawed on ice and 1 µl plasmid DNA was added to a 50 µl aliquot of the competent cells. The cells were mixed gently and incubated on ice for 25 minutes. The cells were heat shocked at 42 °C for 1 minute and incubated on ice for a further 5 minutes. To each transformation reaction, LB broth without antibiotic was added. The cells were incubated at 37 °C for 1 hour with shaking at 180-200 rpm. The transformation cultures were plated onto LB-Agar plates containing 100 µg/ml ampicillin (pGEX constructs) and 100 µg/ml kanamycin (pET constructs). The plates were incubated overnight at 37 °C in an inverted position.

2.2.2 Long Term Storage of Expression Constructs

A single transformation colony was inoculated into LB broth containing 100 µg/ml ampicillin or kanamycin and incubated with shaking overnight at 37 °C. Sterile glycerol was added to an 850 µl aliquot of the overnight culture to a final concentration of 17 % (v/v) and the culture was stored at -80 °C.

2.2.3 Small-scale Protein Expression

A scraping of the expression construct glycerol stocks was inoculated into 2 ml LB broth containing 100 µg/ml ampicillin or kanamycin. The cultures were incubated with shaking at 37 °C. A 500 µl aliquot of the overnight cultures was inoculated into 10 ml LB broth containing 100 µg/ml ampicillin or kanamycin. The cultures were incubated at 37 °C with shaking until the OD_{600} was between 0.6 and 0.8 - measured by a UVmini-1240 (Shimadzu). To each culture, IPTG (Isopropyl β-D-1-thiogalactopyranoside; Sigma-Aldrich, Germany) was added to a final concentration of 1 mM and the cultures were incubated with shaking at 37 °C for a further 3 hours. IPTG addition was omitted in parallel control cultures. The cells were harvested by centrifugation in a JA-20 rotor at 4 °C, 5000 *xg* for 10 minutes using an Avanti® J-E Centrifuge (Beckman Coulter). The pellets were washed in 20 mM Tris-HCl (pH 8.0) and re-centrifuged at 5000 *xg* for 10 minutes. The bacterial pellets were stored at -80 °C overnight. The pellets

were thawed on ice and resuspended in 1 ml 20 mM Tris-HCl (pH 8.0) and sonicated for two cycles (60 amps for 45 seconds) using a Vibra-Cell™ sonicator (Sonics & Materials Inc). The expression samples were centrifuged at 5000 *xg* for 10 minutes and the soluble (supernatant) and insoluble (pellet) fractions were separated and analysed by SDS-PAGE.

2.2.4 SDS-PAGE Analysis

Protein expression samples were analysed on a 12 % SDS-PAGE gel according to the protocol described by Laemmli (1970). The gel was made up of a 12 % (w/v) resolving gel (4 ml [30% (w/v)] acrylamide, 2.5 ml lower gel buffer [1.5 M Tris-HCl, 0.4 % (w/v) SDS, pH 8.8], 3.5 ml water, 35 µl 10 % (w/v) ammonium persulfate and 7 µl TEMED [N,N,N',N'-Tetramethyl-ethylenediamine]) and a 4 % stacking gel (0.7 ml [30% (w/v)] acrylamide, 1.25 ml stacking gel buffer [0.5 M Tris-HCl, 0.4 % (w/v) SDS, pH 6.8], 3 ml water, 25 µl 10 % (w/v) ammonium persulfate and 6 µl TEMED. The expression samples were mixed with 4X SDS sample buffer (10 ml stacking buffer, 8 ml glycerol, 0.8 g SDS, 0.8 ml 2-mercapto-ethanol, 0.2 mg bromophenol blue, 1.2 ml water) in a 3:1 sample to sample buffer ratio. The samples were heated at 100 °C for 5 minutes and loaded onto the SDS-PAGE gel alongside a Color Prestained Protein Standard (New England Biolabs, (MA) USA). Electrophoresis was conducted in a Mini-PROTEAN Tetra System (Bio-Rad) in SDS running buffer (25 mM Tris-HCl, 0.2 M glycine, 3.5 mM SDS) at 120 V –constant voltage- for 1.5 hours. The gel was stained with Coomassie stain (45 % (v/v) water, 45 % (v/v) methanol, 10 % (v/v) acetic acid, 0.25 % (w/v) Coomassie Brilliant Blue R-250) overnight at room temperature with gentle shaking (Enduro™ Minimix). The gel was destained with destain solution (44 % (v/v) water, 44 % (v/v) methanol, 11 % (v/v) acetic acid) at room temperature with gentle shaking. The destain solution was changed every 15 minutes until the protein bands were visible. The gel was photographed using a ChemiDoc™ XRS+ gel documentation system (Bio-Rad).

2.2.5 Large-scale Protein Expression

Large scale expression cultures of pET-hCdom, pET-*Pf*C-dom, pET-GST, pGEX-4T-1, pGEX-*Pf*TPR2A and pGEX-mTPR2A were grown up for protein purification. A scraping of the expression construct glycerol stock was inoculated into 7 ml LB broth containing 100 µg/ml ampicillin (pGEX constructs) or 100 µg/ml kanamycin (pET constructs). The culture was incubated with shaking overnight at 37 °C. A 5ml aliquot of the overnight culture was inoculated into 250 ml LB broth (500 ml for *Pf*C-domain expression) containing 100 µg/ml ampicillin or kanamycin. The culture was incubated with shaking at 37 °C until the OD_{600} was

between 0.6 and 0.8 - measured by a UVmini-1240. IPTG (Sigma-Aldrich, Germany) was added to the culture to a final concentration of 1 mM and the culture was incubated at 37 °C for a further 3 hours. The cells were harvested by centrifugation in a JA-14 rotor at 4°C, 5000 *xg* for 10 minutes using an Avanti® J-E Centrifuge. The bacterial pellet was washed in equilibration buffer -50 mM Tris-HCl containing 20 mM imidazole, pH 8.0 for His-tagged proteins (expressed from the pET plasmids) and 40 mM Tris, 150 mM NaCl, 1mM PMSF (phenylmethylsulfonyl fluoride), 0.2 % (v/v) Triton X-100, pH 8.0 for GST-tagged proteins (expressed from the pGEX plasmids). The sample was re-centrifuged at 5000 *xg* for 10 minutes and the pellet was stored overnight at -80 °C.

2.2.6 Protein Purification of His-tagged Proteins

A Ni-NTA column (Qiagen, Germany) was used to purify hC-domain, *Pf*C-domain and His-GST from large scale protein expression cultures containing the corresponding pET constructs. The pellet was thawed on ice for 30 minutes, resuspended in equilibration buffer (50 mM Tris-HCl, 20 mM imidazole, pH 8.0) and 10 mg/ml lysozyme was added. The sample was incubated on ice for 30 minutes and sonicated for two cycles (60 amps for 1 minute) using a Vibra-Cell™ sonicator. The lysate was centrifuged in a JA-14 rotor at 4°C, 14,000 *xg* for 30 minutes. The supernatant was filtered sequentially using 0.45 µm and 0.2 µm filters. A 120 µl aliquot of the cleared lysate was collected for protein concentration determination and SDS-PAGE analysis. The Ni-NTA column was washed with water and equilibrated by washing with equilibration buffer. The cleared lysate was loaded onto the column and a 120 µl aliquot of the flow-through was collected for protein concentration determination and SDS-PAGE analysis. The column was washed twice with equilibration buffer. A 120 µl aliquot of each wash was collected for protein concentration determination and SDS-PAGE analysis. The bound protein was eluted from the column by addition of 3 ml elution buffer (50 mM Tris-HCl, 0.5M imidazole, pH 8.0). A 120 µl aliquot of the eluted protein was protein concentration determination and SDS-PAGE analysis and the remaining eluate was stored at 4 °C. The Ni-NTA column was rinsed with water and stored in 50 % (v/v) ethanol at 4 °C. All purification steps were conducted at 4 °C when possible.

2.2.7 Protein Concentration Determination

The protein concentration of the purification samples was determined by Bradford's method according to the protocol described by Bradford (1976). A set of protein standards was prepared using Bovine Serum Albumin (BSA; Roche Diagnostics, Germany) (1.5 - 0.125 mg/ml serial

dilution). The standard samples, collected purification samples, equilibration buffer and elution buffer were added to a clear 96 well plate - 5µl in each well – in duplicate and 250 µl Bradford reagent (Sigma-Aldrich, Germany) was added. The plate was incubated at room temperature for 5 minutes and absorbance was read at 595 nm using a SpectraMax® M3 (Molecular Devices) plate reader. The absorbance values obtained for the standard samples were used to construct a standard curve which was subsequently used to determine the concentration of the purification samples.

2.2.8 Desalting

The protein purification eluate (section 2.2.6) was desalted to remove imidazole using an 8.3 ml Sephadex™ G-25 PD-10 Desalting Column (GE Healthcare, (IL) USA). The column was equilibrated with TBS (40 mM Tris, 150 mM NaCl, pH 7.4) and 2.5 ml of the eluate containing purified protein was loaded onto the column. The protein was eluted with 3.5 ml TBS under gravity. The concentration of the eluate was determined by Bradford's method as described in section 2.2.7. A 120 µl aliquot of the eluted protein was set aside for SDS-PAGE analysis and protein concentration determination. The desalted protein eluate was mixed with glycerol to a final concentration 40 % (v/v) and stored at -20 °C. The column was washed with 2 bed volumes of water and stored in 50 % (v/v) ethanol.

2.2.9 Protein Concentration

After desalting, purified *Pf*C-domain was concentrated using a Centrisart® I column (Sigma-Aldrich, Germany). The protein was loaded onto the column and kept on ice for 5 minutes. The column was centrifuged at 2500 *xg* for 40 minutes using a Megafuge 1.0R (Heraeus). A 120 µl aliquot of the concentrated protein was collected for SDS-PAGE analysis and protein concentration determination. The concentrated protein was stored at 4 °C.

The purification samples, desalted protein samples and concentrated protein aliquots were analysed by SDS-PAGE as described in section 2.2.4.

2.2.10 Recharging the Ni-NTA Column

After each purification, the Ni-NTA column was recharged. The column was rinsed with water and stripping buffer (20 mM sodium phosphate, 500 mM NaCl, 50 mM EDTA, pH 7.4) was loaded onto the column. The column was rinsed with water and 0.1 M $NiSO_4$ was loaded onto the column. After a final rinse with water, 50 % (v/v) ethanol was added to the resin and the column was stored at 4 °C.

2.2.11 Preparation of a Glutathione-Agarose Column

Lyophilised glutathione-agarose (Sigma-Aldrich, Germany) was hydrated in water (70 mg agarose in 14 ml water) overnight at 4 °C. The resin was packed in a repurposed Ni-NTA column and the column was washed with 10 bed volumes of water. Storage buffer (2 M NaCl, 1 mM NaN_3) was added to the resin and the column was stored at 4 °C.

2.2.12 Protein Purification of GST-tagged Proteins

The glutathione-agarose column was used to purify GST-mTPR2A, GST-*Pf*TPR2A and GST (expressed from pGEX-4T-1) from large scale protein expression cultures. The pellet was thawed on ice for 30 minutes, resuspended in equilibration buffer (40 mM Tris, 150 mM NaCl (pH 8.0), 1 mM PMSF, 0.2 % (v/v) Triton X-100) and 10 mg/ml lysozyme was added. The sample was incubated on ice for 30 minutes and sonicated for two cycles (60 amps for 1 minute) using a Vibra-Cell™ sonicator. The lysate was centrifuged in a JA-14 rotor at 4°C, 14,000 *xg* for 30 minutes. The supernatant was filtered by a 0.45 µm and then by a 0.2 µm filter. A 120 µl aliquot of the cleared lysate was collected for protein concentration determination and SDS-PAGE analysis. The column was rinsed with water and equilibrated by washing with equilibration buffer. The cleared lysate was loaded onto the column and a 120 µl aliquot of the flow-through was collected for protein concentration determination and SDS-PAGE analysis. The column was washed twice with equilibration buffer. A 120 µl aliquot of each wash was collected for protein concentration determination and SDS-PAGE analysis. The bound protein was eluted from the column by addition of elution buffer (50 mM Tris-HCl (pH 9.5), 10 mM reduced L-glutathione) in three 1 ml fractions. A 120 µl aliquot of each elution fraction was collected for SDS-PAGE analysis and protein concentration determination. The eluted protein was mixed with glycerol to a final concentration of 40 % (v/v) and stored at -20 °C.

The purification samples were analysed by SDS-PAGE and the protein concentration was determined as described in sections 2.2.4 and 2.2.7 respectively.

2.2.13 Glutathione-Agarose Column Cleaning

After each purification, the glutathione-agarose column was cleaned by washing with: 2 bed volumes of water, 2 bed volumes of cleansing buffer 1 (0.1 M borate buffer (pH 8.5), 0.5 M NaCl), 2 bed volumes of water, 2 bed volumes of cleansing buffer 2 (0.1 M potassium acetate (pH 4.5), 0.5 M NaCl) and 2 bed volumes of water. The resin was stored in storage buffer.

2.3 C-domain–TPR2A Interaction Assays

2.3.1 Nickel plate GST Assay

Purified His-tagged C-domain and GST-TPR2A protein samples were diluted to a final concentration of 1 µM in TBS (40 mM Tris, 150 mM NaCl, pH 7.4) containing 1% (w/v) BSA (Roche Diagnostics, Germany). His-tagged GST was used a positive control and untagged GST was used as a negative control. The GST assay was performed according to the protocol described by Habig *et al.* (1974). One hundred microliters of the His-tagged protein was added to a Ni-NTA HisSorb™ plate (Qiagen, Germany), followed by 100 µl of the GST-tagged protein. The plate was incubated at room temperature with gentle shaking for 1 hour on an Enduro™ Minimix. In parallel, aliquots of DPBS (Sigma-Aldrich GST Assay Kit, Germany) and CDNB (2,4,-Dinitrochlorobenzene) (Sigma-Aldrich GST Assay Kit, Germany) were incubated at 25 ºC for an hour. The plate was washed twice (each wash 1 minute with shaking) with TBS containing 0.1 % (v/v) Tween-20 and then washed four times with TBS (each wash 1 minute with shaking). A substrate mastermix was prepared by adding 200 mM reduced L-glutathione reduced (Sigma-Aldrich GST Assay Kit, Germany) to a mixture of the 25 ºC-equilibrated CDNB and DPBS respectively (100 µl reduced L-glutathione and CDNB for every 9.8 ml PBS). To each well, 200 µl substrate mastermix was added and absorbance was read immediately at 340 nm using a SpectraMax® M3 plate reader every 30 seconds over 30 minutes. To control for the contribution of non-specific plate binding and background, readings obtained from wells containing GST-TPR2A proteins alone (i.e. without the His-tagged C-domain binding partner) or TBS-1% BSA buffer alone were averaged and subtracted from the other readings. Progress curves were constructed to demonstrate C-domain–TPR2A interaction. The GST assay was also conducted using prepared PBS (10 mM Na_2HPO_4, 1.8 mM KH_2PO_4, 2.7 mM KCl, 140 mM NaCl), 100 mM CDNB in ethanol and 200 mM reduced L-glutathione in water in substitution of the DPBS, CDNB and glutathione reagents of the commercial Sigma-Aldrich GST assay kit.

Inhibition of the C-domain-TPR2A interaction was performed using *Pf*TPR and hTPR peptides (AKLYNRLAISYIN and AKAYARIGNSYFK respectively) custom synthesised by GenScript. A 1 mM stock of the peptides was prepared using dimethyl sulfoxide (DMSO). The GST assay was conducted using 1 µM His-tagged C-domain and GST-TPR2A protein samples. After addition of the protein samples, the TPR peptides were added to a final concentration of 100 µM and the assay was performed as described above.

2.3.2 Preparation of Ni-NTA plates

Nickel coated plates were prepared according to the protocol described by Cressey *et al.* (2008). A Nunc-Immuno™ Microwell™ 96-well plate (Sigma-Aldrich, Germany) was coated with 1 mg/ml Nα, Nα,-Bis(carboxymethyl)-L-lysine hydrate (Sigma-Aldrich, Germany) in 0.1 M sodium phosphate (pH 8) without shaking at room temperature overnight. The plate was washed 3 times with TBS (50 mM Tris, 150 mM NaCl, pH 7.5) containing 0.05 % (v/v) Tween-20 (each wash 1 minute with shaking) and subsequently blocked with 3 % (w/v) BSA (Roche Diagnostics, Germany) in TBS at room temperature for 1 hour with gentle shaking on an Enduro™ Minimix. The plate was washed with TBS-0.05 % (v/v) Tween-20 followed by a wash with TBS containing 50 mM EDTA. The plate was washed five times with TBS to remove residual EDTA and the wells were charged with 10 mM $NiSO_4$ for 20 minutes at room temperature without shaking followed by a final wash with TBS prior use.

2.3.3 Glutathione plate HRP Assay

Purified His-tagged C-domain and GST-TPR2A protein samples were diluted to a final concentration of 1 µM in TBS (40 mM Tris, 150 mM NaCl, pH 7.4) containing 1% (w/v) BSA (Roche Diagnostics, Germany). His-tagged GST was used a positive control. A glutathione plate (Thermo Scientific) was washed three times with wash buffer (TBS-0.05 % (v/v) Tween-20) - each wash 1 minute with shaking. The protein samples were added to the glutathione plate (GST-tagged protein first). The plate was incubated at room temperature with gentle shaking for 1 hour on an Enduro™ Minimix. The plate was washed three times with wash buffer (each wash 1 minute with shaking) and HisDetector™ Nickel-HRP (SeraCare, (MA) USA), diluted 1:10,000 in TBS containing 1 % (w/v) BSA and 0.05 % Tween 20 was added. The plate was incubated stationary at room temperature for 30 minutes and then washed three times with wash buffer (each washing step stationary for 3 minutes). SureBlue Reserve (SeraCare, (MA) USA) was added to each well and absorbance was read at 630 nm using a SpectraMax® M3 plate reader every 30 seconds over 30 minutes. The readings obtained with wells containing the C-domain alone and TBS-1% (w/v) BSA buffer were subtracted from experimental readings to control for background signals. Progress curves were constructed to demonstrate C-domain–TPR2A interaction.

Chapter 3

Cloning, Expression and Purification of pET-hCdom, pET-*Pf*Cdom, pET-GST, pGEX-mTPR2A and pGEX-*Pf*TPR2A

3.1 Introduction

The purpose of this study was to explore a novel conceptual protein-protein interaction assay format in which one interaction partner is prepared as a polyhistidine (His)-tagged protein and the other as a glutathione-S-transferase (GST) fusion protein. The His-tagged protein could be immobilised on nickel-coated plates and binding of the GST-tagged interaction partner may be detected using a colorimetric GST enzyme assay (described in more detail in the introduction of Chapter 4). Based on its potential as a novel drug target, malaria and mammalian Hsp90-Hop interaction was chosen as a model to explore the assay. The goal was to:

i) Demonstrate feasibility of the assay approach;

ii) Directly demonstrate that *P. falciparum* Hsp90 and Hop interact *in vitro*;

iii) Establish an assay that can be used to screen compounds for Hsp90-Hop inhibition in a medium - to high-throughput mode.

To facilitate expression in *E. coli*, it was opted not to use the full-length proteins (approx. 85 and 65 kDa for Hsp90 and Hop respectively), but rather the domains of the two proteins that are directly involved in Hsp90-Hop interaction, i.e. the C-terminal domain of Hsp90 and TPR2A domain of Hop (approx. 10 and 16 kDa respectively). Development of the assay thus required the cloning of the coding sequences, *E. coli* expression and purification of 6 recombinant proteins:

His-tagged human and *P. falciparum* Hsp90 C-domains (hCdom, *Pf*Cdom);

GST-tagged murine and *P. falciparum* TPR2A domains (mTPR2A, *Pf*TPR2A);

His-tagged and untagged GST (hGST and uGST as positive and background controls, respectively).

Note that murine instead of human TPR2A domain was used based on the availability of a murine Hop template plasmid from a collaborating laboratory (Prof. A. Edkins) and the domains from the two species share a 98% sequence identity.

Molecular cloning allows for isolation and insertion of a gene of interest into a vector for propagation (Lodish *et al.*, 2000). To isolate the gene of interest, PCR is frequently used to amplify a particular gene fragment from a DNA 'template' (Valones *et al.*, 2009). The most commonly used method for cloning PCR products involves introduction of restriction enzyme sites to the gene of interest - through primers - which are subsequently used to ligate the gene into a plasmid vector as first described by Jackson *et al.* (1972). The gene of interest and plasmid vector are cut with the same restriction enzymes, producing cohesive ends which are ligated by DNA ligase to form a recombinant DNA molecule (Alberts *et al.*, 2008). Most plasmids used in molecular cloning are optimized for replication in *E. coli* and for use as vectors by reducing their length, leaving only essential DNA sequences required for cloning i.e. a selectable marker e.g. a drug resistance gene, a replication origin and a region containing restriction sites in which DNA fragments can be inserted (Lodish *et al.*, 2000). The recombinant DNA molecule is introduced into a bacterial host for propagation (typically competent *E. coli* cells) by transformation (Hanahan *et al.*, 1991). The selectable marker in the recombinant DNA molecule allows for selection of transformed cells (Alberts *et al.*, 2008).

Once cloning is successful and presence of the gene insert is confirmed (usually by sequencing or restriction digestion), the recombinant DNA molecule is transformed into an expression host. A number of expression host are available for protein expression - bacteria, yeast, human cells and insect cells - however *E. coli* remains the standard choice as it's easy to use and cost effective (Esposito and Chatterjee, 2006). Despite its extensive use, a number of problems can occur during expression of recombinant proteins in *E. coli.* Common problems faced in heterologous protein expression include cell death due to protein toxicity, the formation of inclusion bodies, no protein activity or no protein expression at all (Terpe, 2006). The percentage of soluble recombinant proteins expressed in *E. coli* continues to decrease due to the formation of inclusion bodies or protein misfolding (Grãslund *et al.*, 2008). Consequently, it is important to evaluate the expression profile of recombinant proteins by small-scale expression before large-scale expression can be considered (Lesley, 2001). Expression of recombinant proteins can be achieved by induction of a strong promoter system such as T7, *tac* or lambda P_L by IPTG or by autoinduction which involves manipulating the carbon sources during *E. coli* growth (Grãslund *et al.*, 2008). Small-scale expression typically involves separation of the pellet and supernatant fractions after centrifugation of an expression culture that has undergone lysis followed by analysis by SDS-PAGE (Lesley, 2001). This analysis allows for the determination of optimal growth conditions for large-scale expression and also

indicates whether the expressed protein is soluble or insoluble (soluble proteins are present in the supernatant fraction and insoluble proteins are present in the pellet fraction). There are concerns that expression levels and solubility of recombinant proteins are influenced by factors that do not always change with increase in culture volume e.g. culture conditions and the degree of aeration (Grãslund *et al.*, 2008).

Once the optimal growth conditions for the protein have been determined, large-scale protein expression allows for the production of relatively high concentrations of protein which can be isolated from the expression culture by protein purification methods – often affinity purification (Esposito and Chatterjee, 2006). Affinity purification requires fusion tags on the recombinant protein (usually incorporated into the plasmid vector) which allow for one-step chromatographic purification that yields sufficiently pure protein (Lesley, 2001). Commonly used affinity tags include: the polyhistidine tag, the GST tag, the calmodulin-binding peptide tag and the streptavidin-binding peptide tag (Esposito and Chatterjee, 2006). In this study, the polyhistidine (His) tag and the GST tag were used. The His-tag was introduced at the N-termini of the recombinant C-domain proteins and GST by using the plasmid pET-28a(+) (Novagen). It contains a T7 promoter and a *lacI* expression cassette and lac operon for IPTG-inducible expression and a kanamycin resistance gene for selection. The GST tag was attached to the N-termini of the TPR2A domains using pGEX-4T-1 (GE Healthcare, (IL) USA). It contains a *tac* promoter and *lacI* expression cassette for IPTG-inducible expression and ampicillin resistance gene for selection.

His-tagged proteins are purified from the expression culture by immobilised metal-affinity chromatography (IMAC) (Bornhorst and Falke, 2000). IMAC is based on interactions between amino acid side chains such as the polyhistidine tag and transition metal ions - such as nickel – immobilised on a matrix due to the formation of co-ordination bonds between the histidine imidazole ring and the transition metal (Bornhorst and Falke, 2000). Proteins containing the polyhistidine tag are strongly retained on the IMAC matrix and are eluted by adjusting the pH of the wash buffer or by increasing the concentration of imidazole in the wash buffer (Bornhorst and Falke, 2000). IMAC is a preferred purification method as it is fast, allows for strong, specific binding and has high yields and mild elution conditions (Grãslund *et al.*, 2008). Purification of GST-tagged proteins is often through a gravity-flow chromatography system using an immobilised glutathione Sepharose column – the GST-tagged protein binds to the glutathione matrix in an enzyme-substrate binding reaction (Harper and Speicher, 2011).

Proteins purified on this column are also eluted under mild conditions by an elution buffer containing reduced glutathione (Harper and Speicher, 2011).

The aim of this section was to: clone human and *Pf* Hsp90 C-terminal domains and GST into pET-28a(+) and *Pf* and mouse TPR2A domains into pGEX-4T-1; transform the recombinant DNA constructs into competent XL-10 gold *E. coli* cells for proliferation and T7 Express *lysY E. coli* cells for expression; determine the expression profile of the recombinant proteins and subsequent over-expression and purification of the proteins by affinity purification. The presence of the insert in the recombinant plasmids was confirmed by agarose gel electrophoresis following restriction digestion of the cloned constructs and sequencing. SDS-PAGE analysis of the small-scale expression samples was used to determine the solubility of the expressed proteins and SDS-PAGE analysis of the purification samples was used to confirm the presence and determine the purity of the purified protein.

3.2 Results

3.2.1 PCR amplification

Gene amplification by PCR of human Hsp90 C-terminal domain (hCdom), *Pf*Hsp90 C-terminal domain (*Pf*Cdom), *Pf*Hop TPR2A domain (*Pf*TPR2A), murine Hop TPR2A domain (mTPR2A) and GST was performed using primers designed and sequence templates described in Appendix A and Appendix B respectively. BamHI and XhoI restriction sites were incorporated into the 5' and 3' end of the primers respectively. Hot start PCR was conducted for 30 cycles under the following parameters: 94 ºC for 40 seconds, 66 ºC for 45 seconds and 70 ºC for 2 minutes followed by a final step at 70 ºC for 5 minutes. The PCR products were analysed on a 0.8 % agarose gel for 1 hour. The following sizes were expected: hCdom: 291 bp, *Pf*Cdom: 279 bp, GST: 679 bp, mTPR2A: 393 bp and *Pf*TPR2A: 411bp.

A 1 Kb DNA ladder was used to determine the sizes of the PCR products and as seen in Figure 3 below, the obtained PCR products agreed with the expected sizes and were sufficiently free of other artefacts to allow purification for subsequent cloning, indicating successful PCR amplification of the sequences.

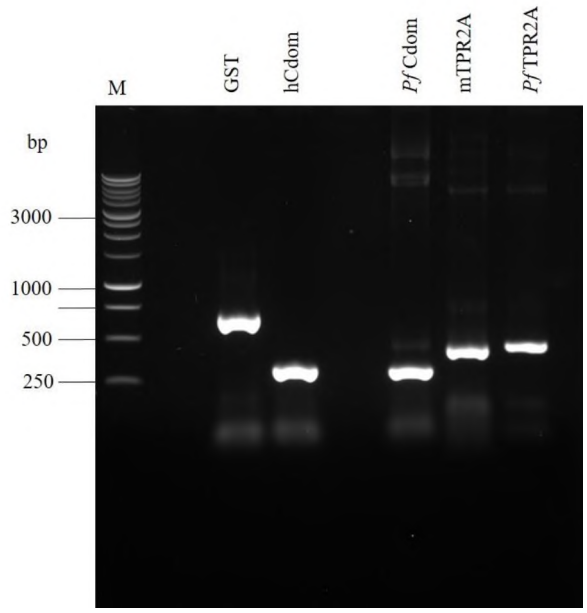

Figure 3: Agarose gel of GST, hCdom, *Pf*Cdom, mTPR2A and *Pf*TPR2A PCR products.

PCR amplified gene fragments were analysed on a 0.8% agarose gel at 80V for 1 hour and stained with ethidium bromide. M: 1 Kb DNA ladder. Bands at approximately 679 bp, 291 bp, 279 bp, 393 bp and 411 bp were expected respectively for the PCR products indicated in the lane labels.

3.2.2 Cloning

pET-HPPK and pGEX-4T-1 plasmids were restricted with BamHI and XhoI in overnight restriction enzyme digestion reactions to release pET-28a(+) and pGEX-4T-1 plasmid backbones, the restriction digests were analysed by agarose gel electrophoresis (not shown) and the plasmids bands were excised and purified using the Wizard® SV Gel and PCR Clean-Up Kit (Promega, (WI) USA). The PCR products were also digested with BamHI and XhoI, purified from an agarose gel following electrophoresis using the Isolate II PCR Gel Purification Kit (Bioline, UK) and ligated into the BamHI/XhoI restriction sites of pET-28a(+) (for GST, hCdom and *Pf*Cdom) and pGEX-4T-1 (for mTPR2A and *Pf*TPR2A).

Once the cloned constructs were isolated from transformed XL-10 gold *E. coli* colonies, cloning was verified by restriction digestion of the pET-GST, pGEX-mTPR2A and pGEX-*Pf*TPR2A constructs using BamHI and XhoI. The restriction digests were analysed on an 0.8 % agarose gel containing 1.2 µM ethidium bromide (Fig. 4). For pET-GST, DNA bands at 5369 bp (plasmid backbone) and 657 bp (insert) were expected. For pGEX-mTPR2A, DNA bands at 4969 bp and 393bp and for pGEX-*Pf*TPR2A, DNA bands at 4969 bp and 411 bp were expected.

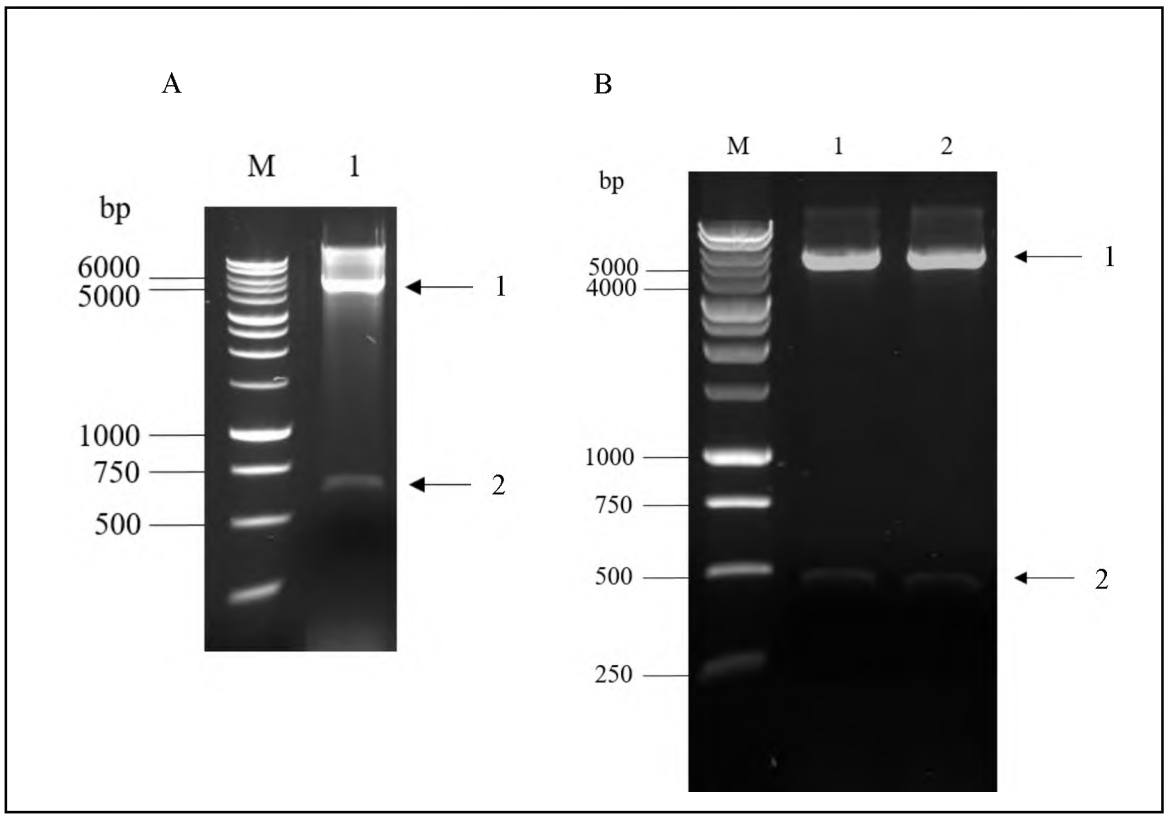

Figure 4: Agarose gel showing diagnostic restriction digests of pET-GST, pGEX-*Pf*TPR2A and pGEX-mTPR2A using BamHI and XhoI.

The cloned constructs were isolated from successful *E. coli* XL-10 gold transformants by alkaline lysis miniprep and used to set up overnight restriction enzyme digestion reactions that were analysed on a 0.8 % agarose gel at 80 V for 1 hour. **(A)** pET-GST restriction digestion. Lane 1: DNA bands at approximately 5500 bp and 650 bp. **(B)** Lane 1: pGEX-*Pf*TPR2A restriction digest. DNA bands at approximately 5000 bp and 480 bp; Lane 2: pGEX-mTPR2A restriction digest. DNA bands at approximately 5000 bp and 470 bp. M: 1 Kb DNA ladder, Arrow 1: Plasmid vector backbone, Arrow 2: Cloned DNA insert.

Two bands were observed for each restriction digestion analysis indicating successful digestion of the constructs. The DNA bands at arrow 1 are indicative of the plasmid vector backbones which were observed at their expected sizes. The DNA bands at arrow 2 are indicative of the cloned inserts at the expected sizes.

Attempts at cloning verification by restriction digestion of pET-hCdom were unsuccessful (no insert bands were observed on the gels) thus the construct was isolated from transformed XL-10 gold cells and cloning was verified by PCR, using pET-hCdom plasmid isolated from three independent transformed *E. coli* colonies as the DNA template. PCR was conducted as described in Section 2.1.2 and the PCR products were analysed on a 0.8 % agarose gel containing 1.2 µM ethidium bromine at 90 V for 1 hour 10 minutes (Fig. 5). An expected PCR band at 291 bp was obtained. Further confirmation of the construct was obtained by DNA sequencing (carried out by Inqaba Biotech – Appendix D).

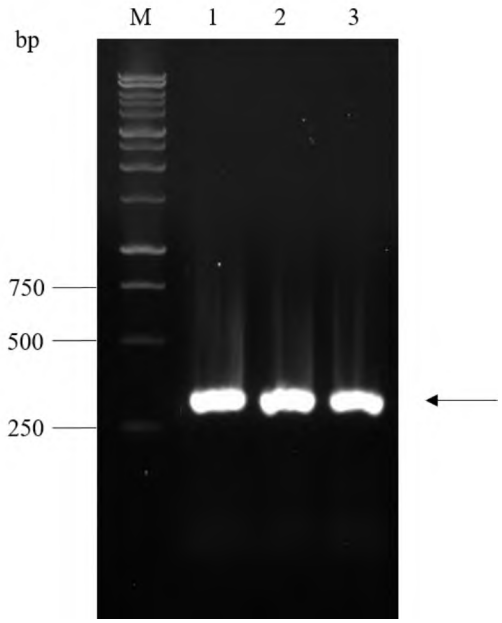

Figure 5: Agarose gel showing PCR confirmation of hCdom cloned into pET-28a(+).

PCR amplified hCdom fragments using pET-hCdom from three different plasmid samples as the DNA template were analysed on a 0.8 % agarose gel at 90 V for 1 hour. M: 1 Kb DNA ladder; Lane 1: hCdom sample 1; Lane 2: hCdom sample 2; Lane 3: hCdom sample 3. Arrow shows the PCR products expected at 291 bp.

Repeated attempts to obtain the pET-*Pf*Cdom construct were unsuccessful. The construct was therefore custom prepared and supplied by GenScript, transformed into competent XL-10 gold *E. coli* cells and the presence of *Pf*Cdom was determined by restriction digestion (Fig. 6). Overnight restriction digestion of pET-*Pf*Cdom with NheI and XhoI followed by agarose gel electrophoresis on a 0.8 % agarose gel was performed and expected DNA bands at 285 bp and 5369 bp for the gene insert and plasmid vector, respectively, were obtained.

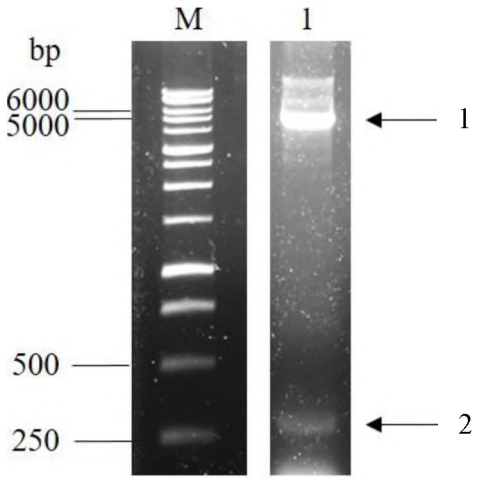

Figure 6: Agarose gel showing restriction of pET-*Pf*Cdom using NheI and XhoI.

The cloned construct was isolated from successful XL-10 gold transformants by alkaline lysis miniprep and overnight restriction digestion was performed. The restriction digest was analysed on a 0.8 % agarose gel at 80 V

for 1 hour. M: 1 Kb DNA ladder; Lane 1: pET-*Pf*Cdom restriction digest. Arrow 1: Plasmid vector DNA fragment, Arrow 2: Gene insert DNA fragment. The molecular weight lane (M) and lane 1 were separated and edited individually in order to display the weakly fluorescent insert band 2 in lane 1.

Cloning of pET-hCdom, pET-*Pf*Cdom, pET-GST, pGEX-mTPR2A and pGEX-*Pf*TPR2A was further verified by sequencing performed by Inqaba Biotec™ (Appendix D). The sequencing data shows the presence of the insert in all five constructs indicating successful cloning. The first two codons of the *Pf*TPR2A construct were not in the sequenced region but the identical match of the sequenced area to the initial coding sequence (Appendix B) suggests the presence of the correct insert.

3.2.3 Small-scale expression analysis

Small-scale expression was performed to determine the expression levels of $(His)_6$-hCom, $(His)_6$-*Pf*Cdom, $(His)_6$-GST, GST-mTPR2A and GST-*Pf*TPR2A and solubility of the recombinant proteins in T7 Express *lys*Y *E. coli* cells.

An overnight culture of transformed T7 cells was inoculated into 10 ml LB broth containing 100 µg/ml ampicillin (pGEX constructs) or kanamycin (pET constructs). The cultures were incubated at 37 ºC with shaking until the OD_{600} was between 0.6 and 0.8. Expression was induced by addition of IPTG. The cultures were incubated at 37 ºC for a further 3 hours. In parallel control cultures, IPTG was omitted. The cells were harvested by centrifugation and stored at -80 ºC. The cells were lysed by the freeze-thaw method and sonication. The soluble (supernatant) and insoluble (pellet) fractions were separated by centrifugation and the expression samples were analysed by SDS-PAGE on 12 % polyacrylamide gels at 120 V for 1.5 hours and stained with Coomassie. Results obtained for hCdom (His-tagged human Hsp90 C-domain expressed from pET-hCdom) and hGST (His-tagged GST expressed from pET-GST) are shown in Fig. 7 and 8, respectively.

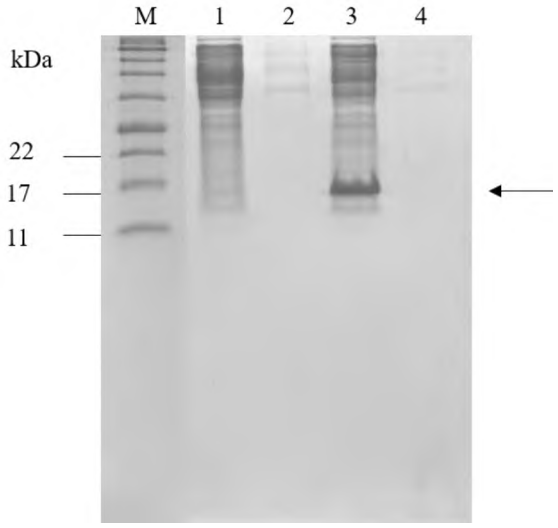

Figure 7: SDS-PAGE analysis of hCdom small-scale expression samples.

Small-scale hCdom expression samples analysed by SDS-PAGE on a 12 % gel. M: Molecular mass marker; Lane 1: uninduced soluble fraction; Lane 2: uninduced insoluble fraction; Lane 3: induced soluble fraction; Lane 4: induced insoluble fraction.

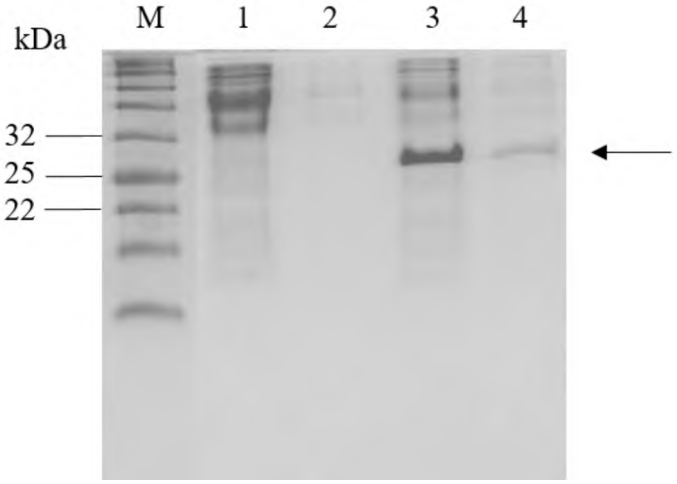

Figure 8: SDS-PAGE analysis of hGST small-scale expression samples.

Small-scale hGST expression samples analysed by SDS-PAGE on a 12 % gel. M: Molecular mass marker; Lane 1: uninduced soluble fraction; Lane 2: uninduced insoluble fraction; Lane 3: induced soluble fraction; Lane 4: induced insoluble fraction.

In both gels in Figures 7 and 8, very few, faint bands were observed in both the induced and uninduced insoluble fractions indicating complete lysis of the cells. Relatively intensely stained distinct bands were observed at the expected sizes (14 kDa for hCdom and 29 kDa for hGST) in the induced soluble fractions of *E. coli* containing pET-hCdom and pET-GST, suggesting both corresponding recombinant proteins were expressed at high levels and were soluble.

A similar expression profile was observed for pGEX-mTPR2A and pGEX-*Pf*TPR2A transformed cells (Fig. 9 and 10). No bands were observed in the induced and uninduced insoluble fractions, suggesting complete lysis of cells. The distinct bands observed in the

induced soluble fractions were at the expected sizes (41 kDa and 42 kDa for mTPR2A and *Pf*TPR2A respectively) indicating the proteins were expressed and soluble. The bands were stained more intensely than those observed for the pET constructs (Fig. 7 and 8), suggesting higher expression levels for pGEX constructs.

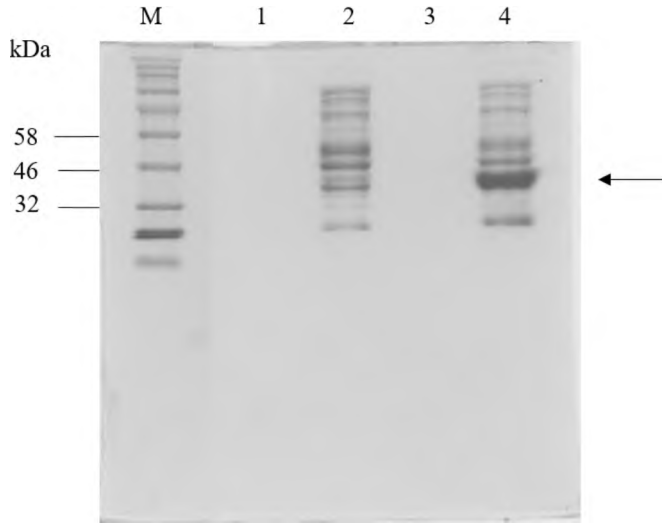

Figure 9: SDS-PAGE analysis of mTPR2A small-scale expression samples.

Small-scale mTPR2A expression samples analysed by SDS-PAGE on a 12 % gel. M: Molecular mass marker; Lane 1: uninduced insoluble fraction; Lane 2: uninduced soluble fraction; Lane 3: induced insoluble fraction; Lane 4: induced soluble fraction.

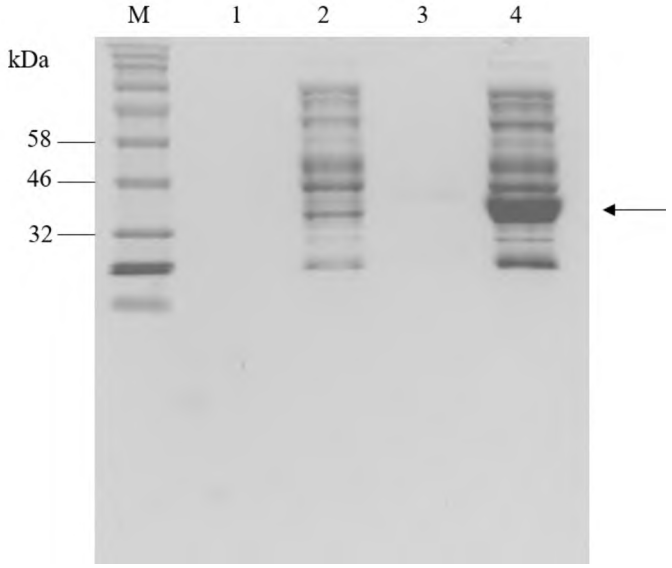

Figure 10: SDS-PAGE analysis of *Pf*TPR2A small-scale expression samples.

Small-scale *Pf*TPR2A expression samples analysed by SDS-PAGE on a 12 % gel. M: Molecular mass marker; Lane 1: uninduced insoluble fraction; Lane 2: uninduced soluble fraction; Lane 3: induced insoluble fraction; Lane 4: induced soluble fraction.

Attempts at small-scale expression of $(His)_6$-*Pf*Cdom in 10 ml cultures were unsuccessful - no obvious unique bands were observed in the IPTG induced vs. uninduced samples (not shown).

Thus a 50 ml expression culture was used to increase bacterial biomass. In addition, a parallel culture was set up containing LB broth supplemented with 1% glucose in an attempt to enhance expression (Fig. 11) (Rosano and Ceccarelli, 2014).

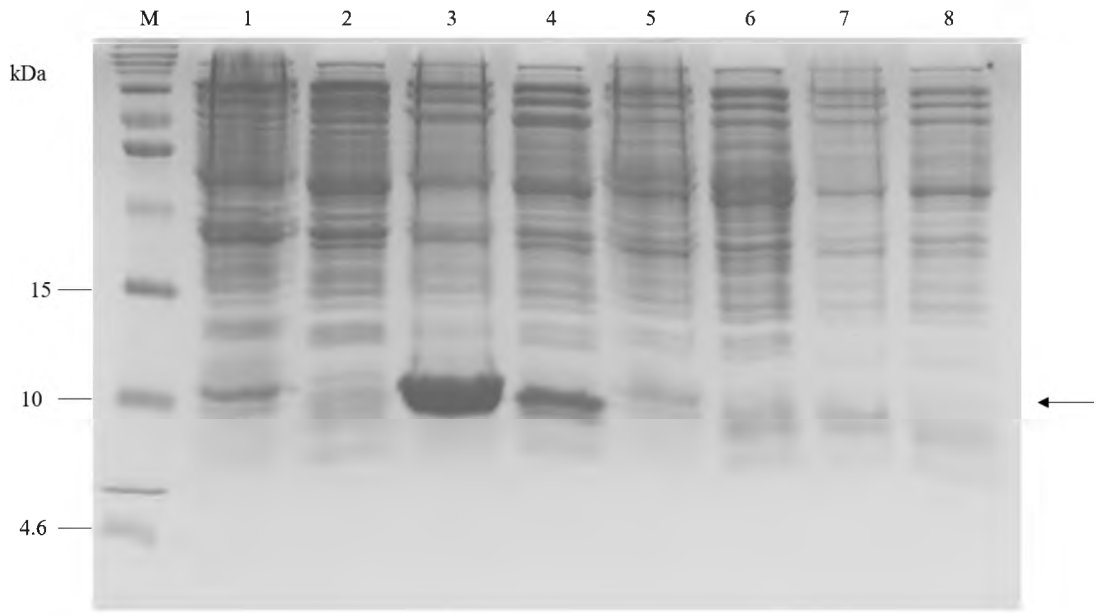

Figure 11: SDS-PAGE analysis of *Pf*Cdom small-scale expression samples.

Small-scale *Pf*Cdom expression samples analysed by SDS-PAGE on a 12 % gel. M: Molecular mass marker (ProSieve Quad Color™); Lanes 1-4: cultures containing 1% glucose; Lanes 5-8: cultures without glucose. Lane 1 and 5: uninduced insoluble fraction; Lane 2 and 6: uninduced soluble fraction; Lane 3 and 7: induced insoluble fraction; Lane 4 and 8: induced soluble fraction.

The expression profile observed for *Pf*Cdom was different from those previously observed for the other constructs. The bands observed for the insoluble fractions were similar to those observed for the soluble fractions indicating poor lysis of cells, perhaps due to the increased *E. coli* biomass. However, a distinct band was observed close to the expected size of *Pf*Cdom (13 kDa) in the glucose containing induced insoluble and induced soluble fraction (Fig. 11, lanes 3 and 4). No *Pf*Cdom bands were observed for the samples lacking glucose, implying glucose is a requirement for *Pf*Cdom expression. *Pf*Cdom was observed at higher protein concentrations in the induced insoluble fraction containing glucose, however the band observed in the soluble fraction suggested concentrations high enough to allow for purification form the soluble fraction without further attempts to increase soluble expression or resorting to protein solubilisation/re-folding protocols using the insoluble fraction.

3.2.4 Protein purification

Once optimal expression conditions for the construct were determined, large-scale expression of the proteins was used to generate high concentrations of protein for purification purposes. Large-scale expression was performed under similar conditions to the small-scale expression cultures except that 250 ml cultures were used. After expression, the cells were harvested by centrifugation and stored at -80 ºC. The cells were lysed by the freeze-thaw method, addition of lysozyme and sonication. The soluble fraction was obtained from the cell suspension by centrifugation, filtered and loaded onto a Ni-NTA column (Qiagen, Germany) for the His-tagged proteins (hCdom, *Pf*Cdom) and a glutathione-agarose column for GST fusion proteins (mTPR2A and *Pf*TPR2A). Excess imidazole was removed from purified His-tagged proteins by size-exclusion column desalting as detailed in section 2.2.8. Protein eluates with concentrations lower than 0.09 mg/ml were concentrated using a Centrisart® I ultrafiltration column as detailed in section 2.2.9. The purification samples were analysed by SDS-PAGE performed at 120 V for 1.5 hours and stained with Coomassie. Results obtained for the His-tagged C-domains are shown in Fig. 12 and 13.

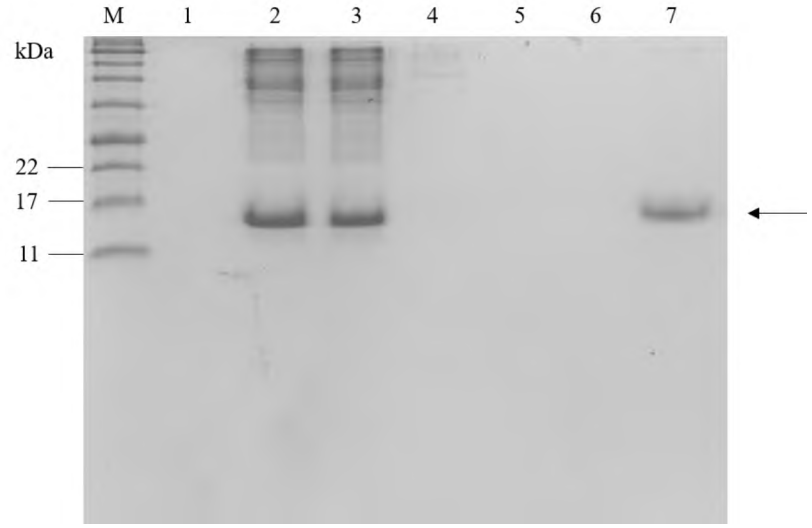

Figure 12: SDS-PAGE analysis of hCdom protein purification samples.

A Ni-NTA column was used to purify hCdom from a large-scale expression culture. The purification samples were analysed by SDS-PAGE on a 12 % gel. M: Molecular mass marker; Lane 2: Filtered lysate (soluble supernatant); Lane 3: Sample flow-through; Lane 4: Wash 1; Lane 5: Wash 2; Lane 7: Elution. Lanes 1 and 6: empty.

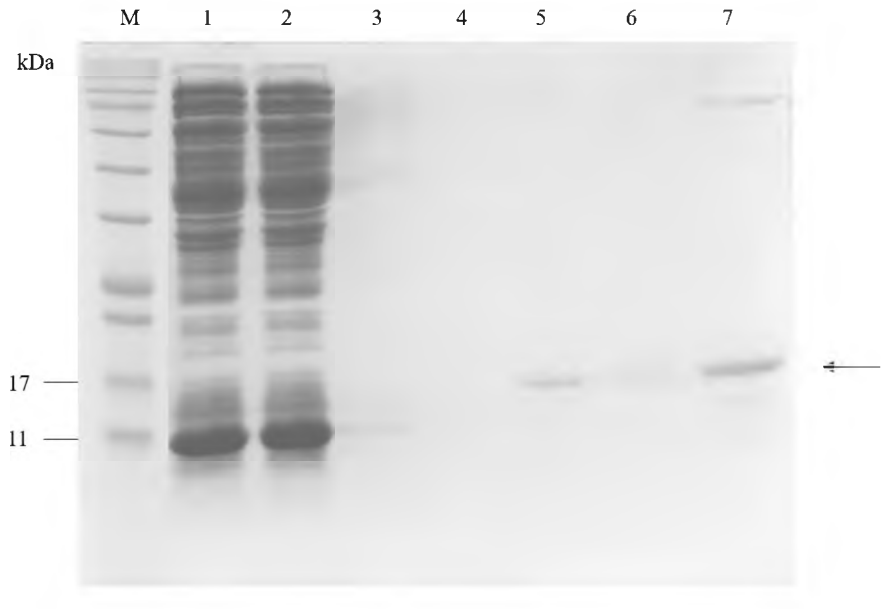

Figure 13: SDS-PAGE analysis of *Pf*Cdom protein purification samples.

A Ni-NTA column was used to purify *Pf*C-dom from a large-scale expression culture. The purification samples were analysed by SDS-PAGE on a 12 % gel. M: Molecular mass marker; Lane 1: Filtered lysate (soluble supernatant); Lane 2: Sample flow-through; Lane 3: Wash 1; Lane 4: Wash 2; Lane 5: Elution; Lane 6: Desalted *Pf*C-domain; Lane 7: Concentrated *Pf*C-domain.

Purification of hCdom and *Pf*Cdom using the Ni-NTA column was successful as observed by the presence of one distinct protein band in the elution fractions. Initial low concentrations of purified *Pf*Cdom lead to scaling up of the large-scale expression culture for purification to 500 millilitres. Scaling up the *Pf*Cdom expression culture still yielded very low protein concentration in the elution fraction – the faint band in Lane 5 – likely due to poor binding of the protein to the column (compare the *Pf*Cdom band in the applied cleared lysate, lane 1, and the flow-through in lane 2), thus protein concentration was performed. Protein concentration was successful as is evident from the distinct band observed in Lane 7 of Figure 13.

GST-mTPR2A and GST-*Pf*TPR2A proteins were purified using a prepared glutathione agarose column as described in Section 2.2.12. The protein was separated from the cell suspension by specific GST-glutathione interaction between the GST-tagged protein and the glutathione column matrix. The bound protein was eluted in three 1ml fractions using 10 mM glutathione. Results are shown in Fig. 14 and 15.

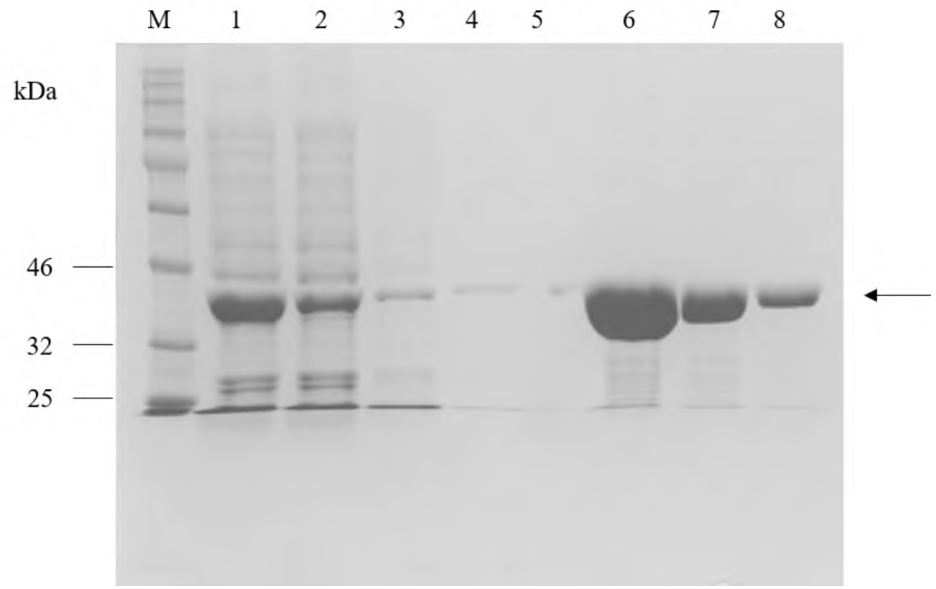

Figure 14: SDS-PAGE analysis of mTPR2A protein purification samples.

A glutathione-agarose column was used to purify mTPR2A from a large-scale expression culture. The purification samples were analysed by SDS-PAGE on a 12 % gel. M: Molecular mass marker; Lane 1: Filtered lysate (soluble supernatant); Lane 2: Sample flow-through; Lane 3: Wash 1; Lane 4: Wash 2; Lane 6: Elution 1; Lane 7: Elution 2; Lane 8: Elution 3. Lane 5: empty.

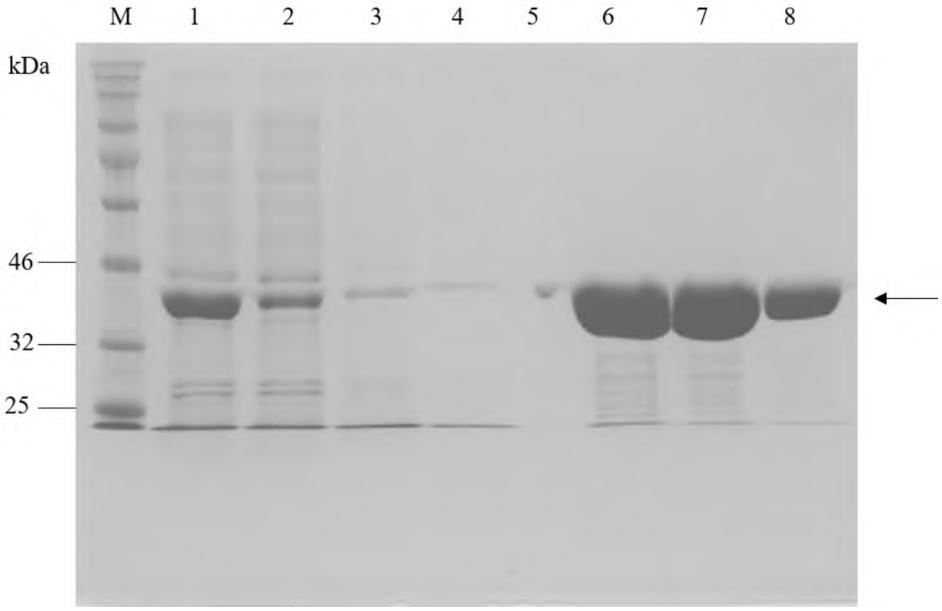

Figure 15: SDS-PAGE analysis of *Pf*TPR2A protein purification samples.

A glutathione-agarose column was used to purify *Pf*TPR2A from a large-scale expression culture. The purification samples were analysed by SDS-PAGE on a 12 % gel. M: Molecular mass marker; Lane 1: Filtered lysate (soluble supernatant); Lane 2: Sample flow-through; Lane 3: Wash 1; Lane 4: Wash 2; Lane 6: Elution 1; Lane 7: Elution 2; Lane 8: Elution 3. Lane 5: empty.

Purification of mTPR2A and *Pf*TPR2A confirms the results observed in small-scale expression of the two proteins which is that pGEX constructs have much higher expression levels than

pET constructs as evidenced by three very large bands in the elution fractions of the proteins and that binding to the column was also more efficient – there was a more pronounced decrease in the recombinant protein in the column flow-through (Fig. 14 and 15, lane 2) compared to the applied filtered lysate (lane 1). This may be due to the use of a longer purification column i.e. more glutathione-agarose was used to pack the column thus the column had a higher binding capacity. Very minor bands were observed in the elution fractions below the purified protein band, most likely as a result of protein overloading on the gels.

Development of the proposed assay format required a positive control (His-tagged GST) and background control (untagged GST). To prepare the latter, empty pGEX-4T-1 vector was used. pGEX-4T-1 was transformed into T7 Express *lysY E. coli* cells and large-scale protein expression and purification was performed as described for the GST-tagged TPR2A domains above (Fig. 16). His-tagged GST (hGST) was expressed form the pET-GST construct prepared in this study and purified according to the procedures described for the His-tagged C-domain constructs above (Fig. 17).

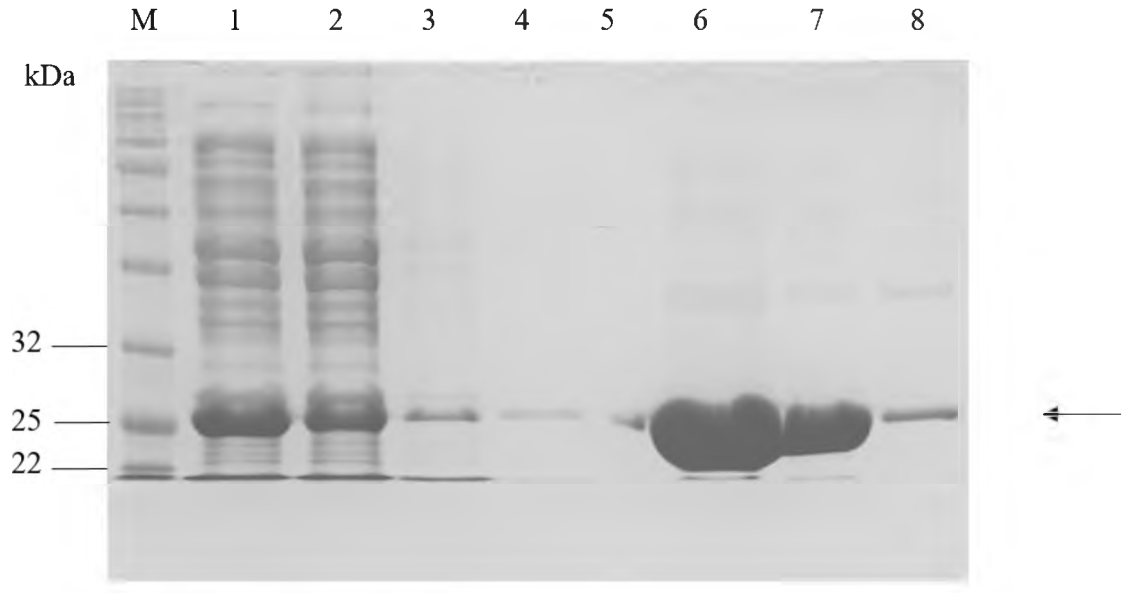

Figure 16: SDS-PAGE analysis of uGST protein purification samples from *E. coli* transformed with pGEX-4T-1.

A glutathione-agarose column was used to purify GST from a large-scale expression culture. The purification samples were analysed by SDS-PAGE on a 12 % gel. M: Molecular mass marker; Lane 1: Filtered lysate (soluble supernatant); Lane 2: Sample flow-through; Lane 3: Wash 1; Lane 4: Wash 2; Lane 6: Elution 1; Lane 7: Elution 2; Lane 8: Elution 3. Lane 5: empty.

GST from pET-GST was purified from a large-scale expression culture using a Ni-NTA column.

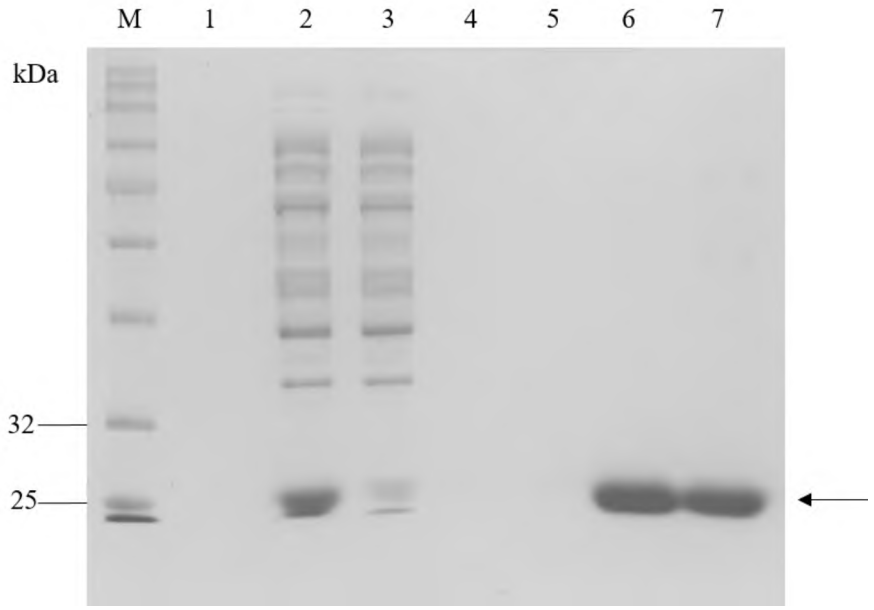

Figure 17: SDS-PAGE analysis of hGST protein purification samples from *E. coli* transformed with pET-GST.

A Ni-NTA column was used purify GST from a large-scale expression culture. The purification samples were analysed by SDS-PAGE on a 12 % gel. M: Molecular mass; Lane 2: Filtered lysate (soluble supernatant); Lane 3: Sample flow-through; Lane 4: Wash 1; Lane 5: Wash 2; Lane 6: Elution; Lane 7; Desalted protein. Lane 5: empty.

A much higher concentration of GST was obtained in untagged GST (pGEX-GST) purification than in His-tagged GST (pET-GST) purification. This is most likely also due to the high expression levels observed for pGEX constructs as well as the higher binding capacity of the glutathione-agarose column than that of the Ni-NTA column, as found previously for the TPR2A and Cdom purification experiments.

3.2.5. Final protein work-up and storage

The His-tagged purified protein eluates were passed through a size exclusion desalting column to remove the excess imidazole used in the affinity chromatography elution buffers and for buffer exchange into TBS (40 mM Tris, 150 mM NaCl, pH 7.4). Where necessary (*Pf*Cdom), proteins were concentrated using ultrafiltration columns. Protein concentrations were determined using a Bradford assay (Table 3) using a standard curve generated with BSA (Appendix E) and stored after adding glycerol to a final concentration of 40 % as aliquots at -20 °C with the exception of *Pf*Cdom which was stored at 4 °C.

Table 3: Concentration of the purified proteins determined using a Bradford assay.

Protein	Concentration (mg/ml)
hCdom	0.77
*Pf*Cdom	0.42
mTPR2A	2.1
*Pf*TPR2A	1.9
uGST	2.7
hGST	2.8

3.3 Discussion

Molecular cloning of human C-domain, GST, *Pf*TPR2A and mouse TPR2A was successful although confirmation by restriction digestion was troublesome and ineffective for hC-domain cloning. Failure to confirm hC-domain cloning by restriction digestion may have been due to the small size of the insert which results in poor gel resolution and low binding of ethidium bromide, causing poor visualisation, or possibly incomplete restriction enzyme digestion. PCR was performed to confirm the presence of the insert using the cloned construct as the template DNA and hC-domain specific primers (a method based on colony PCR). In colony PCR, positive clones are resuspended in water, heated at 100 ºC for 5 minutes for cell lysis and the released DNA is used in a PCR reaction using vector specific primers or insert specific primers (Singh and Jain, 2013). PCR is very sensitive which is a great advantage but also increases the risk of mispriming and contamination. For reliable results, the reaction was conducted in triplicate and hot start PCR was used which reduces the risk of mispriming and primer dimer formation thus the likelihood that the bands observed were the hC-domain insert and not contamination or primer dimers is high (Lebedev *et al.*, 2008). Ultimately all constructs were verified to be correct by DNA sequencing (Appendix D).

Bacterial expression systems are popular in recombinant protein expression as they are inexpensive, faster than eukaryotic systems and have well characterised genetics (Terpe, 2006). A variety of host strains and promoter systems are available (Stevens, 2000). *E. coli* is the most commonly used expression host (Terpe, 2006). In this study, T7 Express *lys*Y cells – a BL21 derivative – were used as the host strain. These cells have high transformation efficiency and a T7 RNA polymerase promoter system which utilises IPTG as an inducer, has very high expression levels and demonstrates tight control of induction (Stevens, 2000). The latter is due to basal 'leaky' expression of recombinant proteins being minimised by the presence of the *lys*Y vector in the host which expresses T7 lysozyme. T7 lysozyme binds to and inhibits T7

RNA polymerase from binding to the *lac* operon thus very little to no protein expression is observed in the absence of the IPTG inducer. The AT-rich genome of *P. falciparum* has made heterologous overexpression of *P. falciparum* genes in *E. coli* difficult due to rare codon usage (Matambo *et al.*, 2004). Codon optimisation is often used to solve this issue by using synonymous codon changes to increase protein production in recombinant protein expression by mimicking codon-bias (Mauro and Chappell, 2014). Alternatively, increasing the expression of underrepresented tRNAs in the host can be done but studies show this leads to protein misfolding and aggregation (Mauro and Chappell, 2014). In this study, the *P. falciparum* C-domain sequence was *E. coli* codon optimised and synthesized by Genscript, while the *Pf*TPR2A sequence cloned into pGEX-4T-1was human codon optimised. The latter was due to the fact that the template plasmid used for PCR and cloning of the sequence was originally prepared to express this domain in human cells in a parallel project. Although human and *E. coli* codon biases differ, it was expected that the higher GC-content of the humanised sequence would still enhance expression in *E. coli* compared to the native AT-rich *P. falciparum* sequence.

Small-scale expression of hC-domain, mTPR2A, hGST, and *Pf*TPR2A indicated the proteins were soluble and expressed at high levels at 37 °C after 3 hours thus very little optimization was required prior to scaling up. In addition, no leaky expression was seen in the uninduced small-scale expression cultures, confirming the tight regulation of expression in T7 *lysY E. coli*. However, small-scale expression of *Pf*C-domain showed no expression of the recombinant protein in the absence of glucose. Glucose is often added to the expression media when the recombinant protein is toxic (Rosano and Ceccarelli, 2014). Glucose prevents induction of the *lac* promoter by inactivating lactose permease, preventing lactose uptake and thus decreasing basal expression levels in uninduced cells (Rosano and Ceccarelli, 2014). This suggests that, although basal expression of the constructs in the absence of IPTG induction was not apparent in the Coomassie-stained SDS-PAGE gels, there was sufficient basal expression of *Pf*C-domain to cause *E. coli* toxicity. Addition of glucose to the expression media prevented toxic basal expression of *Pf*C-domain thus the protein was only expressed after addition of IPTG. Furthermore, unlike the other proteins, *Pf*C-domain was observed in both the soluble and insoluble fractions, indicating the formation of inclusion bodies (aggregates of insoluble, misfolded protein) as a result of overexpression. As a solution, Terpe (2006) suggests lowering expression levels by: decreasing expression temperature, using a weaker promoter or by lowering the concentration of IPTG used for induction. As an alternative, the insoluble protein

in the inclusion bodies may be solubilised by denaturants (e.g. urea, guanidinium hydrochloride or sarkosyl), followed by re-folding of the protein by removing the denaturants by dialysis (Singh and Panda, 2005). Another challenge faced in small-scale and large-scale expression of *Pf*C-domain was poor cell lysis. For reasons that are not clear, the freeze-thaw method and sonication that were used to successfully lyse hC-domain, mTPR2A hGST and *Pf*TPR2A expression cells was only partially successful for the cells expressing *Pf*C-domain. For better lysis, addition of lysozyme or multiple freeze-thaw cycles may be required as well as more sonication cycles although the heat generated by sonication may damage the protein (Islam *et al.*, 2017). Despite the presence of the *Pf*C-domain in inclusion bodies and sub-optimal lysis of the *E. coli* cells, it was thought that sufficient *Pf*C-domain was present in the soluble fraction to proceed to purification, thus alternative expression methods, solubilisation/re-folding of inclusion bodies and improved lysis were not attempted.

The recombinant proteins fused to affinity tags were expressed on a larger scale and used in one-step affinity column purification. The polyhistidine tag and GST tag are the most popular affinity tags for one-step purification due to their efficiency, ease of use and minimal effect on the structure and activity of the recombinant protein (Hunt, 2005). In this study, we observed efficient protein purification using the IMAC (Ni-NTA) and glutathione-agarose resins. Although purification of proteins with a His-tag is the most commonly used method, we observed much more efficient purification of proteins with the GST tag despite the slow binding kinetics of GST to glutathione-sepharose (Hunt, 2005). This is possibly a result of two factors: higher binding capacity of the glutathione resin compared to the Ni-NTA resin due to the use of a longer purification column and higher expression levels of pGEX constructs compared to pET constructs. The difference in the expression levels of pGEX and pET constructs implies pGEX is a much more efficient expression vector, or that the presence of the highly expressed GST-tag in front of the mTPR2A domains promotes high level soluble expression of the entire fusion protein.

Similar to the small-scale expression result, poor lysis of *Pf*C-domain expression cells was observed during preparation of the purification cell lysate despite the use of three lysis techniques – the freeze-thaw method, addition of lysozyme and sonication – otherwise effective on the other proteins. To solve this, additional freeze-thaw and sonication cycles may be necessary or alternatively the addition of lysis detergents such as Tween-20 or Triton-X-100 (Islam *et al.*, 2017). Low protein concentration was another major issue faced in *Pf*C-domain purification even after increasing the expression culture volume. A factor which likely

contributed to this was poor binding to the Ni-NTA affinity resin. This is suggested by the presence of significant amounts of *Pf*C-domain and human C-domain proteins in the flow-through after the cleared lysates had been applied to the respective columns. In the future, this may be remedied by using a larger resin volume, re-charging the column with nickel sulfate to ensure optimal nickel concentration in the column and/or re-applying the flow-through to the column to increase exposure of the His-tagged proteins to the affinity resin. Another contributing factor was the presence of *Pf*C-domain at higher concentrations in the insoluble fraction during small-scale expression studies. As mentioned previously, the insoluble protein fraction may potentially be used for *Pf*C-domain purification with prior solubilisation and refolding. However, purification of insoluble proteins is generally avoided due to the high concentration of denaturants required for solubilisation and poor protein recovery during refolding, thus expression optimisation to produce soluble protein is the favoured approach (Singh and Panda, 2005). Possible optimisation methods include: change in expression conditions such as temperature, aeration and inducer concentration, change in incubation time or possibly change in host strain (Terpe, 2006). Another general approach to improve protein solubility is changing the affinity tag as non-peptide affinity tags such as maltose-binding protein and thioredoxin are known as solubility enhancers. However, the assay format explored in this study required one of the interaction partners to be His-tagged (for binding to nickel-coated plates).

In conclusion, molecular cloning of GST, mammalian and *P. falciparum* C-domain and TPR2A genes into pET and pGEX expression vectors respectively was successful, apart from the *Pf*C-domain which required custom cloning by Genscript. Small-scale expression studies indicated the proteins were soluble although *Pf*C-domain is predominantly expressed in an insoluble form. Purification of the proteins yielded pure protein with sufficiently high concentrations with the exception of *Pf*C-domain. Poor lysis, insoluble protein expression and low protein concentration of *Pf*C-domain suggests further optimisation of expression conditions is required to improve protein yield. Nonetheless, sufficient purified *Pf*C-domain was obtained to proceed to assay optimisation. The purified proteins were stored in glycerol at -20 °C to maintain stability – except *Pf*C-domain which was stored at 4 °C – and were used to develop a C-domain-TPR2A interaction assay.

Chapter 4

Establishment and Optimisation of the C-domain - TPR2A interaction assay

4.1 Introduction

Widespread resistance to currently used antimalarial drugs has led to research into alternative drug targets with novel mechanisms of action to combat cross resistance and offer new therapeutic options (Shahinas *et al.*, 2013). Hsp90 is a well-studied heat shock protein found in most organisms including mammalian cells and parasites such as *P. falciparum* and *T. evansi* that helps cells sustain regular function under stress conditions by maintaining the functional conformation of regulatory proteins – proteins involved in assembly, trafficking and signal transduction – when they misfold and aggregate (Kim *et al.*, 2013). Hsp90 has over 200 known client proteins and is widely recognised as a potential drug target for cancer, infectious and neurodegeneration diseases (Shrestha *et al.*, 2016). Numerous studies have been conducted over the past 20 years in Hsp90 inhibitor development with moderate success (Wang *et al.*, 2016).

Recently the co-chaperone Hop has been targeted due to its functional relationship with Hsp90 (Shrestha *et al.*, 2016). Hop mediates the interaction of Hsp70 and Hsp90 by binding to the C-terminus of Hsp70 via its TPR1 and TPR2B domains and by binding to the C-terminus of Hsp90 via its TPR2A domain, allowing for the transfer of client proteins between the chaperones (Butler *et al.*, 2015). Targeting this protein-protein interaction disrupts the Hsp70-Hop-Hsp90 complex, thereby preventing Hsp90 client proteins from chaperoning (Sidera and Patsavoudi, 2014). A study conducted by Cortajarena *et al.* (2008) found a designed TPR domain mimic CTPR390+ bound to the Hsp90 C-terminal domain with higher affinity than the TPR2A domain of Hop, resulting in HER2 degradation and growth inhibition of BT474 breast cancer cells. Another study by Horibe *et al.* (2011) used a designed TPR peptide to inhibit Hsp90-Hop interaction, which induced cell death in multiple cancer cell lines but had no effect on normal cells. These studies indicate the Hsp90-Hop complex is a viable cancer drug target and development of small molecule inhibitors that target the complex is ongoing (Shrestha *et al.*, 2016).

The first *in vitro* HTS assay to screen for small molecule compounds that disrupt Hsp90-Hop interaction was developed by Yi and colleagues (2009) to screen for anti-cancer compounds. The assay is based on AlphaScreen technology in which an N-terminally biotin-tagged Hsp90

C-terminal peptide attached to streptavidin coated donor beads and an N-terminally His-tagged TPR2A peptide attached to nickel-chelated acceptor beads are incubated together (Yi *et al.*, 2009). The donor beads and acceptor beads are brought together by biotin-Hsp90 - $(His)_6$-TPR2A interaction and upon excitation at 680 nm, emission at 520-620 nm occurs if the donor and acceptor beads are within 200 nm of each other (Yasgar *et al.*, 2016; Yi *et al.*, 2009). The assay identified 34 'hit' compounds which require further characterisation. Using this information we hypothesise the Hsp90-Hop complex in *P. facliparum* is potentially a viable drug target in malaria treatment. Development of a plate-based assay for this interaction would enable the screening of compound libraries for potential inhibitors.

The 4 biochemical assays commonly used in PPI inhibitor screening – fluorescence polarization, FRET, ELISA-based assays and AlphaScreen assays – can be used for primary high-throughput screening of PPI inhibitors in 96-, 384- and sometimes 1536-well plates (Arkin *et al.*, 2012). Although relatively simple to set up and often highly sensitive, these assays frequently face interference, high cost (AlphaScreen and FRET) and dye orientation issues (Arkin *et al.*, 2012). In this study we developed a novel PPI screening assay focused on *P. falciparum* Hsp90-Hop interaction that can be used in HTS of small molecule compounds. The assay is simple to set up, efficient and relatively cost effective. The assay is a plate-based ELISA-style assay in which His-tagged Hsp90 C-domain is immobilised on a Ni-NTA-coated plate as a result of the high affinity of Ni-NTA for the polyhistidine tag (electron donor groups on the histidine imidazole ring form coordination bonds with nickel) (Terpe, 2003). GST-tagged TPR2A is added to the plate and GST activity is measured using a colorimetric enzyme assay after washing the plate. GST activity is directly proportional to the presence of TPR2A as a result of C-domain-TPR2A interaction as shown in Figure 18 below.

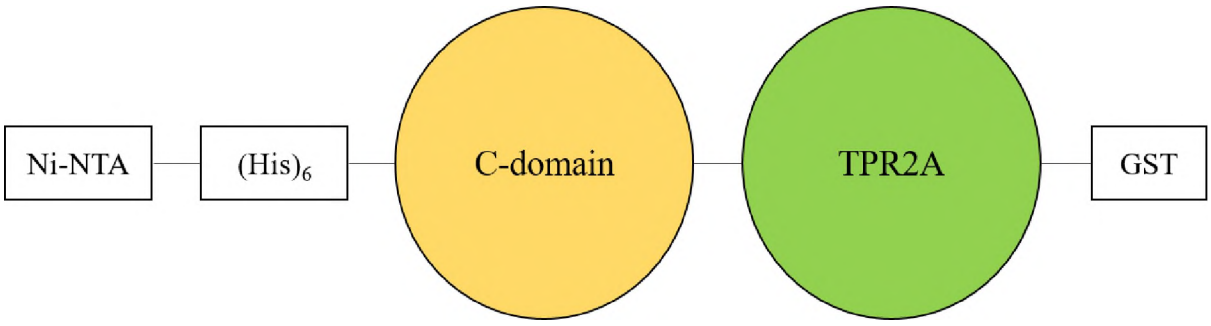

Figure 18: Schematic diagram of the C-domain-TPR2A interaction GST assay.

GST activity was determined by the method described by Habig *et al.* (1974) in which reduced L-glutathione conjugation to CDNB substrate is catalysed by GST resulting in the formation of a GS-DNB conjugate ([*S*-2,4-dinitrophenyl]-GSH) which absorbs at 340 nm.

$$\text{GSH} + \text{CDNB} \xrightarrow{\text{GST}} \text{GS-DNB conjugate} + \text{HCl}$$

GST activity is thus directly proportional to the rate of GS-DNB product formation which is determined by absorbance at 340 nm (Dhar *et al.*, 2003). His-tagged GST (hGST) and untagged GST (uGST) were used as positive and negative controls respectively to confirm binding of His-tagged proteins to the Ni-NTA plate and functionality of the GST colorimetric assay (hGST), as well as to control for non-specific binding of GST to the plate and background absorbance readings produced by the GST assay reagent (uGST) (Figure 19).

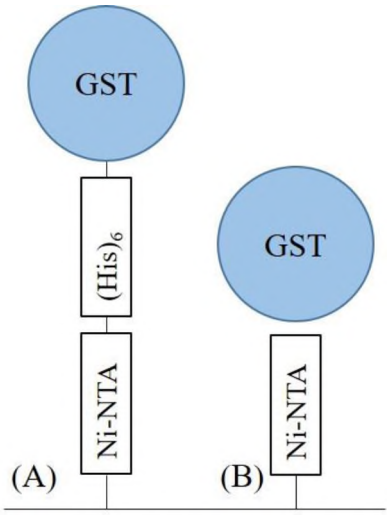

Figure 19: Schematic diagram of the GST positive and negative controls.

(**A**) GST positive control – His-tagged GST binds to the Ni-NTA plate and hence a GST signal is observed upon addition of GST substrate. (**B**) GST negative control – to control for non-specific binding of GST to the plate and background signals produced by the GST assay.

The aims of the work described in this chapter were to:

i) Establish an initial GST colorimetric assay using the hGST and uGST controls to confirm, firstly, the conditions required to bind His-tagged proteins to the Ni-NTA plate and, secondly, that the GST enzyme assay is capable of robustly detecting GST immobilised on the plate vs. background signals;

ii) Establish and optimise a *P. falciparum* C-domain-TPR2A interaction GST assay as well as mammalian C-domain-TPR2A interaction GST assay;

iii) Establish protocols for preparing custom Ni-NTA plates and GST enzyme assay reagents and compare these with commercial plates and GST assay kits;

iv) Determine assay Z'-factor values as a measure of assay robustness;

v) Perform inhibition studies using TPR peptides to demonstrate, in principle, that the assay format can be used to detect Hsp90-Hop interaction inhibitors;

vi) Explore an alternative assay format in which GST-tagged TPR2A is immobilised on glutathione-coated plates and capture of His-tagged C-domain detected using a nickel-HRP conjugate and a colorimetric HRP substrate.

4.2 Results

4.2.1 Initial GST assay

Binding of His-tagged proteins to the commercial Ni-NTA HisSorb™ plates (Qiagen, Germany) and GST enzyme assay efficiency was tested using hGST and uGST as a positive and negative controls. A 2-fold serial dilution (1 µM starting concentration) of hGST and uGST was added to a Ni-NTA plate and incubated at room temperature with gentle shaking for 1 hour. The plate was washed and GST substrate mastermix (containing CDNB and reduced L-glutathione) was added to each well. Absorbance was read immediately at 340 nm over 30 minutes. To control for background signals, readings obtained from wells containing TBS-1% BSA (dilution and washing buffer) were subtracted from the sample readings. GST assay progress curves were generated using GraphPad Prism software.

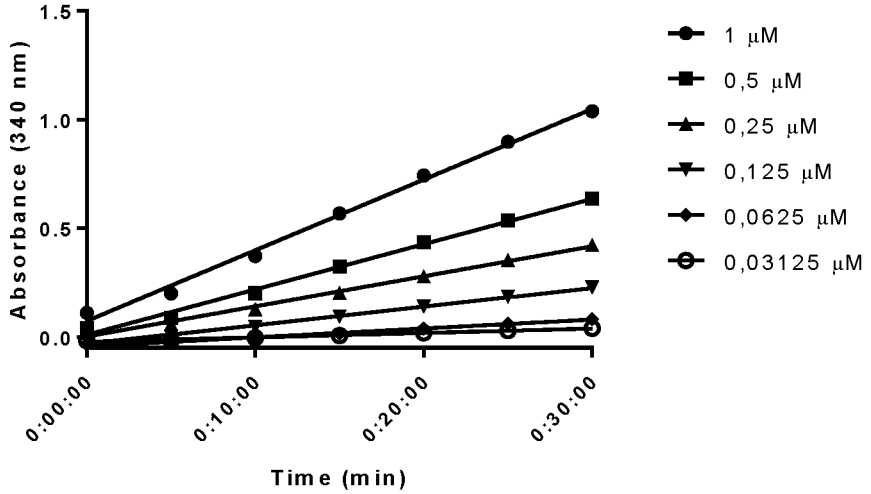

Figure 20: His-tagged GST Ni-NTA plate binding capacity.

The GST assay was performed at various concentrations of hGST. The change in absorbance of the GS-DNB conjugate was measured over 30 minutes at 340 nm. Absorbance readings were corrected for TBS-1% BSA background signal.

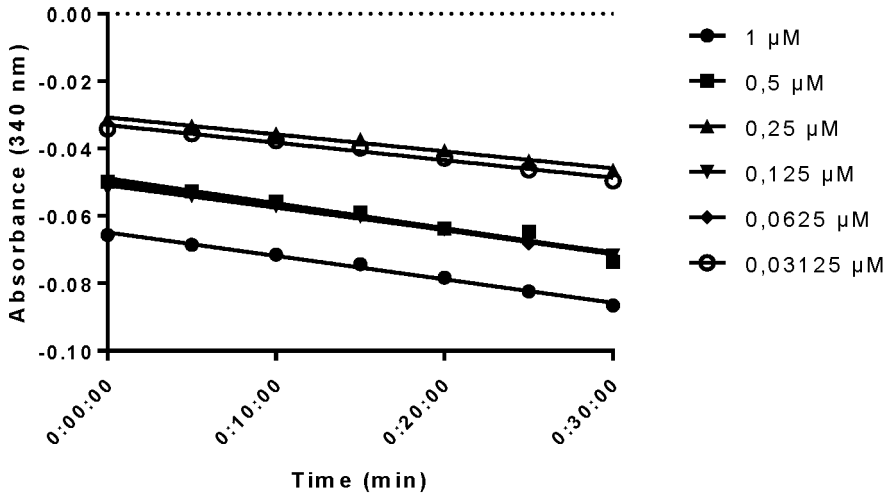

Figure 21: Untagged GST Ni-NTA plate binding capacity.

The GST assay was performed at various concentrations of uGST. The change in absorbance of the GS-DNB conjugate at 340 nm was measured over 30 minutes. Readings were corrected for TBS-1% BSA background signal.

Untagged GST (uGST) was used as a negative control to determine non-specific binding of GST. The results in Figures 20 and 21 indicate GST bound in a concentration-dependent manner to the Ni-NTA plate via the His-tag as expected and no non-specific binding of GST occurred. The results also show the GST assay reaction produced a strong signal which decreased with decrease in GST concentration.

To determine the robustness with which GST plate-binding can be detected compared to the negative control, the assay was repeated using three technical repeats (wells per sample) and the Z'-factor calculated. The Z'-factor is an index for assay quality established by Zhang *et al.* (1999) determined by the following equation:

$$Z' = 1 - \frac{3(\sigma p + \sigma n)}{|\mu p - \mu n|}$$

*σp-standard deviation of positive control; σn-standard deviation of negative control; µp-mean of positive control; µn-mean of negative control

Assays with Z'-factor values ≥ 0.5 are considered 'suitable' as screening assays and capable of confidently discriminating between positive and background signals. The closer the value is to 1 (the maximum attainable value), the bigger the separation between the positive and negative controls (Zhang *et al.*, 1999).

The GST assay was performed using hGST as the positive control and uGST as the negative control. Absorbance was read at 340 nm over 30 minutes incubation with the GST enzyme substrate.

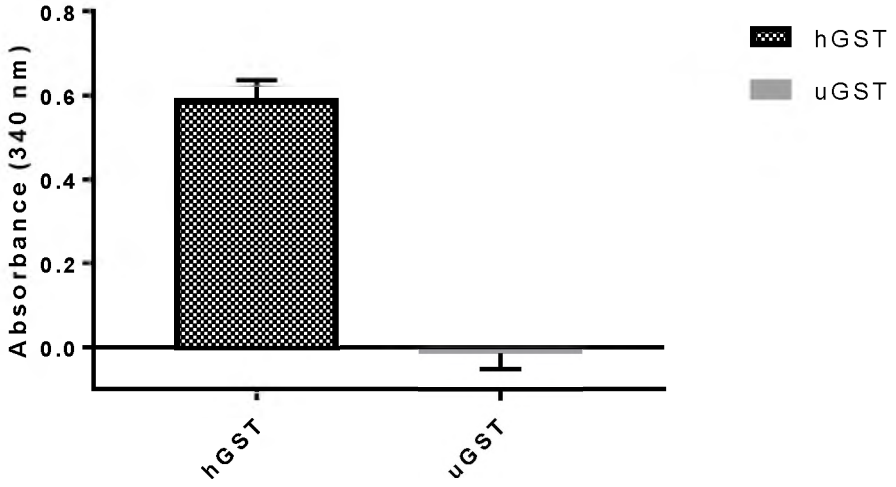

Figure 22: GST assay Z'-factor experiment.

The GST assay was performed with 1 µM hGST and 1 µM uGST. Absorbance of the GS-DNB conjugate was measured at 340 nm over 30 minutes. The absorbance readings were corrected for those obtained in wells incubated with buffer (TBS-1% BSA) alone. The readings obtained at 30 minutes are shown. p-value < 0.001.

Table 4: Z'-factor values at various time points of the GST assay.

Time (min)	Z'-factor
15	0.67
20	0.71
25	0.73
30	0.74

The results in Figure 22 and Table 4 showed the difference between the hGST signal and the uGST signal is statistically significant and produces Z'-factor values after 15 minutes which are usable in screening experiments.

4.2.2 *P. falciparum* C-domain-TPR2A interaction assay

P. falciparum C-domain-TPR2A interaction in the Ni-NTA plate was determined by performing the GST assay. A 2-fold serial dilution (1 µM starting concentration) of His-tagged *Pf*C-domain and GST-tagged *Pf*TPR2A (prepared as described in Chapter 3) was added to the Ni-NTA plate at equimolar concentrations and incubated at room temperature with gentle

shaking for 1 hour. The plate was washed and substrate mastermix was added to each well. Absorbance was read at 340 nm over 30 minutes. To control for background signals, readings obtained from wells containing TBS-1 % BSA (dilution buffer) were subtracted from the sample readings (Fig. 23).

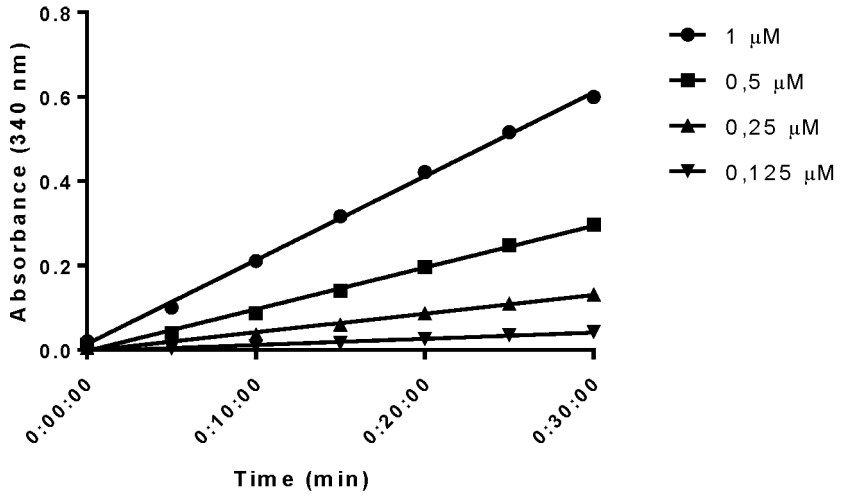

Figure 23: *Pf*C-domain-*Pf*TPR2A interaction GST assay at equimolar concentrations.

The GST assay was performed on a 2-fold serial dilution of *Pf*Cdomain and *Pf*TPR2A at equimolar concentrations. Absorbance of the GS-DNB conjugate was measured at 340 nm over 30 minutes. Readings were corrected for TBS-1% BSA background signal.

To determine to what extent non-specific binding of *Pf*TPR2A to the plate contributed to the signal produced, the assay was performed by using only *Pf*TPR2A (thus, in the absence of *Pf*C-domain). A 2-fold serial dilution of *Pf*TPR2A (1 µM starting concentration) was incubated in a plate, washed and GST substrate mastermix assed. Absorbance was read at 340 nm over 30 minutes (Fig. 24).

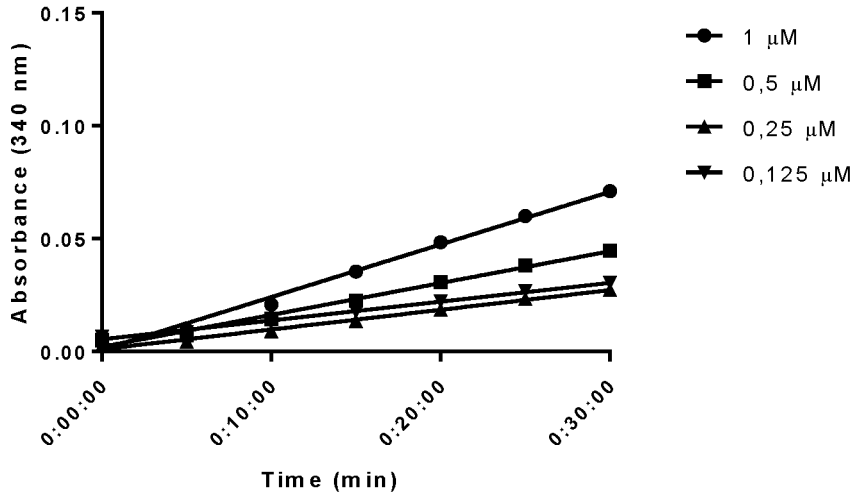

Figure 24: Non-specific binding of *Pf*TPR2A at different concentrations.

The GST assay was performed on a 2-fold serial dilution of *Pf*TPR2A. Absorbance of the GS-DNB conjugate was measured at 340 nm over 30 minutes. Readings were corrected for TBS-1% BSA background signal.

The results showed that, unlike untagged GST (Fig. 21), the GST-*Pf*TPR2A protein displayed some concentration-dependent binding to the plate (Fig. 24) and would thus be a more appropriate background control than wells without protein for future experiments. Nonetheless, readings obtained with equimolar mixtures of *Pf*C-domain and *Pf*TPR2A (Fig. 23) were considerably higher than the corresponding readings obtained with *Pf*TPR2A alone. This result was significant for two reasons: i) It suggests direct binding of *Pf*Hsp90 to *Pf*Hop *in vitro* (to our knowledge, this has not been demonstrated before using purified proteins); ii) It suggests that the proposed novel assay format can be used to detect *Pf*C-domain-*Pf*TPR2A domain interaction.

The GST assay was repeated with 1 µM *Pf*C-domain and various concentrations of *Pf*TPR2A to determine the C-domain-TPR2A concentration ratio that gives the optimal interaction signal, considering the tendency of the GST-tagged *Pf*TPR2A domain to bind non-specifically to the plate. Absorbance was read at 340 nm over 30 minutes. Readings obtained in wells containing *Pf*TPR2A alone were subtracted from those containing the *Pf*Cdomain-*Pf*TPR2A mixtures (Fig. 25).

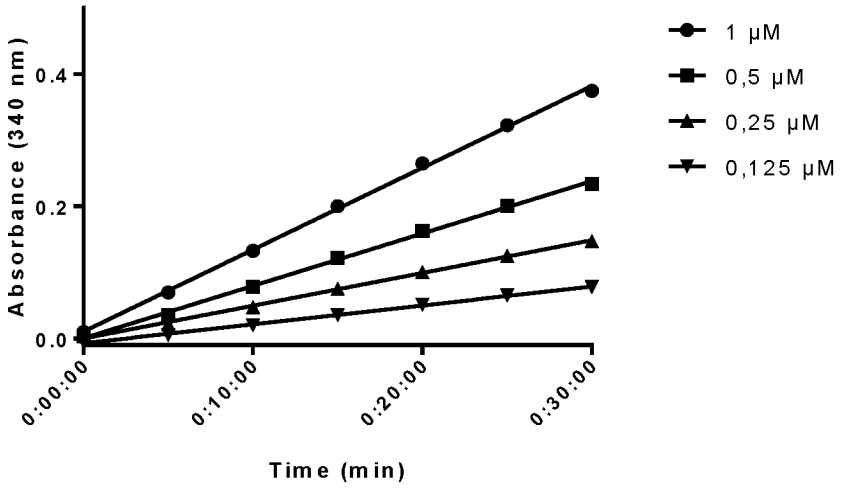

Figure 25: *Pf*C-domain-*Pf*TPR2A interaction GST assay at varying *Pf*TPR2A concentrations.

The GST assay was performed with 1 µM *Pf*C-domain and various concentrations of *Pf*TPR2A. Absorbance of the GS-DNB conjugate was measured at 340 nm over 30 minutes. Readings were corrected for TBS-1% BSA background signal and *Pf*TPR2A non-specific binding.

The results in Figure 25 showed a decreasing C-domain-TPR2A interaction signal with decreasing *Pf*TPR2A concentrations. The highest signal was observed at 1 µM of each protein, suggesting future assays should be performed at 1 µM in a 1:1 concentration ratio.

To determine the robustness with which the *Pf*Cdomain-*Pf*TPR2A interaction can be detected at a 1:1 molar ratio compared to the TPR2A background signal, a Z'-factor analysis was carried out for the 30 minute data points. The readings obtained at the 30 minute time-point and Z'-factor analysis are shown in Fig. 26 and Table 5, respectively.

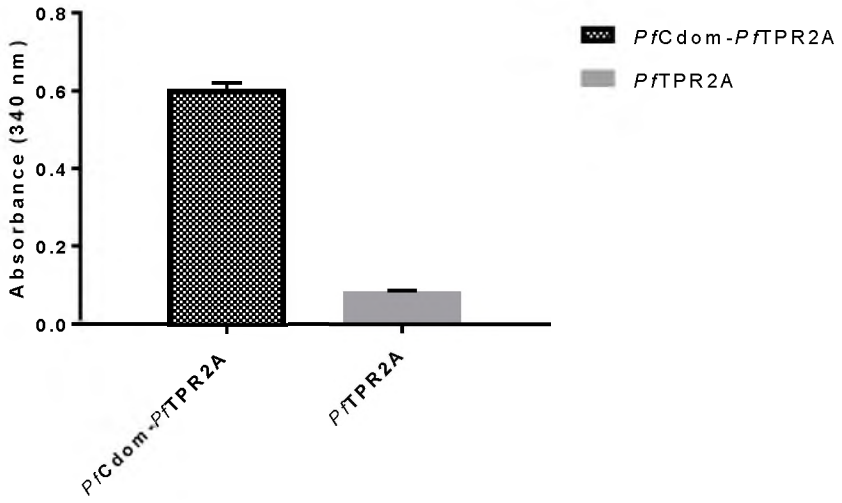

Figure 26: *Pf*C-domain-*Pf*TPR2A interaction GST assay - control for *Pf*TPR2A background signal.

The GST assay was performed with 1 µM *Pf*C-domain and 1 µM *Pf*TPR2A, and 1 µM *Pf*TPR2A. Absorbance of the GS-DNB conjugate was measured at 340 nm over 30 minutes. The final reading was used – corrected for TBS-1% BSA background signal. p-value < 0.0001.

Table 5: Z'-factor values at various time points of the *P. falciparum* C-domain-TPR2A interaction GST assay.

Time (min)	Z'-factor
15	0.79
20	0.85
25	0.89
30	0.90

The results in Figure 26 and Table 5 showed there was good separation between the *Pf*C-domain-*Pf*TPR2A interaction signal and the *Pf*TPR2A background signal indicating the assay signal observed is mostly a result of *Pf*C-domain interaction with *Pf*TPR2A and not *Pf*TPR2A non-specific binding. The Z'-factor values in Table 5 suggest the assay values obtained after 15 minutes are usable for accurate screening.

An additional control experiment that needed to be performed was to confirm that the observed interaction of *Pf*C-domain and *Pf*TPR2A was due to the binding of the two *Pf* domains to each other and not due to interaction of the *Pf*C-domain with the GST tag of the TPR2A domain. The assay was thus performed using the *Pf*C-domain-*Pf*TPR2A interaction as the positive reaction and *Pf*C-domain incubated with untagged GST (uGST) as the negative control.

Absorbance was read at 340 nm over 30 minutes. The readings obtained at the 30 minute time-point and Z'-factor analysis are shown in Fig. 27 and Table 6, respectively.

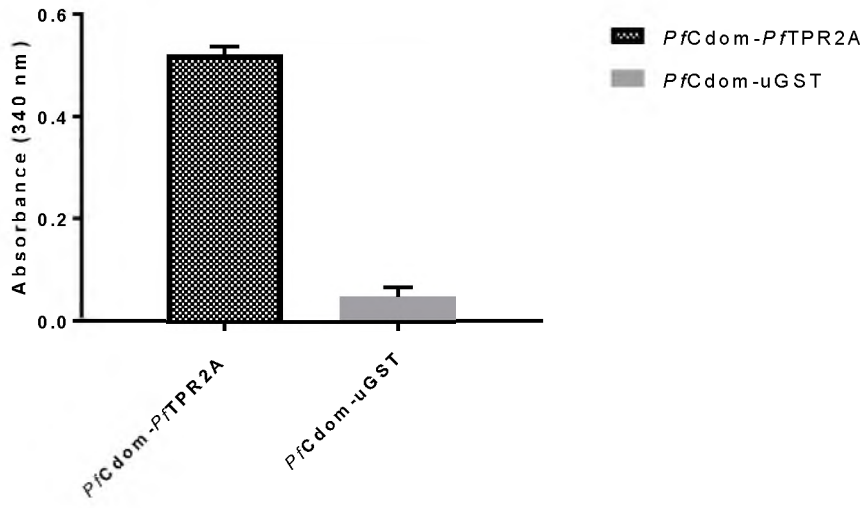

Figure 27: *Pf*C-domain-*Pf*TPR2A interaction GST assay - control for *Pf*C-domain-uGST interaction.

The GST assay was performed with 1 µM *Pf*C-domain + 1 µM *Pf*TPR2A, and 1 µM *Pf*C-domain + 1 µM uGST. Absorbance of the GS-DNB conjugate was measured at 340 nm over 30 minutes. The final reading was used – corrected for TBS-1% BSA background signal and non-specific binding of *Pf*TPR2A (in the case of *Pf*C-domain-*Pf*TPR2A) and uGST (in the case of *Pf*C-domain -uGST). p-value < 0.0001.

Table 6: Z'-factor values at various time points of the *P. falciparum* C-domain-TPR2A and C-domain-uGST interaction GST assay.

Time (min)	Z'-factor
15	0.64
20	0.72
25	0.78
30	0.79

The results in Figure 27 show a clear, statistically significant difference between the assay reaction and the negative control i.e. the observed interaction signal is mostly a result of C-domain-TPR2A interaction and not GST non-specific binding. A low signal was observed for *Pf*C-domain-uGST interaction. The Z'-factor values in Table 6 suggest the assay values obtained after 15 minutes are usable for accurate screening.

4.2.3 Mammalian C-domain-TPR2A interaction assay

Having determined that the GST-based plate assay can be used to detect *Pf*C-domain-*Pf*TPR2A interaction, the corresponding mammalian C-domain-TPR2A interaction assay was set up as a screening control. In compound screening, ideal compounds should be effective against the *P. falciparum* C-domain-TPR2A interaction and have no effect on the mammalian C-domain-TPR2A interaction. Moreover, given the interest in Hsp90-Hop interaction for cancer therapy, the assay may be used as a novel means to screen for potential anti-cancer agents. The GST assay was performed on a 2-fold serial dilution of human His-tagged C-domain and murine GST-tagged TPR2A (1 µM starting concentration) at equimolar concentrations. The samples were incubated at room temperature with gentle shaking for 1 hour. The plate was washed and substrate mastermix was added to each well. Absorbance was read at 340 nm over 30 minutes. To control for background signals, readings obtained from wells containing TBS-1 % BSA (dilution buffer) were subtracted from the sample readings (Fig. 28).

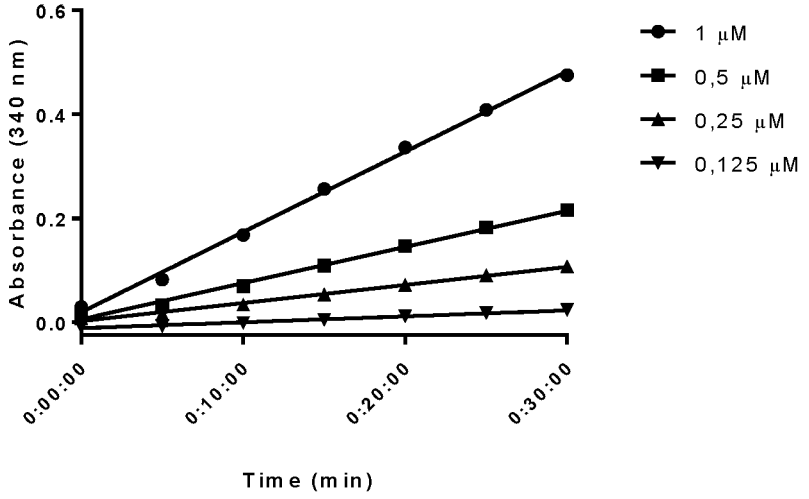

Figure 28: Mammalian C-domain-TPR2A interaction GST assay at equimolar concentrations.

The GST assay was performed on a 2-fold serial dilution of hC-domain and mTPR2A at equimolar concentrations. Absorbance of the GS-DNB was measured at 340 nm over 30 minutes. Readings were corrected for TBS-1% BSA background signal.

Non-specific binding of mTPR2A was determined by performing the GST assay on only mTPR2A. A 2-fold serial dilution of mTPR2A (1 µM starting concentration) was used. Absorbance was read at 340 nm over 30 minutes (Fig. 29).

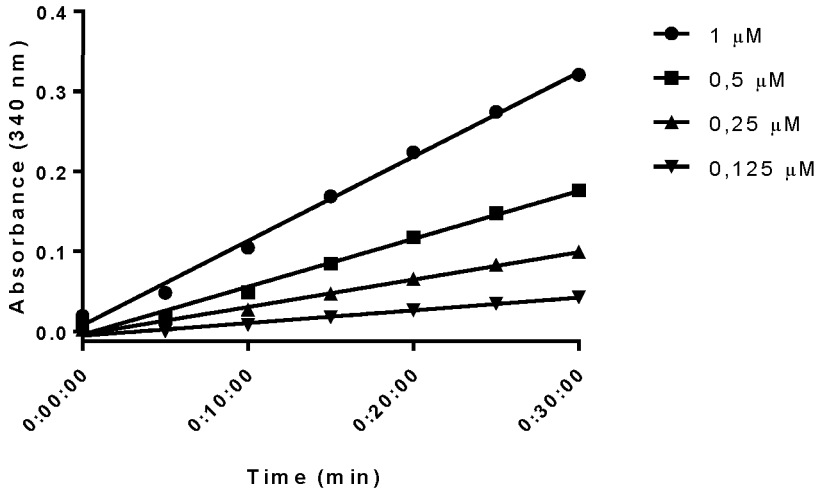

Figure 29: Non-specific binding of mTPR2A at different concentrations.

The GST assay was performed on a 2-fold serial dilution of mTPR2A. Absorbance of the GS-DNB was measured at 340 nm over 30 minutes. Readings were corrected for TBS-1% BSA background signal.

The results in Figure 28 show relatively high binding levels of hC-domain to the Ni-NTA plate which can be inferred from the GST signal observed as result of mTPR2A binding. However, similar to the *Pf*C-domain-*Pf*TPR2A interaction assay, relatively high non-specific binding of mTPR2A was observed (Figure 29) indicating any future assays must be corrected for mTPR2A non-specific binding to obtain an accurate C-domain-TPR2A interaction signal.

As for the *P. falciparum* assay, the GST assay was performed with 1 µM hC-domain and various concentrations of mTPR2A to determine the C-domain-TPR2A concentration ratio that gives the best signal and the lowest TPR2A background signal. Absorbance was read at 340 nm over 30 minutes and hC-domain-mTPR2A readings corrected for background by subtracting readings obtained with mTPR2A alone (Fig. 30)

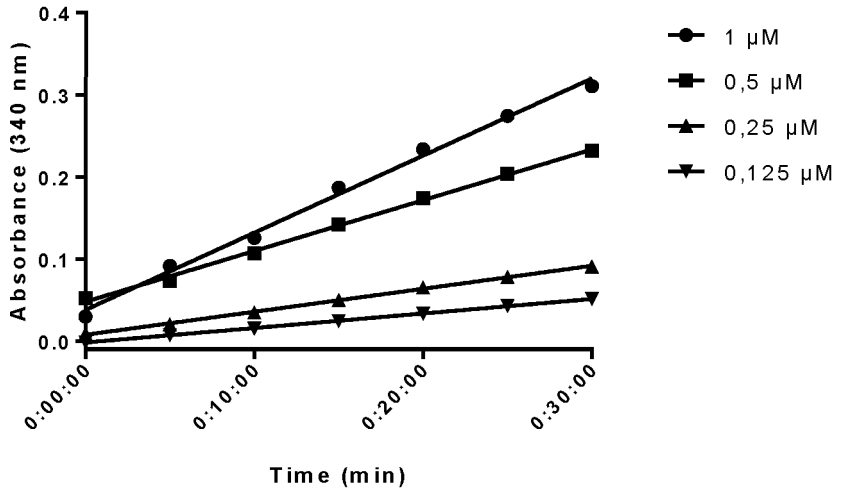

Figure 30: Mammalian C-domain-TPR2A interaction GST assay at different mTPR2A concentrations.

The GST assay was performed with 1 µM hC-domain and various concentrations of mTPR2A. Absorbance of the GS-DNB conjugate was measured at 340 nm over 30 minutes. Readings were corrected for TBS-1% BSA background signal and mTPR2A non-specific binding.

The results show the highest interaction signal was obtained at 1 µM hC-domain and 1 µM mTPR2A despite the high non-specific binding signal observed in Figure 29 at 1 µM MTPR2A alone. Although a relatively small signal difference was observed between the 1:1 ratio and the 1:0.5 ratio, the mammalian C-domain-TPR2A interaction signals were generally lower than the *P. falciparum* C-domain-TPR2A interaction signals (a direct comparison was made in later experiments – section 4.2.4) thus the ratio giving the highest signal (1:1) was used for future assays to allow distinct differences to be observed when testing potential inhibitors.

To confirm that the assay format was able to robustly detect hC-domain-mTPR2A interaction, despite the high non-specific binding of mTPR2A to the plate, a Z'-factor analysis was performed for the 30 minute time-point using a 1:1 ratio of the two interaction partners. The readings obtained at the 30 minute time-point and Z'-factor analysis are shown in Fig. 31 and Table 7, respectively.

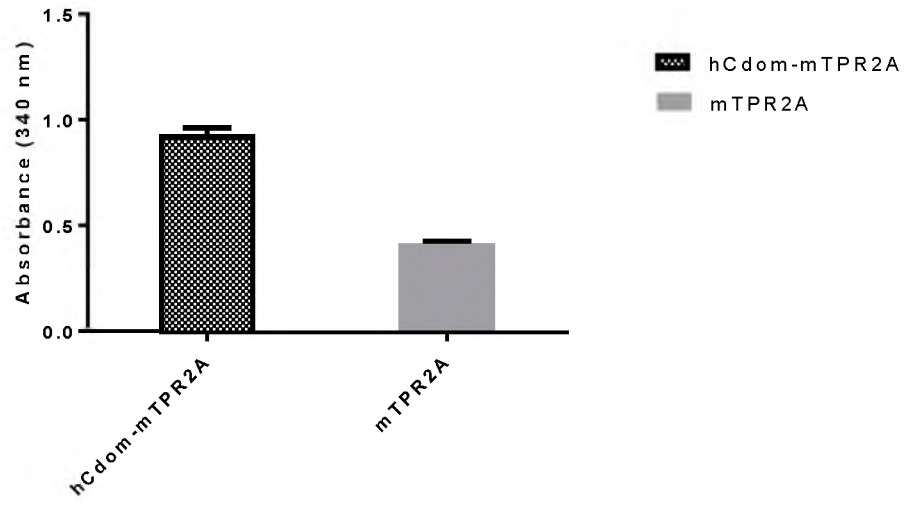

Figure 31: hC-domain-mTPR2A interaction GST assay - control for mTPR2A background signal.

The GST assay was performed with 1 µM hC-domain + 1 µM mTPR2A, and 1 µM mTPR2A. Absorbance of the GS-DNB conjugate was measured at 340 nm over 30 minutes. The final reading was used – corrected for TBS-1% BSA background signal. p-value < 0.001.

Table 7: Z'-factor values at various time points of the mammalian C-domain-TPR2A interaction GST assay.

Time (min)	Z'-factor
15	0.32
20	0.49
25	0.72
30	0.76

The results in Figure 31 and Table 7 showed there was good separation between the hC-domain-mTPR2A interaction signal and the mTPR2A background signal suggesting the assay signal observed is mostly as a result of hC-domain interaction with mTPR2A and not mTPR2A non-specific binding. The Z'-factor values in Table 7 suggest only the assay values obtained after 25 minutes are usable for accurate screening.

As before, the Z'-factor of the mammalian C-domain-TPR2A interaction assay was determined using the hC-domain-mTPR2A interaction as the positive reaction and hC-domain-uGST as the negative control in the GST assay, to confirm that the interaction signal was not due to binding of the human C-domain to GST as opposed to mTPR2A. Absorbance was read at 340

nm over 30 minutes. The readings obtained at the 30 minute time-point and Z'-factor analysis are shown in Fig. 32 and Table 8, respectively.

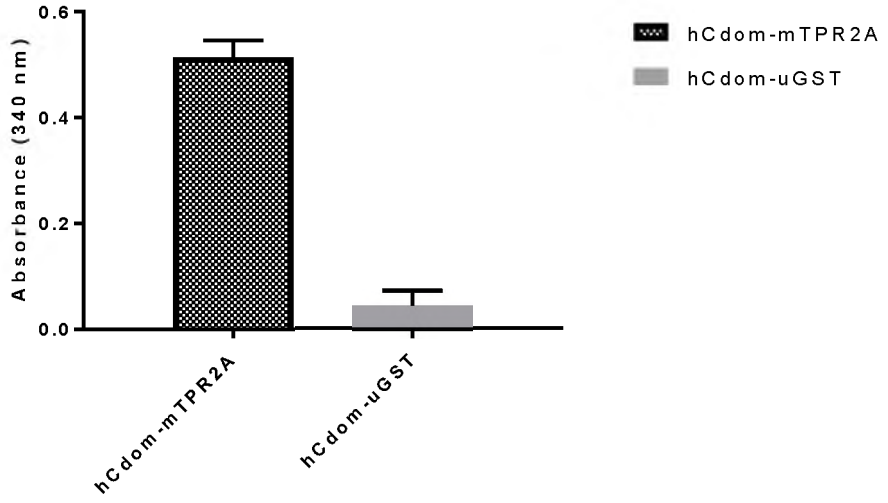

Figure 32: Mammalian C-domain-TPR2A interaction GST assay – control for hC-domain-uGST interaction.

The GST assay was performed with 1 µM hC-domain +1 µM mTPR2A and 1 µM hC-domain + 1 µM uGST. Absorbance of the GS-DNB conjugate was measured at 340 nm over 30 minutes. The final reading was used – corrected for TBS-1% BSA background signal and non-specific binding of mTPR2A (in the case of hC-domain-mTPR2A) and uGST (in the case of hC-domain-uGST). p-value <0.001.

Table 8: Z'-factor values at various time points of the mammalian C-domain-TPR2A and C-domain-uGST interaction GST assay.

Time (min)	Z'-factor
15	0.11
20	0.44
25	0.55
30	0.62

The results in Figure 32 show a clear, statistically significant difference between the assay reaction and the negative control. Similar to the *P. falciparum* C-domain-uGST interaction, a low signal was observed for the hC-domain-uGST interaction. Very low Z'-factor values were observed for the hC-domain-mTPR2A interaction assay at earlier time points suggesting the signals obtained are only produce accurate screening results after 25 minutes where the Z'-factor is higher than 0.5. In conclusion, the results suggest that, as with the *P. falciparum* domains, the novel assay format described here can detect the interaction of mammalian Hsp90 C-domains and Hop TPR2A domains.

4.2.4 Comparison of *P. falciparum* and mammalian C-domain-TPR2A interaction

Earlier experiments to establish the interaction assays had suggested that the *P. falciparum* interaction yielded higher signals than that obtained with the mammalian domains. Mammalian and *P. falciparum* C-domain-TPR2A interaction signals were therefore directly compared. The GST assay was performed at 1 µM of each protein. The proteins were incubated in the Ni-NTA plate at room temperature with gentle shaking for 1 hour. The plate was washed and substrate mastermix was added to each well. Absorbance was read at 340 nm after 30 minutes (Fig. 33)

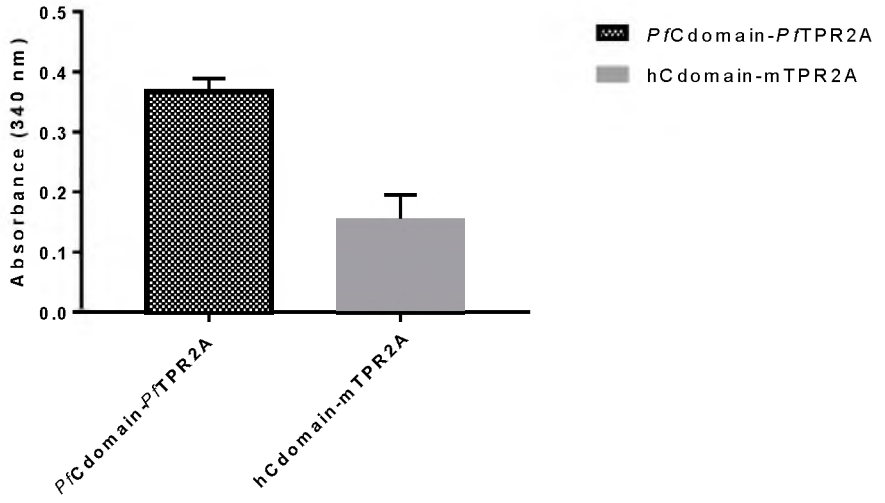

Figure 33: Comparison of the *P. falciparum* and mammalian C-domain-TPR2A interaction signals.

The GST assay was performed to compare hC-domain-mTPR2A and *Pf*C-domain-*Pf*TPR2A interaction signals. Absorbance of the GS-DNB conjugate was measured at 340 nm after 30 minutes. Readings were corrected for TBS-1% BSA background signal and TPR2A non-specific binding. p-value < 0.01.

The results suggest C-domain-TPR2A interaction is more efficient for the *P. falciparum* proteins. The *P. falciparum* interaction signal is more than double the mammalian interaction signal at equimolar concentrations, suggesting *Pf*TPR2A has a higher affinity for *Pf*C-domain than mTPR2A has for hC-domain.

4.2.5 Determining C-domain-TPR2A affinity

Having established that the *P. falciparum* proteins appear to interact with a higher affinity than the mammalian proteins, an interesting question was to what extent the domains can cross-react. The affinity of the *Pf*C-domain and hC-domain for their opposite TPR2A counterparts was determined by repeating the GST assay with hC-domain + *Pf*TPR2A and *Pf*C-domain + mTPR2A. Absorbance was read at 340 nm after 30 minutes (Fig. 34).

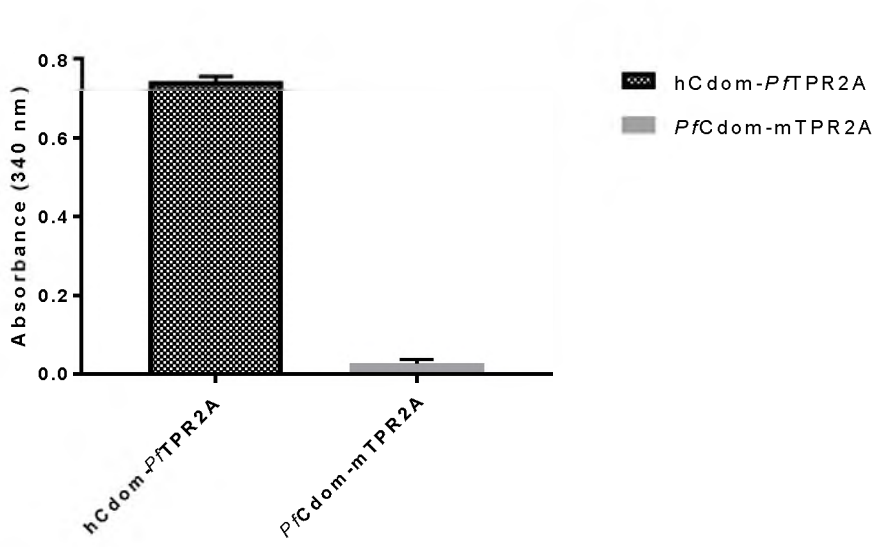

Figure 34: hC-domain-*Pf*TPR2A and *Pf*C-domain-mTPR2A interaction.

GST assays were performed in parallel with 1 µM hC-domain + 1 µM *Pf*TPR2A and 1 µM *Pf*C-domain + 1 µM mTPR2A. Absorbance of the GS-DNB conjugate was measured at 340 nm after 30 minutes. Readings were corrected for TBS-1% BSA background signal and TPR2A non-specific binding. p-value < 0.0001

Figure 34 suggests *Pf*TPR2A binds as effectively to the hC-domain as it binds to *Pf*C-domain suggesting the protein doesn't have high specificity for its C-domain binding partner. Conversely, the low GST signal observed for *Pf*C-domain-mTPR2A indicates mTPR2A has very high specificity for its C-domain binding partner.

4.2.6 Comparing kit and lab-prepared GST assay components

An important aspect of assay development is cost-efficiency. In initial assay development experiments, GST enzyme activity was detected using a commercial colorimetric GST assay kit (Sigma-Aldrich). We prepared GST assay reagents based on the kit protocol and performed parallel GST assays using the prepared reagents and the kit reagents. The GST assay was performed as previously described using the *P. falciparum* proteins. Absorbance was measured at 340 nm and the readings obtained were corrected for TBS-1 % BSA background signal and non-specific binding of TPR2A (Fig. 35).

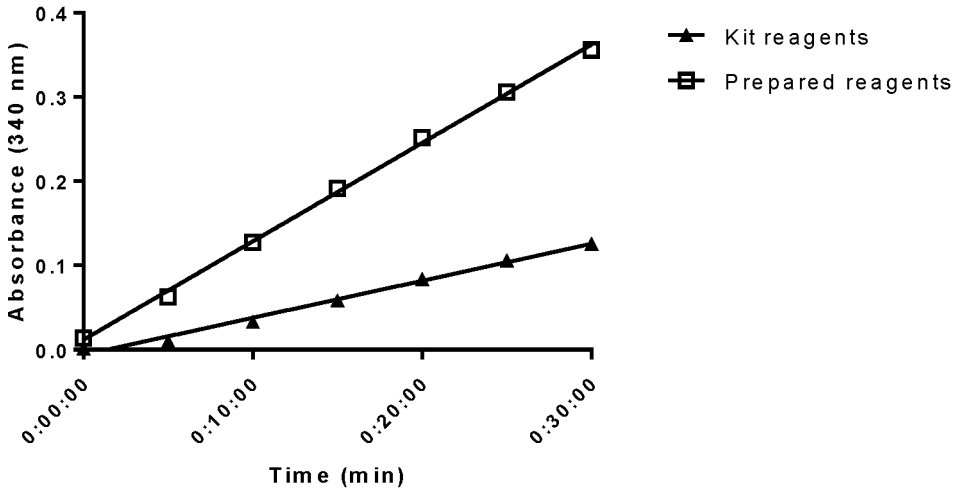

Figure 35: *P. falciparum* C-domain-TPR2A interaction GST assay using kit reagents and lab-prepared reagents.

GST assays were performed in parallel with 1 µM *Pf*C-domain and 1 µM *Pf*TPR2A using GST assay kit reagents and lab-prepared assay reagents. Absorbance of the GS-DNB conjugate was measured at 340 nm over 30 minutes. Readings were corrected for TBS-1%BSA background signal and *Pf*TPR2A non-specific binding.

The results suggested that the custom prepared reagents yielded considerably improved signals compared to the commercial kit. To confirm, the assay was repeated using the mammalian proteins (Fig. 36). The mammalian GST assay was performed using 5 µM of the interaction partners to improve the signal intensity, given that the mammalian proteins appear to interact more weakly than the malaria counterparts.

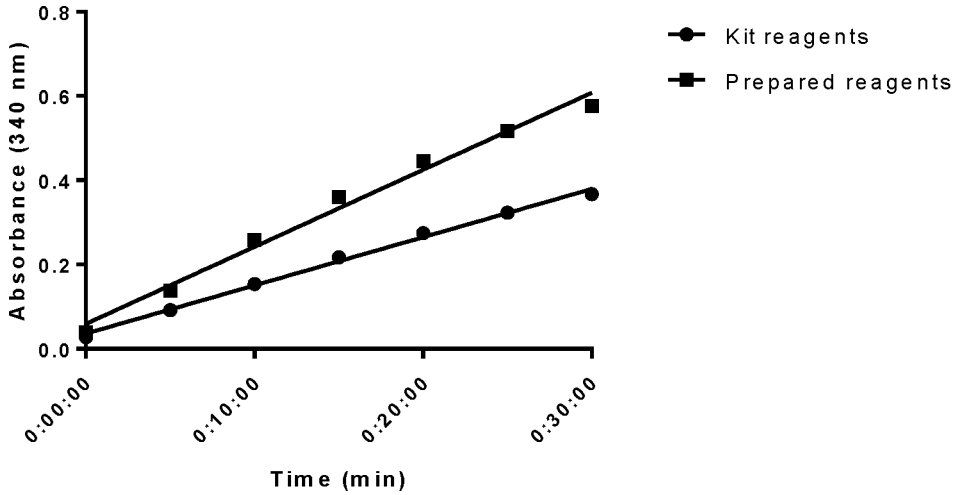

Figure 36: Mammalian C-domain-TPR2A interaction GST assay using kit reagents and lab-prepared reagents.

GST assays were performed in parallel with 5 µM hC-domain and 5 µM mTPR2A using GST assay kit reagents and lab-prepared assay reagents. Absorbance of the GS-DNB conjugate was measured at 340 nm over 30 minutes. Readings were corrected for TBS-1% BSA background signal and non-specific binding of mTPR2A.

Higher GST signals were again observed in the GST assays performed with the lab-prepared reagents indicating lab-prepared reagents are more effective than assay kit reagents. This is most likely a result of lab-prepared reagents being used immediately after preparation whereas kit reagents are unused for an undetermined amount of time between preparation and use which may affect reagent stability and efficacy.

The major cost consideration in the assay is the commercial Ni-NTA plates used. To determine whether this can be ameliorated by generating custom plates, a Nunc-Immuno™ Microwell™ 96-well plate was coated with Nα,-Bis(carboxymethyl)-L-lysine hydrate overnight and the plate was subsequently blocked with 3 % (w/v) BSA, washed and incubated in 10 mM $NiSO_4$. The plate was washed prior to use and mammalian hC-domain-mTPR2A GST assays were performed in parallel using a purchased Ni-NTA plate and the prepared Ni-NTA plate.

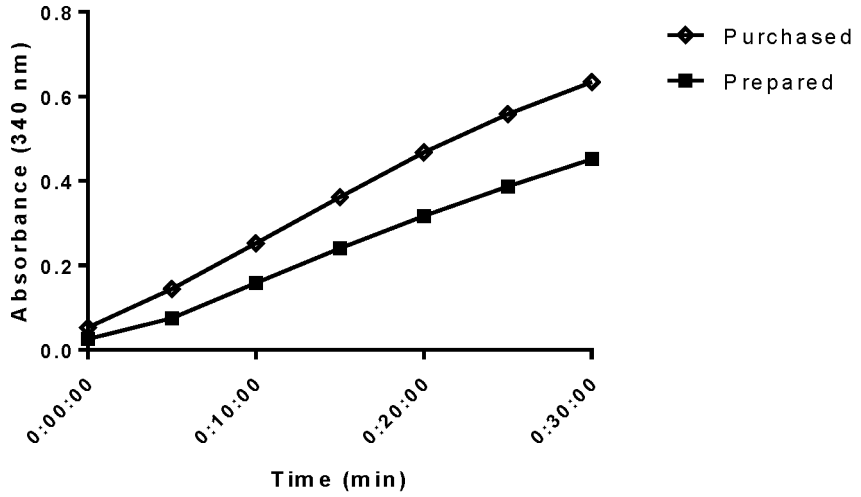

Figure 37: Mammalian C-domain-TPR2A interaction GST assay in purchased and prepared Ni-NTA plates.

GST assays were performed in parallel in purchased and prepared Ni-NTA plates with 5 µM hC-domain and 5 µM mTPR2A. Absorbance of the GS-DNB conjugate was measured at 340 nm over 30 minutes. Readings were corrected for TBS-1% BSA background signal and non-specific binding of mTPR2A.

Higher GST signals were observed for the GST assay performed in the purchased Ni-NTA plate. This may be due to the presence of more Ni-NTA binding sites on the purchased plate compared to the prepared plate – more binding sites, more C-domain binding and consequently more GST-tagged TPR2A binding. Further optimisation of custom plate preparation was not attempted.

4.2.7 C-domain-TPR2A inhibition

Having established that the GST assay format can detect the interaction of the respective *P. falciparum* and mammalian C- and TPR2A domains, the next question was whether it can detect inhibition of the interaction and thus be used for drug screening. In the absence of a small molecule inhibitor of the interaction, TPR peptides (*P. falciparum* TPR and human TPR) were used to inhibit the C-domain-TPR2A interaction. The human peptide was previously described by Horibe *et al.* (2011) and contains the Hop sequence critical for interaction with the EEVD motif of human Hsp90 (AKAYARIGNSYFK), notably K301 and R305. Based on sequence alignment, a corresponding *P. falciparum* peptide was designed (AKLYNRLAISYIN). The peptides were custom synthesized and supplied by GenScript. The GST assay was performed as previously described in the presence of a *Pf*TPR peptide and a hTPR peptide. Absorbance was measured at 340 nm over 30 minutes. The readings obtained were corrected for TBS-1 % BSA background and non-specific binding of TPR2A (Fig. 38 and 39).

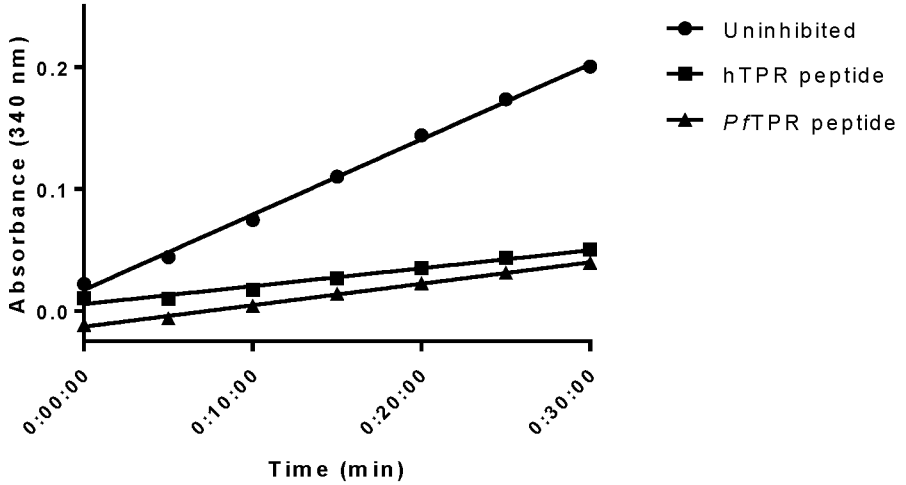

Figure 38: Mammalian C-domain-TPR2A inhibition with hTPR peptide and *Pf*TPR peptide.

Three GST assays were performed in parallel using 1 µM hC-domain and 1 µM mTPR2A: one assay without inhibitor, one containing 100 µM hTPR peptide and one containing 100 µM *Pf*TPR peptide. Absorbance of the GS-DNB conjugate was measured at 340 nm over 30 minutes. Readings were corrected for TBS-1% BSA background signal and non-specific binding of mTPR2A.

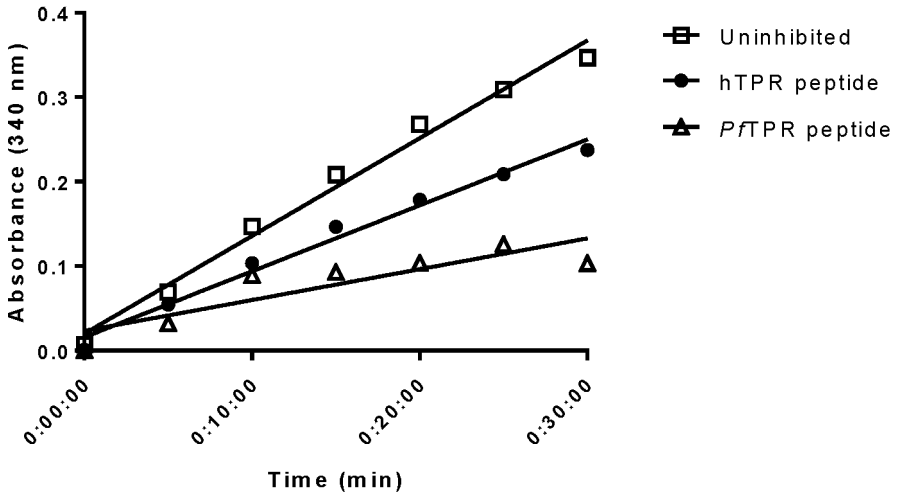

Figure 39: *P. falciparum* C-domain-TPR2A inhibition with *Pf*TPR peptide and hTPR peptide.

Three GST assays were performed in parallel using 1 µM *Pf*C-domain and 1 µM *Pf*TPR2A: one assay without inhibitor, one containing 100 µM *Pf*TPR peptide and one containing 100 µM hTPR peptide. Absorbance of the GS-DNB conjugate was measured at 340 nm over 30 minutes. Readings were corrected for TBS-1% BSA background signal and non-specific binding of *Pf*TPR2A.

Table 9: Percentage inhibition of the mammalian and *P. falciparum* C-domain-TPR2A interaction by *Pf*TPR and hTPR peptides.

	Inhibition	
	*Pf*Cdom-*Pf*TPR2A	hCdom-mTPR2A
***Pf*TPR**	44 %	83 %
hTPR	32 %	75 %

The results in Figures 38 and 39 showed decreased GST assay signals as a result of decreased C-domain-TPR2A interaction. The results in Table 9 quantitatively show the inhibitory effect of the peptides on the C-domain-TPR2A interaction calculated from the 30 minute time-point readings. In the *P. falciparum* interaction assay, the *Pf*TPR peptide was more effective than the hTPR peptide, while the peptides appeared to have similar inhibitory activity in the mammalian assay. The mammalian C-domain-TPR2A interaction was also more sensitive to inhibition – the decrease in the GST signal was more significant in the presence of the peptides. This might be symptomatic of the lower affinity of the mammalian interaction.

4.2.8 C-domain-TPR2A Glutathione plate assay

Having established that the GST assay format can be used to robustly detect C-domain-TPR2A interaction and inhibition of the interaction, a remaining question was whether the assay sensitivity could be improved when the protein immobilised on the plate was reversed. In this format, the GST-TPR2A domains were immobilised on glutathione coated plates and bound His-tagged C-domains detected using a Ni-NTA-horseradish peroxidase (HRP) conjugate, followed by adding a colorimetric HRP substrate. We did not initially opt for this format, since it requires an additional incubation and washing step, i.e. the incubation with the Ni-NTA-HRP. The assay was performed with 1 µM mammalian and *P. falciparum* C-domain and TPR2A protein samples. The proteins were added to the glutathione plate and incubated at room temperature with gentle shaking for 1 hour. The plate was washed and HisDetector™ Nickel-HRP (1:10,000 dilution; SeraCare, (MA) USA) was added to each well and incubated at room temperature for 30 minutes. The plate was washed and protein interaction was determined by adding SureBlue Reserve colorimetric HRP substrate (SeraCare, (MA) USA) and measuring the absorbance at 630 nm after 30 minutes (Fig. 40).

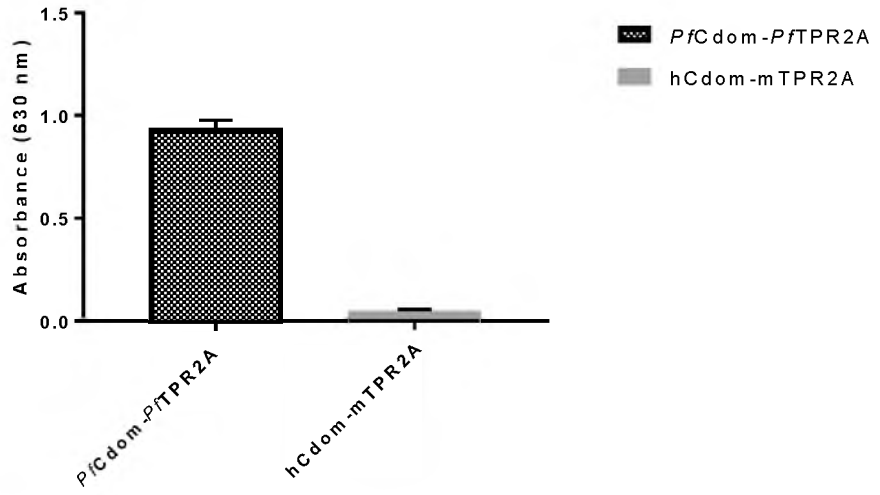

Figure 40: *P. falciparum* and mammalian C-domain-TPR2A interaction HRP assay.

C-domain-TPR2A interaction assays were performed in a glutathione-coated plate. Absorbance of SureBlue Reserve HRP reagent was measured at 630 nm. Readings were corrected for TBS-1% BSA background signal and non-specific binding of C-domain. p-value < 0.0001.

The results in Figure 40 correlate with results previously obtained with the GST assay in which more C-domain-TPR2A interaction was observed for the *P. falciparum* proteins. The interaction signal for the mammalian proteins was extremely low.

To determine the sensitivity of this assay format for the *P. falciparum* interaction, Z'-factor analysis was performed. The assay was repeated as previously described using the *Pf*C-domain-*Pf*TPR2A interaction as the positive reaction and *Pf*C-domain as the negative control. Absorbance was read at 630 nm over 30 minutes (Fig. 41).

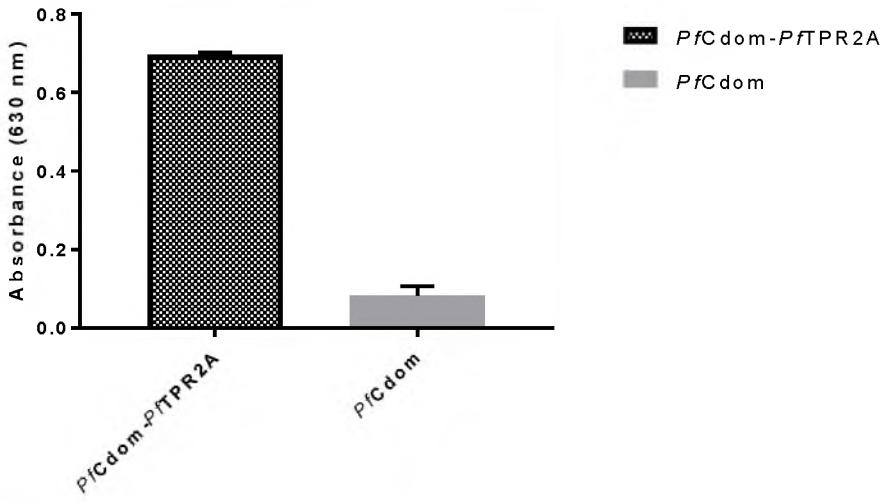

Figure 41: *P. falciparum* C-domain-TPR2A interaction HRP assay: Z'-factor experiment.

The HRP assay was performed with 1 µM *Pf*C-domain and 1 µM *Pf*TPR2A alone. Absorbance of SureBlue Reserve was measured at 630 nm over 30 minutes. The final reading was used, corrected for TBS-1% BSA background signal. p-value < 0.001.

Table 10: Z'-factor values at various time points of the *P. falciparum* C-domain-TPR2A interaction HRP assay.

Time (min)	Z'-factor
15	0.86
20	0.84
25	0.85
30	0.85

The results in Table 10 show that, in addition to yielding higher absorbance readings, higher Z'-factor values were obtained for this assay format than the corresponding GST assay (Table 5).

Although the mammalian assay yielded disappointing results when first attempted at 1 µM, the assay was repeated at a higher concentration of the two interaction partners (5 µM) using the hC-domain-mTPR2A interaction as the positive reaction and hC-domain as the negative

control. Absorbance was read at 630 nm over 30 minutes and Z'-factors calculated (Fig. 42, Table 11).

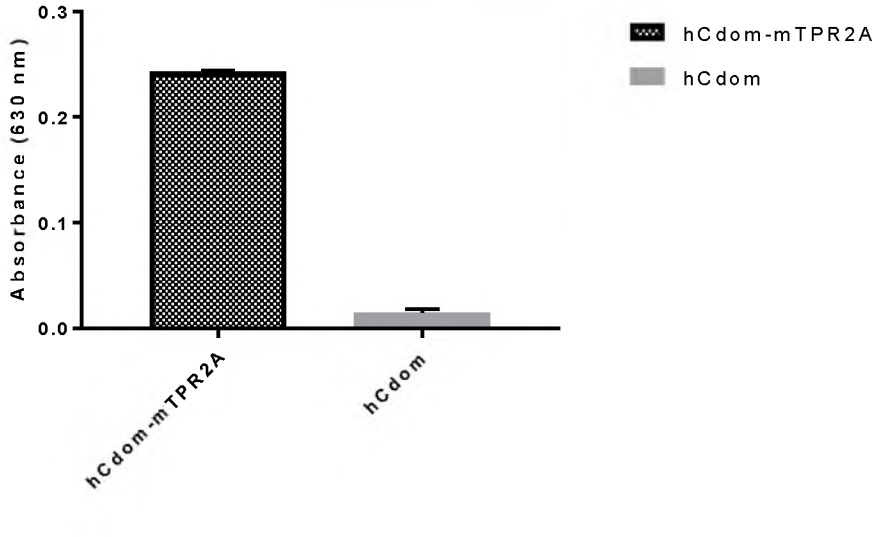

Figure 42: Mammalian C-domain-TPR2A interaction HRP assay: Z'-factor experiment.

The HRP assay was performed with 5 µM hC-domain and 5 µM mTPR2A, and 5 µM hC-domain alone Absorbance of the SureBlue reserve was measured at 630 nm over 30 minutes. The final reading was used – corrected for TBS-1% BSA background signal. p-value < 0.0001.

Table 11: Z'-factor values at various time points of the mammalian C-domain-TPR2A interaction HRP assay.

Time (min)	Z'-factor
15	0.92
20	0.92
25	0.93
30	0.94

The results show a clear difference between the sample and control experiments although the signal observed for the mammalian interaction was still significantly lower than that of the *P. falciparum* interaction. The signal observed for the negative controls was low but suggests future assays may require the signals to be corrected for C-domain background. The results indicate any interaction signals observed are likely due to C-domain-TPR2A interaction and not due to non-specific binding of C-domain. For both mammalian and *P. falciparum* Z'-factor experiments, very high Z'-factor values were observed i.e. very close to 1 (particularly the mammalian interaction) which suggests separation between the positive signal and negative signal is large which is indicative of an excellent screening assay.

4.3 Discussion

An efficient, robust and sensitive *Pf*C-domain-*Pf*TPR2A interaction assay was developed using recombinant proteins. As the assay was intended for small molecule compound screening, a mammalian C-domain-TPR2A interaction assay was developed as a control for specificity of inhibition of the *Pf* vs. mammalian interaction. As an alternative, the assay may be used to identify inhibitors of the mammalian interaction for exploration as potential anti-cancer agents. His-tagged GST was used as a positive control to confirm binding of His-tagged proteins to the Ni-NTA plate and functionality of the GST colorimetric enzyme assay, whereas untagged GST was used to confirm non-specific binding of GST to the Ni-NTA plate did not occur. These controls allowed us to establish that GST did not bind to the plate and any GST signals observed in the interaction assay were most likely due to the presence of GST-tagged TPR2A. The signal observed for the positive control was due to GST immobilisation as a result of the interaction between the polyhistidine tag and the Ni-NTA complex.

C-domain-TPR2A interaction was confirmed for both the *P. falciparum* proteins and the mammalian proteins. The interaction between *P. falciparum* C-domain and TPR2A was significantly higher than the mammalian interaction. This suggests the *P. falciparum* proteins have a higher affinity for each other than the mammalian proteins. Interestingly, this was corroborated in a FRET assay format for C-domain-TPR2A interaction developed by another student in the group (Leigh-anne Derry, MSc dissertation). Although this may partly be due to the different species of the mammalian protein partners, the human and murine TPR2A domains share 98% sequence identity. The choice of the mammalian sequences used in this study was dictated by the availability of template sequences from collaborating partners (Prof. Adrienne Edkins). Use of mouse C-domain or human TPR2A may possibly improve the interaction signal of the mammalian assay. The affinity of the C-domain proteins for their TPR2A binding partners was further determined by performing the assay with the opposite TPR2A binding partner. The MEEVD motif at the C-terminus of Hsp90 which is critical for Hop binding is conserved in both *P. falciparum* and human C-domains, as are the Lys(301) and Arg(305) residues in the Hop TPR2A domains required for binding to the MEEVD motif. However, overall the respective TPR2A domains display a 36% amino acid sequence identity (63% similarity), while the C-domains align with a 57% identity (78% similarity). Unexpectedly, a significantly high signal was observed for the hC-domain-*Pf*TPR2A interaction which implies the hC-domain has very low specificity for its TPR2A binding partner, whereas *Pf*C-domain has high specificity for its TPR2A binding partner, demonstrated

by the very low interaction signal observed. The low interaction signal may also be a result of high specificity of mTPR2A for a mammalian C-domain counterpart. The structural basis for these apparent differences in interaction affinity may be explored in future using *in silico* modelling and docking studies, coupled to analysis of the interaction using proteins containing point mutations and the assay format developed in this study.

For both assays, TPR2A non-specific binding to the plate was observed. However, non-specific binding of mammalian TPR2A was much higher than non-specific binding of *P. falciparum* TPR2A. As untagged GST did not bind to the Ni-NTA plate, the signal observed for the GST-fusion proteins is most likely due to TPR2A. Swaffield and Johnston (1996) suggest there may be 'sticky' surfaces on GST-fusion proteins which lead to artefactual interaction of the protein with other proteins and surfaces. Decreasing the concentration of the GST-fusion protein reduced the non-specific binding signal observed, but this did not significantly improve the interaction signal, thus equimolar concentrations of C-domain and TPR2A were used and the TPR2A background signal was accounted for by subtracting it from the C-domain-TPR2A interaction signal. The difference between the mammalian and *P. falciparum* TPR2A non-specific binding signals suggests there is a difference between the protein structures that causes mammalian TPR2A to be much 'stickier' than *P. falciparum* TPR2A.

Determining the Z'-factor is the most widely used parameter to monitor assay quality as well as assay evaluation and validation (Kummel *et al.*, 2010). The Z'-factor is a measure of the distribution of the positive signal/sample signal and the background signals (Sui and Wu, 2007). According to Zhang *et al.* (1999), a Z'-factor between 0.5 and 1 shows good separation of the sample and background signals indicating the assay is 'suitable' for screening purposes. The larger the Z'-factor value, the higher the quality of the assay and the more 'suitable' it is for HTS (Zhang *et al.*, 1999). The Z'-factors obtained for the *P .falciparum* C-domain-TPR2A interaction GST assay were all above 0.5 and increased over time suggesting better signals were obtained at later time points in the assay. The mammalian C-domain-TPRA2A interaction assay Z'-factors were relatively low but after 25 minutes, the assay Z'-factors were above 0.5 indicating suitability of the assay for screening using signals at later time points. For comparing any possible 'hits' in a screening campaign for inhibition of the *Pf* vs. mammalian interaction, later time points will thus have to be used.

Designed TPR peptides encompassing the Lys(301) and Arg(305) residues required for Hsp90 binding (Horibe *et al.*, 2011) were used to inhibit the C-domain-TPR2A interaction, allowing

for evaluation of the assay's ability to respond to small molecule inhibitors. Both peptides inhibited the C-domain-TPR2A interaction, however, the *P. falciparum* C-domain-TPR2A interaction was only partially inhibited while the mammalian interaction was markedly inhibited. This may be due to the low affinity of human C–domain for its TPR2A binding partner thus the interaction is more sensitive to disruption by inhibitors. As expected, the *Pf*TPR peptide was more effective than hTPR peptide at inhibiting the interaction of the *P. falciparum* domains, but inhibition of the mammalian domains was similar with both peptides. *In silico* modelling of peptide structure and docking studies may shed light on this difference. A relatively high peptide concentration of 100 µM was used, considering that small molecule inhibitors that are exploitable in drug discovery projects should ideally have inhibitory concentrations in the low micromolar to nanomolar range. However, inhibition of human Hsp90-Hop interaction (using a surface plasmon resonance assay) with the mammalian peptide was also achieved only at relatively high concentrations (170 µM) by Horibe *et al.* (2011).Overall, the inhibition study demonstrated the assay's ability to respond to inhibitor compounds and thus its potential as a screening assay.

The assay developed in this study offers a relatively sensitive and robust method for identifying novel *P. falciparum* Hsp90-Hop inhibitors, however using purchased GST assay kit reagents and purchased Ni-NTA plates is significantly cost-intensive. To lower assay cost, we prepared the reagents required for the GST assay as well as Ni-NTA coated 96-well plates. The GST signal observed when using prepared reagents was significantly higher than the signal observed when using GST assay kit reagents suggesting the assay is more efficient when recently prepared reagents are used. Conversely, a lower GST signal was observed for the prepared Ni-NTA plate compared to the purchased Ni-NTA plate. This is possibly due to the presence of fewer Ni-NTA binding sites on the prepared plates resulting in decreased C-domain binding and subsequently decreased TPR2A binding. As 'cost per assay' is an important factor to consider when developing a HTS assay, cost reduction is a key aspect of assay optimisation. Although lower GST signals were observed using the prepared Ni-NTA plate, the GST signal was high enough to provide significant results thus in principle, prepared Ni-NTA plates could be used instead of purchased Ni-NTA plates in future screening. However, for this to occur, further optimisation of Ni-NTA plate preparation is required as results varied with each prepared plate. The optimisation and inhibition studies performed indicate the GST assay is ready for validation screening using compound libraries to identify possible 'hit' compounds and determine their potency using dose response analysis. (Zhang *et al.*, 1999).

The C-domain-TPR2A interaction assays were performed on a glutathione plate to determine if similar results would be observed if TPR2A was the immobilised protein instead of the C-domain. Similar to the C-domain-TPR2A interaction GST assay, higher interaction signals were observed for the *P. falciparum* proteins while significantly lower non-specific binding of the C-domain was observed for both *P. falciparum* and mammalian proteins. Extremely low interaction signals were observed for the mammalian proteins at the same concentration as the *P. falciparum* assay. This may be due to low binding of mTPR2A to the plate as well as low affinity of mTPR2A for hC-domain. Z'-factor values for both the mammalian and *P. falciparum* assays were much higher than those observed for the GST assay indicating that performing the assay in this format may be more suitable for screening in terms of assay robustness. However, the assay format requires an additional incubation and washing step which should be taken into consideration when large compound libraries are to be screened. One possibility is to use it as a follow-up assay to corroborate 'hits' obtained in a primary screen using the simpler GST assay. Although early results suggest the glutathione plate format works better than the Ni-NTA plate format, the high concentration of mammalian proteins required to produce a significant signal is not ideal for HTS thus further optimisation of this assay format is required i.e. determination of optimal protein concentration and ratio of C-domain to TPR2A, determination of optimal incubation times, determination of optimal HisDetector dilution as well as inhibition studies before we can accurately compare the two formats.

Chapter 5

General Conclusions

Hsp90 is an extensively studied cancer drug target and in recent times has been considered a possible malaria drug target (Shahinas *et al.*, 2013). The majority of Hsp90 drug candidates in development target the N-terminal ATP binding site of the chaperone while a few target the C-terminal domain (Brandt and Blagg, 2009). Recently, it has been suggested that targeting Hsp90 interaction partners such as Hop may be an alternative way to inhibit Hsp90 (Sidera and Patsavoudi, 2014). Inhibition of the *P. falciparum* Hsp90-Hop interaction has yet to be confirmed as a possible drug target using specific inhibitors. The aim of this research project was to develop a novel Hsp90-Hop interaction assay which may be used to identify inhibitors of the protein-protein interaction for drug target validation purposes in *P. falciparum*. The objectives pursued were achieved by: cloning human and *P. falciparum* Hsp90 C-terminal domains into pET-28a(+) and murine and *P. falciparum* TPR2A domains into pGEX-4T-1; expression and purification of the recombinant proteins and detection of the mammalian and *P. falciparum* Hsp90-Hop interaction using the developed nickel-plate capture and GST enzyme assay format.

There are three main implications of the results obtained in this study:

Firstly, to our knowledge, this is the first demonstration of the interaction of *Pf*Hsp90 and *Pf*Hop using purified proteins (or at least their respective interaction domains). Previous experimental evidence that the proteins interact in malaria parasites included their co-localisation in the parasite cytoplasm by fluorescence microscopy, co-immunoprecipitation from parasite lysates using anti-*Pf*Hop antibodies and their co-elution in a complex also containing *Pf*Hsp70 by gel filtration of parasite lysates (Gitau *et al.*, 2012). In addition, the *Pf*Hsp90 C-terminal domain and *Pf*Hop TPR2A domain were reported to interact in *E.coli* using a GFP complementation assay (Zininga *et al.*, 2015). In this assay format, the N- and C-terminal domains of GFP were fused to the C-terminal and TPR2A domains respectively and expressed in *E. coli*. Interaction of the domains was suggested by the reconstitution of GFP fluorescence in the *E. coli* cells.

Secondly, we have developed an Hsp90-Hop interaction assay that is suitably for compound library screening and undemanding in terms of reagents, procedure or instrumentation, requiring only a standard plate-reading spectrophotometer (the need for nickel-coated plates

may be the only complicating factor and is addressed below). As a comparison, the commonly used FRET assay format for protein-protein interactions that was also applied in our group for *Pf*Hsp90-*Pf*Hop interaction using the C-terminal and TPR2A domains yielded Z'-factor values that were below the 0.5 ideal due to high fluorescence background readings – a common complication in fluorescence assays (Leigh-anne Derry, MSc dissertation). Although the focus of the study was on developing an assay for the malaria interaction partners, the mammalian assay that was developed as a screening control may also be applied for the screening of compounds for potential anti-cancer activity. Future work will include screening experiments – we have acquired a BioFocus library of 2000 α-helix mimetics (potential PPI inhibitors) for this purpose. Potent hit compounds could then be tested for anti-malarial activity using *P. falciparum* cultures as a starting point for exploring the validity of the *Pf*Hsp90-*Pf*Hop interaction as a malaria drug target. The same applies to hits found in the mammalian assay and cancer cell viability assays to more firmly establish Hsp90-Hop interaction as a possible cancer drug target.

Thirdly, we have established an assay format that can be readily adapted for other relevant protein-protein interactions, given the interest in pursuing this category of targets for novel drug discovery. We have, for example, used it to robustly detect the activation and interaction of *P. falciparum* and human Arf 1 GTPases with an effector protein (GGA3) (Tarryn Swart, unpublished results). Interestingly, an alternative novel assay format that was attempted (capture on glutathione plates and detection using nickel-conjugated HRP) produced more robust interaction signals due to reduced non-specific binding and background. The drawback is that it requires an additional incubation and wash step. Currently, we would envision using it as a secondary assay to confirm the validity of hit compounds obtained during screening, but further optimisation of the assay (using custom-prepared reagents, e.g. glutathione-coated plates and HRP substrate; optimising protein and reagent concentrations and incubation times) may reverse this.

Besides screening, adopting the assay for alternative protein-protein interactions and optimising the glutathione plate capture assay, future work is motivated by the fact that compound screening presupposes a sufficient supply of recombinant protein. The protocol for expressing and purifying the His-tagged *Pf*C-domain protein may thus have to be re-visited to improve yields, since the majority of the protein was in in the insoluble *E. coli* fraction and bacterial lysis was also insufficient. The former may possibly be rectified by using lower temperatures for bacterial growth and induction, lower IPTG induction concentrations and/or

alternative *E. coli* expression hosts. Alternative lysis protocols may include the use of commercial lysis and protein extraction reagents, e.g. BugBuster® (Novagen). In addition, the Ni-NTA affinity column binding capacity may be improved by using more resin, regularly re-charging of the column with nickel sulfate and/or re-applying the eluate to the column (this should also improve the TPR2A domain yields). Finally, if the assay format is to be extensively used for screening, the preparation of custom plates as opposed to using commercial sources needs to be explored to save costs. The cost of commercial plates approach approx. R 1000 per plate, while using the custom plates (and the current preparation protocol) entails a cost of less than 10% of that price. However, the custom plates produced interaction signals that were not as high as those obtained with commercial plates and also yielded significant variation between plates. Plate preparation may be explored using alternative well surface chemistries. For this study, Nunc MaxiSorp™ ELISA plates were used, which are claimed by the supplier to be suitable for binding of molecules with mixed hydrophobic/hydrophilic domains. It is possible that the use of plates more suitable for binding of polar molecules (e.g. Nunc MultiSorp™) may improve coating with Bis(carboxymethyl)-L-lysine and chelation of nickel.

References

Acharya, P., Kumar, R. and Tatu, U. (2007). Chaperoning a cellular upheaval in malaria: Heat shock proteins in Plasmodium falciparum. *Molecular and Biochemical Parasitology*, 153(2), pp.85-94.

Ahmad, A. and Muzaffar, M. (2016). Molecular Chaperones and Co-chaperones as Therapeutic Targets for Cancer. *Journal of Molecular Pharmaceutics & Organic Process Research*, 4(1), pp.1-3.

Alberts, B., Johnson, A., Lewis, J., Raff, M., Roberts, K. and Walter, P. (2008). *Molecular biology of the cell*. 5th ed. New York, NY: Garland Science Taylor & Francis, pp.540-541.

Alvira, S., Cuéllar, J., Röhl, A., Yamamoto, S., Itoh, H., Alfonso, C., Rivas, G., Buchner, J. and Valpuesta, J. (2014). Structural characterization of the substrate transfer mechanism in Hsp70/Hsp90 folding machinery mediated by Hop. *Nature Communications*, 5, p.5484.

Ariey, F., Witkowski, B., Amaratunga, C., Beghain, J., Langlois, A., Khim, N., *et al.* (2014). A molecular marker of artemisinin-resistant Plasmodium falciparum malaria. *Nature*, 505(7481), pp.50-55.

Arkin, M., Glicksman, M., Fu, H., Havel, J. and Du, Y. (2017). *Inhibition of Protein-Protein Interactions: Non-Cellular Assay Formats*. [online] Ncbi.nlm.nih.gov. Available at: https://www.ncbi.nlm.nih.gov/books/NBK92000/ [Accessed 17 Oct. 2017].

Ashley, E., Dhorda, M., Fairhurst, R., Amaratunga, C., Lim, P., Suon, S., *et al.* (2014). Spread of Artemisinin Resistance in Plasmodium falciparum Malaria. *New England Journal of Medicine*, 371(8), pp.786-786.

Bagatell, R. and Whitesell, L. (2004). Altered Hsp90 function in cancer: A unique therapeutic opportunity. *Molecular Cancer Therapeutics*, 3(8), pp.1021-1030.

Banerji, U. (2009). Heat Shock Protein 90 as a Drug Target: Some Like It Hot. *Clinical Cancer Research*, 15(1), pp.9-14.

Banumathy, G., Singh, V., Pavithra, S. and Tatu, U. (2003). Heat Shock Protein 90 Function Is Essential for *Plasmodium falciparum* Growth in Human Erythrocytes. *Journal of Biological Chemistry*, 278(20), pp.18336-18345.

Berggård, T., Linse, S. and James, P. (2007). Methods for the detection and analysis of protein–protein interactions. *PROTEOMICS*, 7(16), pp.2833-2842.

Blatch, G. and Edkins, A. (2015). *The Networking of Chaperones by Co-chaperones*. Cham: Springer International Publishing, pp.69-90.

Bornhorst, J. and Falke, J. (2000). Purification of Proteins Using Polyhistidine Affinity Tags. *Methods in Enzymology*, 326, pp.245-254.

Bradford, M. (1976). A Rapid and Sensitive Method for the Quantitation of Microgram Quantities of Protein Utilizing the Principle of Protein-Dye Binding. *Analytical Biochemistry*, 72(1-2), pp.248-254.

Brandt, G. and Blagg, B. (2009). Alternate Strategies of Hsp90 Modulation for the Treatment of Cancer and Other Diseases. *Current Topics in Medicinal Chemistry*, 9(15), pp.1447-1461.

Broussard, J., Rappaz, B., Webb, D. and Brown, C. (2013). Fluorescence resonance energy transfer microscopy as demonstrated by measuring the activation of the serine/threonine kinase Akt. *Nature Protocols*, 8(2), pp.265-281.

Buchner, J. and Li, J. (2013). Structure, Function and Regulation of the Hsp90 Machinery. *Biomedical Journal*, 36(3), p.106.

Butler, L., Ferraldeschi, R., Armstrong, H., Centenera, M. and Workman, P. (2015). Maximizing the Therapeutic Potential of HSP90 Inhibitors. *Molecular Cancer Research*, 13(11), pp.1445-1451.

Cabantous, S., Nguyen, H., Pedelacq, J., Koraïchi, F., Chaudhary, A., Ganguly, K., Lockard, M., Favre, G., Terwilliger, T. and Waldo, G. (2013). A New Protein-Protein Interaction Sensor Based on Tripartite Split-GFP Association. *Scientific Reports*, 3(1).

Calakos, N., Bennett, M., Peterson, K. and Scheller, R. (1994). Protein-protein interactions contributing to the specificity of intracellular vesicular trafficking. *Science*, 263(5150), pp.1146-1149.

Corbett, K. and Berger, J. (2010). Structure of the ATP-binding domain of Plasmodium falciparum Hsp90. *Proteins: Structure, Function, and Bioinformatics*, 78(13), pp.2738-2744.

Cortajarena, A., Yi, F. and Regan, L. (2008). Designed TPR Modules as Novel Anticancer Agents. *ACS Chemical Biology*, 3(3), pp.161-166.

Couturier, C. and Deprez, B. (2012). Setting Up a Bioluminescence Resonance Energy Transfer High throughput Screening Assay to Search for Protein/Protein Interaction Inhibitors in Mammalian Cells. *Frontiers in Endocrinology*, 3, pp.1-13.

Cressey, R., Pimpa, S., Chewaskulyong, B., Lertprasertsuke, N., Saeteng, S., Tayapiwatana, C. and Kasinrerk, W. (2008). Simplified approaches for the development of an ELISA to detect circulating autoantibodies to p53 in cancer patients. *BMC Biotechnology*, 8(16).

Dacres, H., Michie, M., Wang, J., Pfleger, K. and Trowell, S. (2012). Effect of enhanced Renilla luciferase and fluorescent protein variants on the Förster distance of Bioluminescence resonance energy transfer (BRET). *Biochemical and Biophysical Research Communications*, 425(3), pp.625-629.

De Las Rivas, J. and Fontanillo, C. (2010). Protein–Protein Interactions Essentials: Key Concepts to Building and Analyzing Interactome Networks. *PLoS Computational Biology*, 6(6), pp.1-8.

Degorce, F. (2009). HTRF: A Technology Tailored for Drug Discovery - A Review of Theoretical Aspects and Recent Applications. *Current Chemical Genomics*, 3(1), pp.22-32.

Dhar, K., Dhar, A. and Rosazza, J. (2003). Glutathione S-Transferase Isoenzymes from Streptomyces griseus. *Applied and Environmental Microbiology*, 69(1), pp.707-710.

Dondorp, A., Fairhurst, R., Slutsker, L., MacArthur, J., Breman, J., Guerin, P. and Plowe, C. (2011). The Threat of Artemisinin-Resistant Malaria. *New England Journal of Medicine*, 365(12), pp.1073-1075.

Edkins, A. (2016). Hsp90 Co-chaperones as Drug Targets in Cancer: Current Perspectives. *Topics in Medicinal Chemistry*, 19, pp.21-54.

Esposito, D. and Chatterjee, D. (2006). Enhancement of soluble protein expression through the use of fusion tags. *Current Opinion in Biotechnology*, 17(4), pp.353-358.

Fairhurst, R. and Dondorp, A. (2016). Artemisinin-Resistant Plasmodium falciparum in Africa. *New England Journal of Medicine*, 377(3), pp.305-306.

Fang Yi, Pingjun Zhu, Southall, N., Inglese, J., Austin, C., Wei Zheng and Regan, L. (2009). An AlphaScreenTM-Based High-Throughput Screen to Identify Inhibitors of Hsp90-Cochaperone Interaction. *Journal of Biomolecular Screening*, 14(3), pp.273-281.

Fox, G. (2010). Origin and Evolution of the Ribosome. *Cold Spring Harbor Perspectives in Biology*, 2(9).

Free, R., Hazelwood, L. and Sibley, D. (2009). Identifying Novel Protein-Protein Interactions Using Co-Immunoprecipitation and Mass Spectroscopy. *Current Protocols in Neuroscience*. [online] Available at: https://www.ncbi.nlm.nih.gov/pmc/articles/PMC4752115/pdf/nihms-756913.pdf [Accessed 14 Nov. 2017].

Gitau, G., Mandal, P., Blatch, G., Przyborski, J. and Shonhai, A. (2011). Characterisation of the Plasmodium falciparum Hsp70–Hsp90 organising protein (PfHop). *Cell Stress and Chaperones*, 17(2), pp.191-202.

Gomez-Monterrey, I., Sala, M., Musella, S. and Campiglia, P. (2012). Heat Shock Protein 90 Inhibitors as Therapeutic Agents. *Recent Patents on Anti-Cancer Drug Discovery*, 7(3), pp.313-336.

Grãslund, S., Nordlund, P., Weigelt, J., Hallberg, B., Bray, J., Gileadi, O., *et al.* (2008). Protein production and purification. *Nature Methods*, 5(2), pp.135-146.

Gul, S. and Hadian, K. (2014). Protein–protein interaction modulator drug discovery: past efforts and future opportunities using a rich source of low- and high-throughput screening assays. *Expert Opinion on Drug Discovery*, 9(12), pp.1393-1404.

Gurung, A., Bhattacharjee, A., Ajmal Ali, M., Al-Hemaid, F. and Lee, J. (2017). Binding of small molecules at interface of protein–protein complex – A newer approach to rational drug design. *Saudi Journal of Biological Sciences*, 24(2), pp.379-388.

Habig, W., Pabst, M. and Jakoby, W. (1974). Glutathione S-Transferases - The First Enzymatic Step in Mercapturic Acid Formation. *The Journal of Biological Chemistry*, 249(22), pp.7130-7139.

Hanahan, D., Jessee, J. and Bloom, F. (1991). Plasmid transformation of Escherichia coli and other bacteria. *Methods in Enzymology*, 204, pp.63-113.

Harazono, Y., Nakajima, K. and Raz, A. (2014). Why anti-Bcl-2 clinical trials fail: a solution. *Cancer and Metastasis Reviews*, 33(1), pp.285-294.

Harper, S. and Speicher, D. (2011). Purification of proteins fused to glutathione S-tranferase. *Methods in Molecular Biology*, 681, pp.259-280.

Hartl, F., Bracher, A. and Hayer-Hartl, M. (2011). Molecular chaperones in protein folding and proteostasis. *Nature*, 475(7356), pp.324-332.

Heeres, J. and Hergenrother, P. (2011). High-throughput screening for modulators of protein–protein interactions: use of photonic crystal biosensors and complementary technologies. *Chem. Soc. Rev.*, 40(8), pp.4398-4410.

Hernández, M., Sullivan, W. and Toft, D. (2002). The Assembly and Intermolecular Properties of the hsp70-Hop-hsp90 Molecular Chaperone Complex. *Journal of Biological Chemistry*, 277(41), pp.38294-38304.

Holzbeierlein, J., Windsperger, A. and Vielhauer, G. (2010). Hsp90: A Drug Target?. *Current Oncology Reports*, 12(2), pp.95-101.

Horibe, T., Kohno, M., Haramoto, M., Ohara, K. and Kawakami, K. (2011). Designed hybrid TPR peptide targeting Hsp90 as a novel anticancer agent. *Journal of Translational Medicine*, 9, pp.8-20.

Hou, B., Takanaga, H., Grossmann, G., Chen, L., Qu, X., Jones, A., Lalonde, S., Schweissgut, O., Wiechert, W. and Frommer, W. (2011). Optical sensors for monitoring dynamic changes of intracellular metabolite levels in mammalian cells. *Nature Protocols*, 6(11), pp.1818-1833.

Hughes, J., Rees, S., Kalindjian, S. and Philpott, K. (2011). Principles of early drug discovery. *British Journal of Pharmacology*, 162(6), pp.1239-1249.

Hunt, I. (2005). From gene to protein: a review of new and enabling technologies for multi-parallel protein expression. *Protein Expression and Purification*, 40(1), pp.1-22.

Islam, M.S., Aryasomayajula, A. and Selvaganapathy, P. (2017). A Review on Macroscale and Microscale Cell Lysis Methods. *Micromachines*, 8(3), pp.83-110.

Ivanov, A., Khuri, F. and Fu, H. (2013). Targeting protein–protein interactions as an anticancer strategy. *Trends in Pharmacological Sciences*, 34(7), pp.393-400.

Jackson, D., Symons, R. and Berg, P. (1972). Biochemical Method for Inserting New Genetic Information into DNA of Simian Virus 40: Circular SV40 DNA Molecules Containing Lambda Phage Genes and the Galactose Operon of Escherichia coli. *Proceedings of the National Academy of Sciences*, 69(10), pp.2904-2909.

Janzen, W. (2014). Screening Technologies for Small Molecule Discovery: The State of the Art. *Chemistry & Biology*, 21(9), pp.1162-1170.

Jones, S. and Thornton, J. (1996). Principles of protein-protein interactions. *Proceedings of the National Academy of Sciences*, 93(1), pp.13-20.

Keskin, O., Tuncbag, N. and Gursoy, A. (2016). Predicting Protein–Protein Interactions from the Molecular to the Proteome Level. *Chemical Reviews*, 116(8), pp.4884-4909.

Kim, Y., Hipp, M., Bracher, A., Hayer-Hartl, M. and Ulrich Hartl, F. (2013). Molecular Chaperone Functions in Protein Folding and Proteostasis. *Annual Review of Biochemistry*, 82(1), pp.323-355.

Kumalo, H., Bhakat, S. and Soliman, M. (2015). Heat-Shock Protein 90 (Hsp90) as Anticancer Target for Drug Discovery: An Ample Computational Perspective. *Chemical Biology & Drug Design*, 86(5), pp.1131-1160.

Kumar, R., Pavithra, S. and Tatu, U. (2007). Three-dimensional structure of heat shock protein 90 from Plasmodium falciparum: molecular modelling approach to rational drug design against malaria. *Journal of Biosciences*, 32(3), pp.531-536.

Kummel, A., Gubler, H., Gehin, P., Beibel, M., Gabriel, D. and Parker, C. (2010). Integration of Multiple Readouts into the Z' Factor for Assay Quality Assessment. *Journal of Biomolecular Screening*, 15(1), pp.95-101.

Laemmli, U. (1970). Cleavage of Structural Proteins during the Assembly of the Head of Bacteriophage T4. *Nature*, 227(5259), pp.680-685.

Lea, W. and Simeonov, A. (2011). Fluorescence polarization assays in small molecule screening. *Expert Opinion on Drug Discovery*, 6(1), pp.17-32.

Lebedev, A., Paul, N., Yee, J., Timoshchuk, V., Shum, J., Miyagi, K., Kellum, J., Hogrefe, R. and Zon, G. (2008). Hot Start PCR with heat-activatable primers: a novel approach for improved PCR performance. *Nucleic Acids Research*, 36(20).

Lesley, S. (2001). High-Throughput Proteomics: Protein Expression and Purification in the Postgenomic World. *Protein Expression and Purification*, 22(2), pp.159-164.

Li, J., Soroka, J. and Buchner, J. (2012). The Hsp90 chaperone machinery: Conformational dynamics and regulation by co-chaperones. *Biochimica et Biophysica Acta (BBA) - Molecular Cell Research*, 1823(3), pp.624-635.

Lipinski, C. (2004). Lead- and drug-like compounds: the rule-of-five revolution. *Drug Discovery Today: Technologies*, 1(4), pp.337-341.

Lodish, H., Berk, A. and Zipursky, S., Matsudaira, P., Baltimore, D. and Darnell, J. (2000). *Molecular Cell Biology*. 4th ed. New York: W.H. Freeman, pp.Section 7.1, DNA Cloning with Plasmid Vectors.

Makley, L. and Gestwicki, J. (2012). Expanding the Number of 'Druggable' Targets: Non-Enzymes and Protein-Protein Interactions. *Chemical Biology & Drug Design*, 81(1), pp.22-32.

Markham, K., Bai, Y. and Schmitt-Ulms, G. (2007). Co-immunoprecipitations revisited: an update on experimental concepts and their implementation for sensitive interactome investigations of endogenous proteins. *Analytical and Bioanalytical Chemistry*, 389(2), pp.461-473.

Matambo, T., Odunuga, O., Boshoff, A. and Blatch, G. (2004). Overproduction, purification, and characterization of the Plasmodium falciparum heat shock protein 70. *Protein Expression and Purification*, 33(2), pp.214-222.

Mauro, V. and Chappell, S. (2014). A critical analysis of codon optimization in human therapeutics. *Trends in Molecular Medicine*, 20(11), pp.604-613.

Mayer, M. and Bukau, B. (2005). Hsp70 chaperones: Cellular functions and molecular mechanism. *Cellular and Molecular Life Sciences*, 62(6), pp.670-684.

Miyata, Y., Nakamoto, H. and Neckers, L. (2013). The Therapeutic Target Hsp90 and Cancer Hallmarks. *Current Pharmaceutical Design*, 19(3), pp.347-365.

Moore, K. and Rees, S. (2001). Cell-Based Versus Isolated Target Screening: How Lucky Do You Feel?. *Journal of Biomolecular Screening*, 6(2), pp.69-74.

Morell, M., Ventura, S. and Avilés, F. (2009). Protein complementation assays: Approaches for the in vivo analysis of protein interactions. *FEBS Letters*, 583(11), pp.1684-1691.

Moser, C., Lang, S. and Stoeltzing, O. (2009). Heat-shock Protein 90 (Hsp90) as a Molecular Target for Therapy of Gastrointestinal Cancer. *Anticancer Research*, 29, pp.2031-2042.

Müller, I. and Hyde, J. (2010). Antimalarial drugs: modes of action and mechanisms of parasite resistance. *Future Microbiology*, 5(12), pp.1857-1873.

Neckers, L. (2007). Heat shock protein 90: The cancer chaperone. *Journal of Biosciences*, 32(3), pp.517-530.

O'Neill, P., Barton, V. and Ward, S. (2010). The Molecular Mechanism of Action of Artemisinin-The Debate Continues. *Molecules*, 15(3), pp.1705-1721.

Odunuga, O., Longshaw, V. and Blatch, G. (2004). Hop: more than an Hsp70/Hsp90 adaptor protein. *BioEssays*, 26(10), pp.1058-1068.

Onuoha, S., Coulstock, E., Grossmann, J. and Jackson, S. (2008). Structural Studies on the Co-chaperone Hop and Its Complexes with Hsp90. *Journal of Molecular Biology*, 379(4), pp.732-744.

Ozbabacan, S., Engin, H., Gursoy, A. and Keskin, O. (2011). Transient protein-protein interactions. *Protein Engineering Design and Selection*, 24(9), pp.635-648.

Pallavi, R., Roy, N., Nageshan, R., Talukdar, P., Pavithra, S., Reddy, R., *et al.* (2010). Heat Shock Protein 90 as a Drug Target against Protozoan Infections. *Journal of Biological Chemistry*, 285(49), pp.37964-37975.

Peng, X., Wang, J., Peng, W., Wu, F. and Pan, Y. (2016). Protein–protein interactions: detection, reliability assessment and applications. *Briefings in Bioinformatics*, pp.1-22.

Piehler, J. (2005). New methodologies for measuring protein interactions in vivo and in vitro. *Current Opinion in Structural Biology*, 15(1), pp.4-14.

Pratt, W., Morishima, Y., Peng, H. and Osawa, Y. (2010). Role of the Hsp90/Hsp70-based chaperone machinery in making triage decisions when proteins undergo oxidative and toxic damage. *Experimental Biology and Medicine*, 235(3), pp.278-289.

Puig, O., Caspary, F., Rigaut, G., Rutz, B., Bouveret, E., Bragado-Nilsson, E., Wilm, M. and Séraphin, B. (2001). The Tandem Affinity Purification (TAP) Method: A General Procedure of Protein Complex Purification. *Methods*, 24(3), pp.218-229.

Rao, V., Srinivas, K., Sujini, G. and Kumar, G. (2014). Protein-Protein Interaction Detection: Methods and Analysis. *International Journal of Proteomics*, 2014, pp.1-12.

Reymond Sutandy, F., Qian, J., Chen, C. and Zhu, H. (2013). Overview of Protein Microarrays. *Current Protocols in Protein Science*, 27(Unit 27.1).

Rosano, G. and Ceccarelli, E. (2014). Recombinant protein expression in Escherichia coli: advances and challenges. *Frontiers in Microbiology*, 5.

Saibil, H. (2013). Chaperone machines for protein folding, unfolding and disaggregation. *Nature Reviews Molecular Cell Biology*, 14(10), pp.630-642.

Scheuffler, C., Brinker, A., Bourenkov, G., Pegoraro, S., Moroder, L., Bartunik, H., *et al.* (2000). Structure of TPR domain-peptide complexes: critical elements in the assembly of the Hsp70-Hsp90 multichaperone machine. *Cell*, 101(2), pp.199-210.

Sekar, R. and Periasamy, A. (2003). Fluorescence resonance energy transfer (FRET) microscopy imaging of live cell protein localizations. *The Journal of Cell Biology*, 160(5), pp.629-633.

Shahinas, D., Folefoc, A. and Pillai, D. (2013). Targeting Plasmodium falciparum Hsp90: Towards Reversing Antimalarial Resistance. *Pathogens*, 2(1), pp.33-54.

Shen, J., Zhang, J., Luo, X., Zhu, W., Yu, K., Chen, K., Li, Y. and Jiang, H. (2007). Predicting protein-protein interactions based only on sequences information. *Proceedings of the National Academy of Sciences*, 104(11), pp.4337-4341.

Sheng, C., Dong, G., Miao, Z., Zhang, W. and Wang, W. (2015). State-of-the-art strategies for targeting protein–protein interactions by small-molecule inhibitors. *Chem. Soc. Rev.*, 44(22), pp.8375-8375.

Shonhai, A. (2010). Plasmodial heat shock proteins: targets for chemotherapy. *FEMS Immunology & Medical Microbiology*, 58(1), pp.61-74.

Shrestha, L., Bolaender, A., J. Patel, H. and Taldone, T. (2016). Heat Shock Protein (HSP) Drug Discovery and Development: Targeting Heat Shock Proteins in Disease. *Current Topics in Medicinal Chemistry*, 16(25), pp.2753-2764.

Sidera, K. and Patsavoudi, E. (2014). HSP90 Inhibitors: Current Development and Potential in Cancer Therapy. *Recent Patents on Anti-Cancer Drug Discovery*, 9(1), pp.1-20.

Singh, M. and Jain, V. (2013). Tagging the Expressed Protein with 6 Histidines: Rapid Cloning of an Amplicon with Three Options. *PLoS ONE*, 8(5).

Singh, S. and Panda, A. (2005). Solubilization and refolding of bacterial inclusion body proteins. *Journal of Bioscience and Bioengineering*, 99(4), pp.303-310.

Stevens, R. (2000). Design of high-throughput methods of protein production for structural biology. *Structure*, 8(9), pp.R177-R185.

Sui, Y. and Wu, Z. (2007). Alternative Statistical Parameter for High-Throughput Screening Assay Quality Assessment. *Journal of Biomolecular Screening*, 12(2), pp.229-234.

Swaffield, J. and Johnston, S. (1996). *Current Protocols in Molecular Biology*. New York: John Wiley & Sons Inc.

Szilagyi, A. and Zhang, Y. (2014). Template-based structure modeling of protein–protein interactions. *Current Opinion in Structural Biology*, 24, pp.10-23.

Terpe, K. (2003). Overview of tag protein fusions: from molecular and biochemical fundamentals to commercial systems. *Applied Microbiology and Biotechnology*, 60(5), pp.523-533.

Terpe, K. (2006). Overview of bacterial expression systems for heterologous protein production: from molecular and biochemical fundamentals to commercial systems. *Applied Microbiology and Biotechnology*, 72(2), pp.211-222.

Trepel, J., Mollapour, M., Giaccone, G. and Neckers, L. (2010). Targeting the dynamic HSP90 complex in cancer. *Nature Reviews Cancer*, 10(8), pp.537-549.

Vabulas, R., Raychaudhuri, S., Hayer-Hartl, M. and Hartl, F. (2010). Protein Folding in the Cytoplasm and the Heat Shock Response. *Cold Spring Harbor Perspectives in Biology*, 2(12).

Valones, M., Guimarães, R., Brandão, L., Souza, P., Carvalho, A. and Crovela, S. (2009). Principles and applications of polymerase chain reaction in medical diagnostic fields: a review. *Brazilian Journal of Microbiology*, 40(1), pp.1-11.

Vasaikar, S., Bhatia, P., Bhatia, P. and Chu Yaiw, K. (2016). Complementary Approaches to Existing Target Based Drug Discovery for Identifying Novel Drug Targets. *Biomedicines*, 4(4), p.27.

Vidal, M. (2002). *Encyclopedia of genetics*. San Diego: Academic Press, pp.1551-1552.

Wang, M., Shen, A., Zhang, C., Song, Z., Ai, J., Liu, H., *et al.* (2016). Development of Heat Shock Protein (Hsp90) Inhibitors To Combat Resistance to Tyrosine Kinase Inhibitors through Hsp90–Kinase Interactions. *Journal of Medicinal Chemistry*, 59(12), pp.5563-5586.

Wang, T., Mäser, P. and Picard, D. (2016). Inhibition of Plasmodium falciparum Hsp90 Contributes to the Antimalarial Activities of Aminoalcohol-carbazoles. *Journal of Medicinal Chemistry*, 59(13), pp.6344-6352.

Wells, J. and McClendon, C. (2007). Reaching for high-hanging fruit in drug discovery at protein–protein interfaces. *Nature*, 450(7172), pp.1001-1009.

Whitesell, L. and Lindquist, S. (2005). HSP90 and the chaperoning of cancer. *Nature Reviews Cancer*, 5(10), pp.761-772.

Xu, X., Song, Y., Li, Y., Chang, J., Zhang, H. and An, L. (2010). The tandem affinity purification method: An efficient system for protein complex purification and protein interaction identification. *Protein Expression and Purification*, 72(2), pp.149-156.

Yasgar, A., Jadhav, A., Simeonov, A. and Coussens, N. (2016). AlphaScreen-Based Assays: Ultra-High-Throughput Screening for Small-Molecule Inhibitors of Challenging Enzymes and Protein-Protein Interactions. *Methods in Molecular Biology*, 1439, pp.77-98.

Yi, F. and Regan, L. (2008). A Novel Class of Small Molecule Inhibitors of Hsp90. *ACS Chemical Biology*, 3(10), pp.645-654.

Yin, H. and Hamilton, A. (2005). Strategies for Targeting Protein-Protein Interactions With Synthetic Agents. *Angewandte Chemie International Edition*, 44(27), pp.4130-4163.

Zahiri, J., Bozorgmehr, J. and Masoudi-Nejad, A. (2013). Computational Prediction of Protein–Protein Interaction Networks: Algorithms and Resources. *Current Genomics*, 14(6), pp.397-414.

Zhang, J., Chung, T. and Oldenburg, K. (1999). A Simple Statistical Parameter for Use in Evaluation and Validation of High Throughput Screening Assays. *Journal of Biomolecular Screening*, 4(2), pp.67-73.

Zhu, H. and Snyder, M. (2003). Protein chip technology. *Current Opinion in Chemical Biology*, 7(1), pp.55-63.

Zininga, T., Makumire, S., Gitau, G., Njunge, J., Pooe, O., Klimek, H., *et al.* (2015). Plasmodium falciparum Hop (PfHop) Interacts with the Hsp70 Chaperone in a Nucleotide-Dependent Fashion and Exhibits Ligand Selectivity. *PLOS ONE*, 10(8).

Appendices

Appendix A: Designed Primers

Table 12: Primers used for PCR amplification.

Primer	Sequence	T_m (° C)
GST-PET-F	5' –AAT GGG TCG CGG ATC C ATG TCC CCT ATA CTA GGT TAT TGG-3'	67
GST-PET-R	5'- GGT GGT GGT GCT CGA G TTA TTT TGG AGG ATG GTC GCC AC-3'	70
hCdomPET-F	5'-AAT GGG TCG CGG ATC C AAC CCT GAC CAC CCC ATT GTG-3'	71
hCdomPET-R	5'- GGT GGT GGT GCT CGA G CTA ATC GAC TTC TTC CAT GCG AG-3'	69
*Pf*CdomPET-F	5'-AAT GGG TCG CGG ATC C GAG ATT AAC GCA AGA CAC CCC-3'	69
*Pf*CdomPET-R	5'-GGT GGT GGT GCT CGA G TCA ATC GAC TTC CTC CAT CTT GC-3'	68
mTPR2A-PGEX-F	5'- GGT TCC GCG TGG ATC C AAG AAA CAG GCA CTG AAA GAG AAG-3'	68
mTPR2A-PGEX-R	5'-GAT GCG GCC GCT CGA G TTA CAA GCG CTC CTG TTC CTT C-3'	71
*Pf*TPR2A-PGEX-F	5'-GGT TCC GCG TGG ATC C AAG AAA CAG AAT CGC ACT CCA G-3'	68
*Pf*TPR2A-PGEX-R	5'-GAT GCG GCC GCT CGA G TTA CAA GCG CTC CTG TTC CTT C-3'	70

*F-Forward; R-Reverse; T_m: Melting temperature.

Appendix B: Gene sequences amplified by PCR and cloned into pET-28a(+) and pGEX-4T-1

Human Hsp90 C-domain sequence (highlighted region)

```
1861    ATGGCCAAAAAGCACCTGGAGATCAACCCTGACCACCCCATTGTGGAGACGCTGCGGCAG
621      M  A  K  K  H  L  E  I  N  P  D  H  P  I  V  E  T  L  R  Q

1921    AAGGCTGAGGCCGACAAGAATGATAAGGCAGTTAAGGACCTGGTGGTGCTGCTGTTTGAA
641      K  A  E  A  D  K  N  D  K  A  V  K  D  L  V  V  L  L  F  E

1981    ACCGCCCTGCTATCTTCTGGCTTTTCCCTTGAGGATCCCCAGACCCACTCCAACCGCATC
661      T  A  L  L  S  S  G  F  S  L  E  D  P  Q  T  H  S  N  R  I

2041    TATCGCATGATCAAGCTAGGTCTAGGTATTGATGAAGATGAAGTGGCAGCAGAGGAACCC
681      Y  R  M  I  K  L  G  L  G  I  D  E  D  E  V  A  A  E  E  P

2101    AATGCTGCAGTTCCTGATGAGATCCCCCCTCTCGAGGGCGATGAGGATGCGTCTCGCATG
701      N  A  A  V  P  D  E  I  P  P  L  E  G  D  E  D  A  S  R  M

2161    GAAGAAGTCGATTAG
721      E  E  V  D  *
```

Plasmodium falciparum Hsp90 C-domain sequence (highlighted region)

```
1921    AACAGTATGACCTCATATATGCTGTCCAAAAAGATCATGGAGATTAACGCAAGACACCCC
641      N  S  M  T  S  Y  M  L  S  K  K  I  M  E  I  N  A  R  H  P

1981    ATCATTTCAGCCCTGAAACAGAAGGCTGACGCAGATAAAAGCGACAAGACAGTGAAAGAT
661      I  I  S  A  L  K  Q  K  A  D  A  D  K  S  D  K  T  V  K  D

2041    CTGATCTGGCTGCTGTTTGATACATCCCTGCTGACTTCTGGGTTCGCCCTGGAAGAGCCT
681      L  I  W  L  L  F  D  T  S  L  L  T  S  G  F  A  L  E  E  P

2101    ACCACCTTCAGCAAGCGAATCCATCGGATGATCAAGCTGGGACTGTCAATCGACGAAGAG
701      T  T  F  S  K  R  I  H  R  M  I  K  L  G  L  S  I  D  E  E

2161    GAAAACAATGACATTGATCTGCCCCCTCTGGAGGAAACCGTGGACGCTACAGATAGCAAG
721      E  N  N  D  I  D  L  P  P  L  E  E  T  V  D  A  T  D  S  K

2221    ATGGAGGAAGTCGATTGA
741      M  E  E  V  D  *
```

Mouse TPR2A sequence (highlighted region)

```
661     AATAAGAAACAGGCACTGAAAGAGAAGGAGCTGGGAAATGATGCCTACAAGAAGAAAGAT
221      N  K  K  Q  A  L  K  E  K  E  L  G  N  D  A  Y  K  K  K  D

721     TTTGACAAGGCCCTGAAGCATTATGACAGAGCCAAGGAACTGGACCCTACCAACATGACC
241      F  D  K  A  L  K  H  Y  D  R  A  K  E  L  D  P  T  N  M  T

781     TACATAACTAATCAAGCAGCTGTGCACTTTGAGAAGGGCGACTATAACAAATGCCGGGAG
261      Y  I  T  N  Q  A  A  V  H  F  E  K  G  D  Y  N  K  C  R  E

841     CTCTGTGAGAAGGCCATTGAAGTGGGCAGAGAGAACCGAGAGGACTACCGGCAGATCGCC
281      L  C  E  K  A  I  E  V  G  R  E  N  R  E  D  Y  R  Q  I  A

901     AAAGCTTATGCCCGAATTGGCAATTCCTATTTCAAAGAAGAAAAGTACAAGGATGCTATA
301      K  A  Y  A  R  I  G  N  S  Y  F  K  E  E  K  Y  K  D  A  I

961     CATTTCTACAACAAGTCTCTAGCAGAGCACCGAACCCCAGATGTGCTCAAGAAGTGCCAG
321      H  F  Y  N  K  S  L  A  E  H  R  T  P  D  V  L  K  K  C  Q

1021    CAGGCAGAGAAAATTCTGAAGGAACAGGAGCGCTTGGCTTATATCAACCCTGACTTGGCT
341      Q  A  E  K  I  L  K  E  Q  E  R  L  A  Y  I  N  P  D  L  A
```

Plasmodium falciparum TPR2A sequence (highlighted sequences)

```
661     GAGGAAAGGAAAAAGAAAGAGGAAGAGGAAATGAAGAAACAGAATCGCACTCCAGAGCAG
221      E  E  R  K  K  K  E  E  E  E  M  K  K  Q  N  R  T  P  E  Q

721     ATCCAGGGCGATGAACATAAGCTGAAAGGGAACGAGTTCTACAAGCAGAAGAAATTTGAC
241      I  Q  G  D  E  H  K  L  K  G  N  E  F  Y  K  Q  K  K  F  D

781     GAGGCCCTGAAAGAATATGAGGAAGCTATCCAGATTAACCCCAATGATATCATGTACCAC
261      E  A  L  K  E  Y  E  E  A  I  Q  I  N  P  N  D  I  M  Y  H

841     TATAATAAGGCCGCTGTGCATATTGAGATGAAGAACTACGACAAAGCAGTCGAGACCTGT
281      Y  N  K  A  A  V  H  I  E  M  K  N  Y  D  K  A  V  E  T  C
```

```
901         CTGTACGCCATCGAAAATCGATATAACTTCAAGGCTGAGTTTATTCAGGTGGCAAAACTG
301           L  Y  A  I  E  N  R  Y  N  F  K  A  E  F  I  Q  V  A  K  L

961         TACAATCGGCTGGCCATCAGCTACATCAACATGAAGAAGTACGATCTGGCCATCGAGGCT
321           Y  N  R  L  A  I  S  Y  I  N  M  K  K  Y  D  L  A  I  E  A

1021        TATCGGAAGTCCCTGGTCGAAGACAACAATCGCGCAACACGAAACGCCCTGAAAGAGCTG
341           Y  R  K  S  L  V  E  D  N  N  R  A  T  R  N  A  L  K  E  L

1081        GAAAGGCGCAAGGAGAAAGAGGAAAAGGAAGCTTACATCGACCCTGATAAAGCAGAGGAA
361           E  R  R  K  E  K  E  E  K  E  A  Y  I  D  P  D  K  A  E  E
```

GST sequence (highlighted region)

```
241         CACAGGAAACAGTATTCATGTCCCCTATACTAGGTTATTGGAAAATTAAGGGCCTTGTGC
1                           M  S  P  I  L  G  Y  W  K  I  K  G  L  V

301         AACCCACTCGACTTCTTTTGGAATATCTTGAAGAAAAATATGAAGAGCATTTGTATGAGC
15          Q  P  T  R  L  L  L  E  Y  L  E  E  K  Y  E  E  H  L  Y  E

361         GCGATGAAGGTGATAAATGGCGAAACAAAAAGTTTGAATTGGGTTTGGAGTTTCCCAATC
35          R  D  E  G  D  K  W  R  N  K  K  F  E  L  G  L  E  F  P  N

421         TTCCTTATTATATTGATGGTGATGTTAAATTAACACAGTCTATGGCCATCATACGTTATA
55          L  P  Y  Y  I  D  G  D  V  K  L  T  Q  S  M  A  I  I  R  Y

481         TAGCTGACAAGCACAACATGTTGGGTGGTTGTCCAAAAGAGCGTGCAGAGATTTCAATGC
75          I  A  D  K  H  N  M  L  G  G  C  P  K  E  R  A  E  I  S  M

541         TTGAAGGAGCGGTTTTGGATATTAGATACGGTGTTTCGAGAATTGCATATAGTAAAGACT
95          L  E  G  A  V  L  D  I  R  Y  G  V  S  R  I  A  Y  S  K  D

601         TTGAAACTCTCAAAGTTGATTTTCTTAGCAAGCTACCTGAAATGCTGAAAATGTTCGAAG
115         F  E  T  L  K  V  D  F  L  S  K  L  P  E  M  L  K  M  F  E

661         ATCGTTTATGTCATAAAACATATTTAAATGGTGATCATGTAACCCATCCTGACTTCATGT
135         D  R  L  C  H  K  T  Y  L  N  G  D  H  V  T  H  P  D  F  M

721         TGTATGACGCTCTTGATGTTGTTTTATACATGGACCCAATGTGCCTGGATGCGTTCCCAA
155         L  Y  D  A  L  D  V  V  L  Y  M  D  P  M  C  L  D  A  F  P

781         AATTAGTTTGTTTTAAAAAACGTATTGAAGCTATCCCACAAATTGATAAGTACTTGAAAT
175         K  L  V  C  F  K  K  R  I  E  A  I  P  Q  I  D  K  Y  L  K

841         CCAGCAAGTATATAGCATGGCCTTTGCAGGGCTGGCAAGCCACGTTTGGTGGTGGCGACC
195         S  S  K  Y  I  A  W  P  L  Q  G  W  Q  A  T  F  G  G  G  D

901         ATCCTCCAAAATCGGATCTGGTTCCGCGTGGATCCCCGGAATTCCCGGGTCGACTCGAGC
215         H  P  P  K  S  D  L  V  P  R  G  S  P  E  F  P  G  R  L  E

961         GGCCGCATCGTGACTGACTGACGATCTGCCTCGCGCGTTTCGGTGATGACGGTGAAAACC
235         R  P  H  R  D
```

Appendix C: pET-28a(+) and pGEX-4T-1 plasmid maps

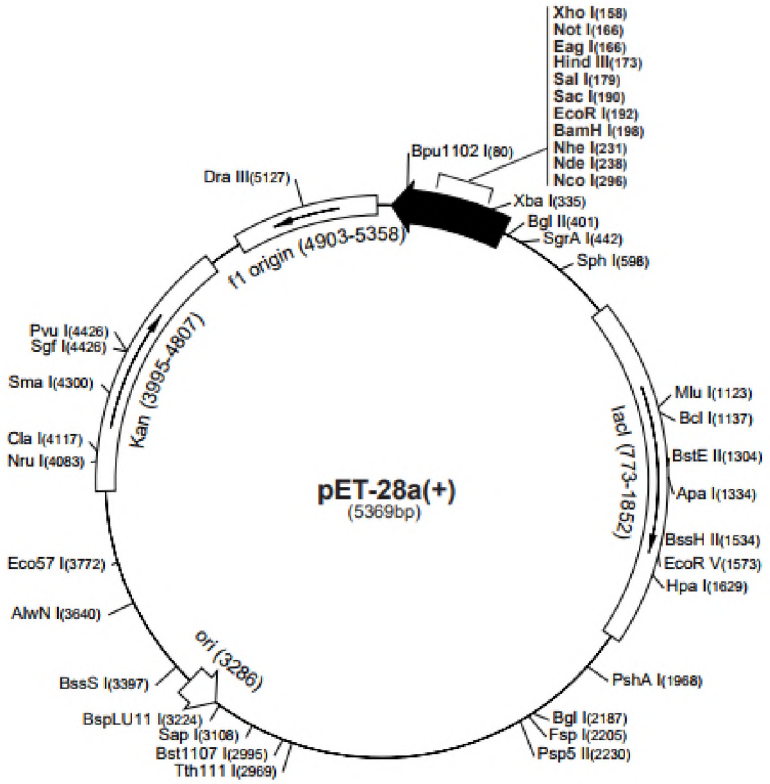

Figure 43: pET-28a(+) plasmid map (obtained from Novagen).

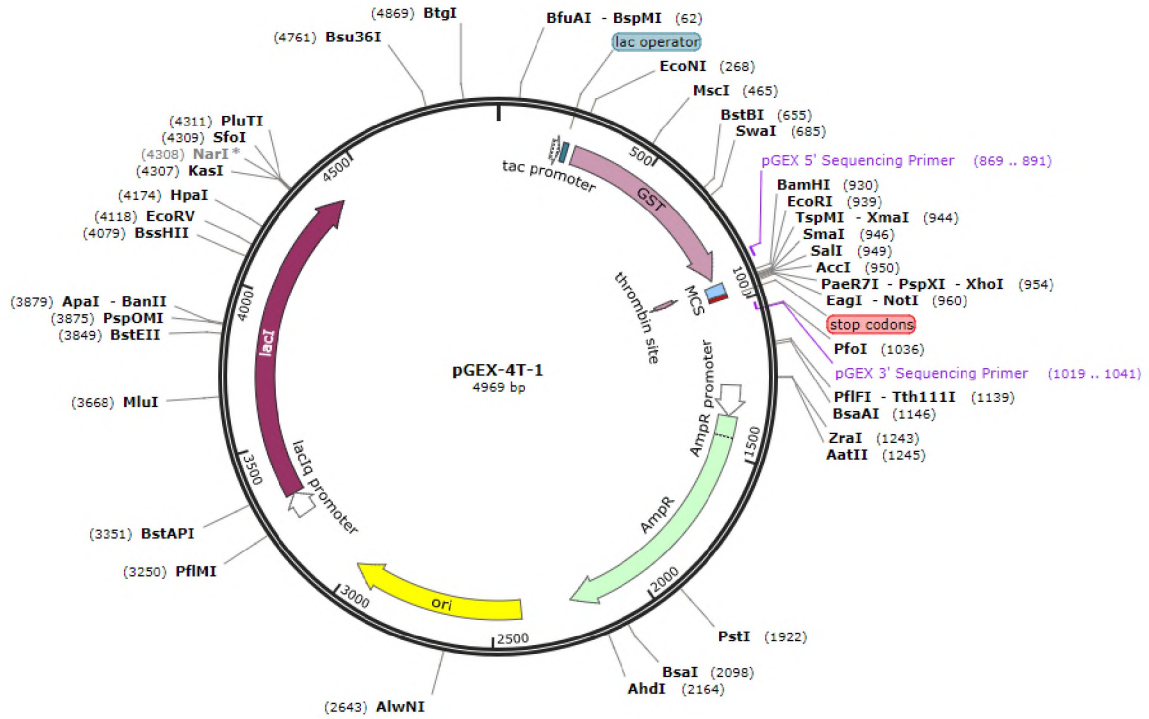

Figure 44: pGEX-4T-1 plasmid map generated by SnapGene.

Appendix D: Summary of sequencing (performed by Inqaba Biotec™ South Africa)

Blue: NheI; Yellow: BamHI; Green: XhoI; Grey: Gene insert

- pET-hC-domain

ACTTTAAGAAGGAGATATACCATGGGCAGCAGCCAYCWTCWTCATCATCACAGCAGCGGCCTGGTGCCGCG
CGGCAGCCATATGGCTAGCATGACTGGTGGACAGCAAATGGGTCGCGGATCCAACCCTGACCACCCCATTGT
GGAGACGCTGCGGCAGAAGGCTGAGGCCGACAAGAATGATAAGGCAGTTAAGGACCTGGTGGTGCTGCTGT
TTGAAACCGCCCTGCTATCTTCTGGCTTTTCCCTTGAGGATCCCCAGACCCACTCCAACCGCATCTATCGCATGA
TCAAGCTAGGTCTAGGTATTGATGAAGATGAAGTGGCAGCAGAGGAACCCAATGCTGCAGTTCCTGATGAGA
TCCCCCCTCTCGAGGGCGATGAGGATGCGTCTCGCATGGAAGAAGTCGATTAGCTCGAGCACCACCACCACCA
CCACTGAGATCCGGCTGCTAACAAAGCCCGAAAGGAAGCTGAGTTGGCTGCTGCCACCGCTGAGCAATAACT
AGCATAACCCCTTGGGGCCTCTAAACGGGTCTTGAGGGGTTTTTTGCTGAAAGGAGGAACTATATCCGGATTG
GCGAATGGGACGCGCCCTGTAGCGGCGCATTAAGCGCGGCGGGTGTGGTGGTTACGCGCAGCGTGACCGCT
ACACTTGCCAGCGCCCTAGCGCCCGCTCCTTTCGCTTTCTTCCCTTCCTTTCTCGCCACGTTCGCCGGCTTTCCCC
GTCAAGCTCTAAATCGGGGGCTCCCTTTAGGGTTCCGATTTAGTGCTTTACGGCACCTCGACCCCAAAAAACTT
GATTAGGGTGATGGTTCACGTAGTGGGCCATCGCCCTGATAGACGGTTTTTCGCCCTTTGACGTTGGAGTCCA
CGTTCTTTAATAGTGGACTCTTGTTCCAAACTGGA

- pET-*Pf*C-domain

ATTTTGTTTAACTTTAAGAAGGAGATATACCATGGGCAGCAGCCATCMTYWTCATCATCACAGCAGCGGCCT
GGTGCCGCGCGGCAGCCATATGGCTAGCAACGCGCGTCACCCGATCATTAGCGCGCTGAAGCAGAAAGCGG
ACGCGGATAAGAGCGACAAAACCGTGAAGGATCTGATCTGGCTGCTGTTCGACACCAGCCTGCTGACCAGCG
GTTTCGCGCTGGAGGAACCGACCACCTTTAGCAAACGTATCCACCGTATGATTAAGCTGGGCCTGAGCATCGA
CGAGGAAGAGAACAACGACATTGATCTGCCGCCGCTGGAAGAGACCGTGGATGCGACCGATAGCAAAATGG
AAGAGGTTGATTAACTCGAGCACCACCACCACCACCACTGAGATCCGGCTGCTAACAAAGCCCGAAAGGAAG
CTGAGTTGGCTGCTGCCACCGCTGAGCAATAACTAGCATAACCCCTTGGGGCCTCTAAACGGGTCTTGAGGGG
TTTTTTGCTGAAAGGAGGAACTATATCCGGATTGGCGAATGGGACGCGCCCTGTAGCGGCGCATTAAGCGCG
GCGGGTGTGGTGGTTACGCGCAGCGTGACCGCTACACTTGCCAGCGCCCTAGCGCCCGCTCCTTTCGCTTTCT
TCCCTTCCTTTCTCGCCACGTTCGCCGGCTTTCCCCGTCAAGCTCTAAATCGGGGGCTCCCTTTAGGGTTCCGAT
TTAGTGCTTTACGGCACCTCGACCCCAAAAAACTTGATTAGGGTGATGGTTCACGTAGTGGGCCATCGCCCTG
ATAGACGGTTTTTCGCCCTTTGACGTTGGAGTCCACGTTCTTTAATAGTGGACTCTTGTTCCAAACTGGAACAA
CACTCAACCCTATCTCGGTCTATTCTTTTGATTTATA

- pET-GST

ATTTTGTTTAACTTTAAGAAGGAGATATACCATGGGCAGCAGCCATCWTCATMATCATCACAGCAGCGGCCT
GGTGCCGCGCGGCAGCCATATGGCTAGCATGACTGGTGGACAGCAAATGGGTCGCGGATCCATGTCCCCTAT
ACTAGGTTATTGGAAAATTAAGGGCCTTGTGCAACCCACTCGACTTCTTTTGGAATATCTTGAAGAAAAATATG
AAGAGCATTTGTATGAGCGCGATGAAGGTGATAAATGGCGAAACAAAAAGTTTGAATTGGGTTTGGAGTTTC
CCAATCTTCCTTATTATATTGATGGTGATGTTAAATTAACACAGTCTATGGCCATCATACGTTATATAGCTGACA
AGCACAACATGTTGGGTGGTTGTCCAAAAGAGCGTGCAGAGATTTCAATGCTTGAAGGAGCGGTTTTGGATA
TTAGATACGGTGTTTCGAGAATTGCATATAGTAAAGACTTTGAAACTCTCAAAGTTGATTTTCTTAGCAAGCTA
CCTGAAATGCTGAAAATGTTCGAAGATCGTTTATGTCATAAAACATATTTAAATGGTGATCATGTAACCCATCC
TGACTTCATGTTGTATGACGCTCTTGATGTTGTTTTATACATGGACCCAATGTGCCTGGATGCGTTCCCAAAATT
AGTTTGTTTTAAAAAACGTATTGAAGCTATCCCACAAATTGATAAGTACTTGAAATCCAGCAAGTATATAGCAT
GGYCTTTGCAGGGCTGGCAAGCCACGTTTGGTGGTGGCGACCATCCTCCAAAATAACTCGAGCACCACCACCA

CCACCACTGAGATCCGGCTGCTAACAAAGCCCGAAAGGAAGCTGAGTTGGCTGCTGCCACCGCTGAGCAATA
ACTAGCATAACCYCTTGGGGCCTCTAAACGGGTCTTGAGGGG

- pGEX-mTPR2A

TCCAAGAACAGGCACTGAAAGAGAAGGAGCTGGGAAATGATGCCYWCAAGAAGAAAGATTTTGACAAGGCC
CTGAAGCATTATGACAGAGCCAAGGAACTGGACCCTACCAACATGACCTACATAACTAATCAAGCAGCTGTGC
ACTTTGAGAAGGGCGACTATAACAAATGCCGGGAGCTCTGTGAGAAGGCCATTGAAGTGGGCAGAGAGAAC
CGAGAGGACTACCGGCAGATCGCCAAAGCTTATGCCCGAATTGGCAATTCCTATTTCAAAGAAGAAAAGTACA
AGGATGCTATACATTTCTACAACAAGTCTCTAGCAGAGCACCGAACCCCAGATGTGCTCAAGAAGTGCCAGCA
GGCAGAGAAAATTCTGAAGGAACAGGAGCGCTTGTAACTCGAGCGGCCGCATCGTGACTGACTGACGATCTG
CCTCGCGCGTTTCGGTGATGACGGTGAAAACCTCTGACACATGCAGCTCCCGGAGACGGTCACAGCTTGTCTG
TAAGCGGATGCCGGGAGCAGACAAGCCCGTCAGGGCGCGTCAGCGGGTGTTGGCGGGTGTCGGGGCGCAG
CCATGACCCAGTCACGTAGCGATAGCGGAGTGTATAATTCTTGAAGACGAAAGGGCCTCGTGATACGCCTATT
TTTATAGGTTAATGTCATGATAATAATGGTTTCTTAGACGTCAGGTGGCACTTTTCGGGGAAATGTGCGCGGA
ACCCCTATTTGTTTATTTTTCTAAATACATTCAAATATGTATCCGCTCATGAGACAATAACCCTGATAAATGCTTC
AATAATATTGAAAAAGGAAGAGTATGAGTATTCAACATTTCCGTGTCGCCCTTATTCCCTTTTTTGCGGCATTTT
GCCTTCCTGTTTTTGCTCACCCAGAAACGCTGGTGAAAGTAAAAGA

- pGEX-*Pf*TPR2A

AATCGCACTCCAGAGCAGATCCAGGGCGATGAACATWAGSTGAAAGGGAACGAGTTCTACAAGCAGAAGAA
ATTTGACGAGGCCCTGAAAGAATATGAGGAAGCTATCCAGATTAACCCCAATGATATCATGTACCACTATAAT
AAGGCCGCTGTGCATATTGAGATGAAGAACTACGACAAAGCAGTCGAGACCTGTCTGTACGCCATCGAAAAT
CGATATAACTTCAAGGCTGAGTTTATTCAGGTGGCAAAACTGTACAATCGGCTGGCCATCAGCTACATCAACA
TGAAGAAGTACGATCTGGCCATCGAGGCTTATCGGAAGTCCCTGGTCGAAGACAACAATCGCGCAACACGAA
ACGCCCTGAAAGAGCTGGAAAGGCGCAAGGAGAAAGAGTAACTCGAGCGGCCGCATCGTGACTGACTGACG
ATCTGCCTCGCGCGTTTCGGTGATGACGGTGAAAACCTCTGACACATGCAGCTCCCGGAGACGGTCACAGCTT
GTCTGTAAGCGGATGCCGGGAGCAGACAAGCCCGTCAGGGCGCGTCAGCGGGTGTTGGCGGGTGTCGGGGC
CGCAGCCATGACCCAGTCACGTAGCGATAGCGGAGTGTATAATTCTTGAAGACGAAAGGGCCTCGTGATACG
CCTATTTTTATAGGTTAATGTCATGATAATAATGGTTTCTTAGACGTCAGGTGGCACTTTTCGGGGAAATGTGC
GCGGAACCCCTATTTGTTTATTTTTCTAAATACATTCAAATATGTATCCGCTCATGAGACAATAACCCTGATAAA
TGCTTCAATAATATTGAAAAAGGAAGAGTATGAGTATTCAACATTTCCGTGTCGCCCTTATTCCCTTTTTTTGCG
GCATTTTGCCTTCCTGTTTTTGC

Appendix E: Bradford assay standard curve

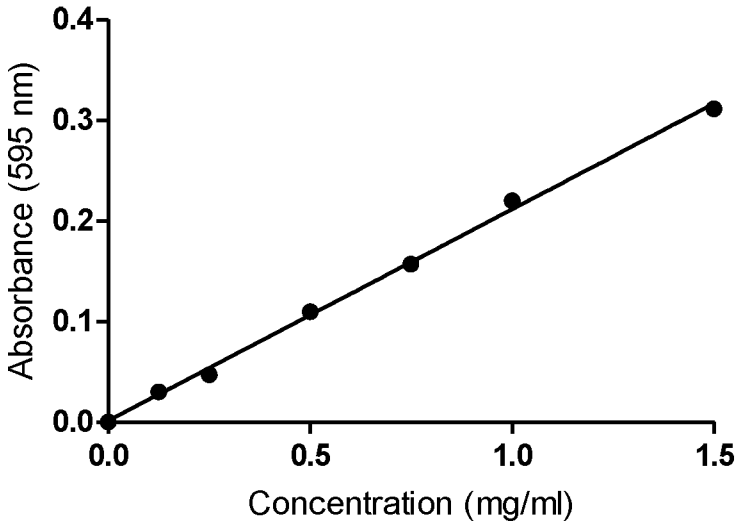

Figure 45: Bradford assay standard curve.

The Bradford protein assay was performed at 0, 0.125, 0.25, 0.5, 0.75, 1 and 1.5 mg/ml BSA concentrations. Absorbance of the Bradford reagent was measured at 595 nm after 5 minutes (Generated by L. Derry).